Optimization and Control of Power Flow in Distribution Networks

Thesis by

Masoud Farivar

In Partial Fulfillment of the Requirements

for the Degree of

Doctor of Philosophy

California Institute of Technology

Pasadena, California

2016

(Defended June 2, 2015)

This thesis is dedicated to
my inspiring parents,
and my twin, Saeid.

Acknowledgments

I would like to express my gratitude to all those who helped me with various aspects in conducting and writing up this dissertation. First and foremost, I am thankful to Professors Steven Low, Babak Hassibi, Mani Chandy, and Adam Wierman for their advice and support throughout my Ph.D work. Special thanks to my collaborators and defense/candidacy committee members Lijun Chen, Xinyang Zhou, John Doyle, Christopher Clarke, Russel Neal, Venkat Chandrasekaran, Yisong Yue, and Ali Hajimiri, for their valuable insights and contributions to the content and the improvement of this thesis. Further, I am thankful for the collaboration opportunities and the financial support from the Southern California Edison, and the Resnick Sustainability Institute at Caltech.

And last, but certainly not least, I am eternally grateful to my parents who have always loved me and encouraged me to constantly distinguish myself and be the best I can be. Without them, I would have never had the educational opportunities I had. And a big shout-out to my twin brother, Saeid, who has been with me from day one, and whom I have grown closer to over these years.

Abstract

Climate change is arguably the most critical issue facing our generation and the next. As we move towards a sustainable future, the grid is rapidly evolving with the integration of more and more renewable energy resources and the emergence of electric vehicles. In particular, large scale adoption of residential and commercial solar photovoltaics (PV) plants is completely changing the traditional slowly-varying unidirectional power flow nature of distribution systems. High share of intermittent renewables pose several technical challenges, including voltage and frequency control. But along with these challenges, renewable generators also bring with them millions of new DC-AC inverter controllers each year. These fast power electronic devices can provide an unprecedented opportunity to increase energy efficiency and improve power quality, if combined with well-designed inverter control algorithms. The main goal of this dissertation is to develop scalable power flow optimization and control methods that achieve system-wide efficiency, reliability, and robustness for power distribution networks of future with high penetration of distributed inverter-based renewable generators.

Proposed solutions to power flow control problems in the literature range from fully centralized to fully local ones. In this thesis, we will focus on the two ends of this spectrum. In the first half of this thesis (chapters 2 and 3), we seek optimal solutions to voltage control problems provided a centralized architecture with complete information. These solutions are particularly important for better understanding the overall system behavior and can serve as a benchmark to compare the performance of other control methods against. To this end, we first propose a branch flow model (BFM) for the analysis and optimization of radial and meshed networks. This model

leads to a new approach to solve optimal power flow (OPF) problems using a two step relaxation procedure, which has proven to be both reliable and computationally efficient in dealing with the non-convexity of power flow equations in radial and weakly-meshed distribution networks. We will then apply the results to fast time-scale inverter var control problem and evaluate the performance on real-world circuits in Southern California Edison's service territory.

The second half (chapters 4 and 5), however, is dedicated to study local control approaches, as they are the only options available for immediate implementation on today's distribution networks that lack sufficient monitoring and communication infrastructure. In particular, we will follow a reverse and forward engineering approach to study the recently proposed piecewise linear volt/var control curves. It is the aim of this dissertation to tackle some key problems in these two areas and contribute by providing rigorous theoretical basis for future work.

Contents

List of Figures

List of Tables

Chapter 1

Introduction

As one of the greatest innovations in human history, the power grid is a complex interconnected network of generators, transmission lines, and distribution facilities, designed to deliver electricity from suppliers to consumers. The traditional architecture of the grid consists of large centralized plants, each injecting hundreds of megawatts of power through a mesh of high-voltage transmission lines over long distances, towards low-voltage radial distribution networks that supply electricity to slowly-varying customer loads. With this perspective in mind, distribution networks were originally built to carry power ***oneway***, and to cope with ***slow*** changes in loading conditions.

Electricity grids, particularly power distribution networks, are rapidly evolving as a result of the growing concerns for the environment and the shift towards renewables, as well as the emergence of new types of controllable loads, such as electrical vehicles (EVs). Worldwide supportive policies have put a strong preference on sustainable energy sources and encouraged fast emergence of related technological advances. The cost of renewables, led by solar photovoltaic (PV) and wind, is already competitive with fossil fuels in some markets around the world, and the prices are expected to further decline in coming decades. Renewable energy resources are highly intermittent and very hard to predict, thus making it difficult to balance real time electricity demand and supply. Figure 1.1 shows plots of solar irradiance data for two typical clear and cloudy days. This kind of volatility introduces several technical issues in renewable integration and limits their penetration. These challenges include regu-
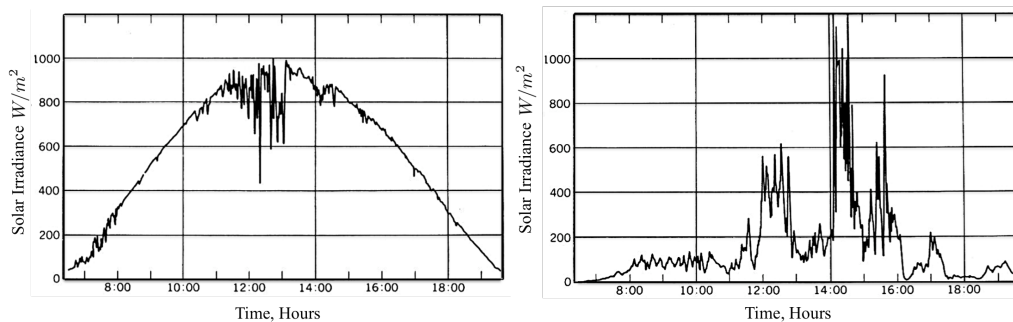
Figure 1.1: Solar irradiance variation on typical clear and cloudy days, respectively.

lating the voltage and frequency, and maintaining the grid stability and the power quality. In this thesis, we will mostly be focused on energy optimization and steady state voltage regulation in radial distribution networks.

With the increased deployment of intermittent distributed resources, the grid does no longer look like a unidirectional network with few large generators. This challenges the classical design paradigms and motivates the need to implement new operation, protection, and control schemes to cope with **fast** variation in generation, and **bi-directional** flows from thousands to millions of new active nodes of all sizes, integrated at every level of the grid. To illustrate the idea, Fig. 1.2 shows the schematic of a real-world distribution network within the Southern California Edison (SCE) service territory, where the red dots represent distributed solar PV installations on this circuit in projection of a possible near future situation.

1.1 Emerging challenges in voltage regulation of distribution networks

As discussed, distributed generation (DG) from intermittent sources presents a number of challenges for voltage regulation. For instance, clouds could drop the outputs of solar panels by as much as 80% in a minute [1], only to spike them back up again when they clear away. The voltage and frequency levels in the distribution feeder can severely fluctuate when large flows of active power are brought on-line and then
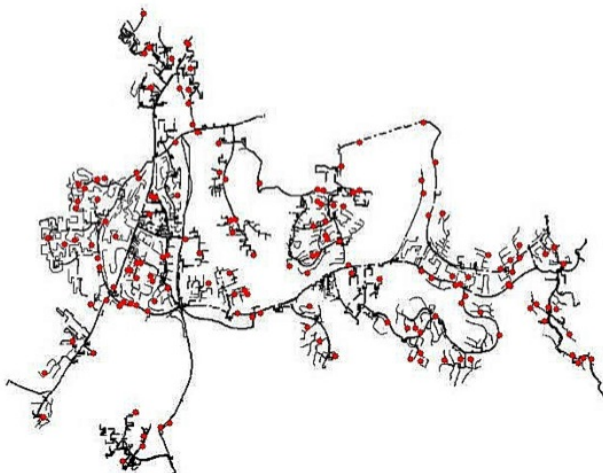
Figure 1.2: Schematic of a distribution network within the Southern California Edison (SCE) service territory filled with distributed rooftop solar PV installations (red dots), in a projection of a possible near future situation.

taken off-line, posing a treat to the system stability. Utility companies are required to continuously regulate the voltage at the distribution level within the ±5% ANSI standard range (0.95 p.u. to 1.05 p.u.), under normal operating conditions. Conventional voltage control equipments, such as switched capacitors and load tap changers, are slow, and work under the assumption that line voltage change slowly and predictably along the feeder. In a traditional unidirectional distribution feeder, the voltage magnitude typically drops with the distance from the substation due to line impedance. However, this is no longer true when DG is present. Conversely, when a generator unit is interconnected to a distribution circuit, the real power it injects causes a local voltage rise at the point of connection. If this rise is too large, it may not be feasible to maintain the line voltage within the desired range. Figure 1.3 illustrates the voltage profile of a distribution feeder with a large DG unit. Notice how the voltage drops along the feeder due to the loads until the point of DG interconnection.

In case of a long feeder with a high concentration of DG units installed towards the end, there will be significant current injection at points where the voltage is normally the lowest. If the load is sufficiently low, current will flow in the reverse direction, i.e., towards the substation and from there into the transmission level, resulting in a
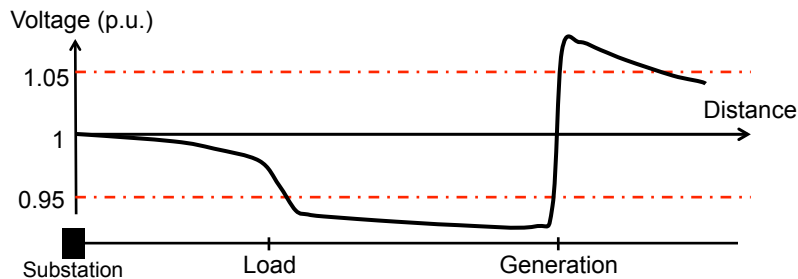
Figure 1.3: Typical voltage profile of a line in a radial distribution feeder. The voltage magnitude typically drops due to the connected loads and rises due to the power injection from the DG units.

voltage profile that increases with distance from the substation. This inverted voltage profile may confuse conventional controls. In such a scenario, load tap changers expecting voltage to decrease with distance from the substation may choose an operating point that in fact causes voltage down the line to exceed operating limits. Later in chapter 3, we will investigate in detail one such example in a realistic rural distribution feeder on the SCE service territory. Voltage fluctuations due to intermittent DG units can also cause the controlling devices such as line regulators and capacitors to operate too frequently, resulting in a reduced life span. What makes the above mentioned issues even worst is the fact that utility companies generally own very little observability and control capabilities along distribution lines. In practice, the **scarcity of information** about the topology, loading and the generation condition, and the absence of sufficient communication infrastructure makes it difficult to make control decisions within operating limits of the controlling devices in distribution networks. This motivates design of decentralized control algorithms to make optimal decisions only based on the available **local measurements**. Although distributed generators from intermittent sources pose a number of significant challenges for voltage regulation at the distribution level, if combined with **smart power electronics**, these DG units can actually contribute to the health of the grid and also serve to save energy. As demonstrated in this work, one such example is solar PV installations connected to the grid through inverters combined with appropriate volt/var control algorithms.

1.2   DC-AC inverters can takeover the control

As investigated in this thesis, DC-AC inverters can potentially address the challenges in integration of high levels of variable renewable resources, if combined with smart and well-designed control algorithms. Inverters are power electronic devices that are used to couple DC or variable-frequency power sources to the AC grid. In practice, all renewable generators are integrated to the grid through inverter interfaces. In this respect, the primary function of the inverter is to deliver the DC power to the AC side as efficiently as possible. Traditionally, inverters were designed with only the basic control functions necessary to perform this primary task, but increasingly now they are expected to also sense the grid's health locally, and react accordingly. In addition to frequency conversion and basic real power delivery, inherent control capabilities of these inverters can also help in maintaining the grid stability during under/over voltage events, by injecting or absorbing reactive power into or from the grid, respectively. Although the term "advanced" inverters in the literature may seem to imply a special type of inverter, many of the inverters already deployed today can provide advanced functionality with some minor software upgrades or parameter adjustments.

Power system loads require a combination of real power (watts) and reactive power, measured in volt-ampere reactive (vars). Control of reactive power flow is the main approach in power systems to regulate line voltages at desirable levels, in order to efficiently transfer active power through transmission and distribution lines. Traditionally, utilities have used switched capacitor banks, inductors, and rotating synchronous condensers to control reactive power flows, all of which are very slow and can take **minutes** to fully react. Though relatively inexpensive, capacitors/inductors can only inject/absorb fixed amounts of var. On the other hand, though synchronous condensers can absorb vars continuously, they incur high energy losses. The unique advantage of inverters in the world of var regulating devices is that not only they can change their reactive power output continuously, but they also are extremely fast. To be more precise, inverters can sense and reach their full output in **milliseconds**,

and this fast response property makes them a great candidate to cope with rapid voltage fluctuations due to high renewable penetration levels. Indeed, a large number of recent studies [2, 3, 4, 5, 6, 7] in the literature have explored the possibility of utilizing inverter-based distributed generators (DGs) to control voltage fluctuations in distribution systems with high renewable penetration levels, and recognized it as a viable solution. As the share of these intermittent sources increase in the future, inverters are likely to take over more and more of the grid control tasks.

1.3   New opportunities for grid optimization

Since 1960s, mathematical optimization approaches have been developed to increase the power system efficiency. Optimal Power Flow (OPF) is an optimization problem over the decision variables of a power system (e.g., voltage magnitudes at generator buses, status of the capacitor banks, transformer taps, etc), subject to the physical laws of the circuit, and the operational constraints of the network. In practice, these approaches have traditionally been mainly applied to OPF problems at the transmission level. The reason, as discussed earlier, is due to the lack of sufficient monitoring, communication, and controlling elements installed on distribution networks.

But the stakes are high, and the opportunity is there! Indeed, the majority of the 5-8% energy loss in a power system typically occurs in highly resistive lines of distribution networks. It is well-known that the installation of DG units can significantly cut these losses by feeding the loads locally and avoiding long distance power transfers. Conservation voltage reduction (CVR) can further reduce energy consumption without impacting the customer loads. In short, the utility companies prefer to push customer voltages to the lower half of the ANSI C84.1 range for CVR purposes. Studies have shown that doing so reduces the overall system demand by a factor of about 0.7%–1.0% for every 1% reduction in voltage, depending on the nature of the loads. But this is difficult to achieve with traditional voltage controllers such as capacitor banks, as they tend to create non-smooth voltage profiles.

The emergence of renewable energy sources provides a big opportunity to re-

imagine the optimization at the distribution level. One major change will be the implementation of smart inverter volt/var control functionalities to minimize energy consumption while regulating the voltages within the specified system constraints. In chapter 3, we will formally formulate the inverter var control problem and use the relaxation-based algorithm developed in chapter 2 to solve it. We demonstrate, through experimental studies on two real-world distribution feeders on SCE service territory that the optimal inverter var control algorithms can result in an overall 2%–4% reduction in distribution network energy consumption by carefully flattening the voltage profile curve (using the continuous var control capability of the inverters) and then lowering it. However, it is important to note that these benefits are achieved at the cost of increasing the internal losses in inverters when they actively participate in volt/var control. In chapter 3, we also provide a model to formally account for this type of loss and weigh it against the overall energy saving benefits in different scenarios. Our findings suggest that, contrary to the common beliefs, there's no simple solution due to the fact that the components of objective work against each other. The key message is that the optimal inverter var control is a highly non-trivial problem that needs to be properly formulated and rigorously solved. We will see how the additional cost of the internal inverter losses may completely offset the benefits in some scenarios.

1.4   The big picture

With the shift toward distributed renewable generators, inverters are being rapidly added to the distribution networks. While it is broadly accepted that the ability of inverters to regulate the reactive power flow is a useful feature that can be managed to the benefit of distribution networks, there has been little consensus on how this capability should be deployed. Furthermore, the implementation of this idea requires a departure from our current standards for interconnection of DG units in a long, multi-year process [8]. Indeed, a series of IEEE SCC21 1547 standard development initiatives [9, 10] have been underway to identify the best practices in upgrading the

inverter's role in providing ancillary services to facilitate more reliable integration of renewable resources. Proposed approaches to inverter-based voltage control in distribution networks can be broadly divided into the following three main categories:

(i) Approaches that propose a centralized control scheme by solving a global optimal power flow (OPF) problem. These methods implicitly assume an underlying complete two-way communication system between a central computing authority and the controlled nodes [4, 11, 12];

(ii) Distributed message-passing algorithms in which communications are limited to neighboring nodes [5, 13, 12, 14];

(iii) Local control methods that require no communications and rely only on local measurements and computations [3, 6, 15]. These include reactive power control based on local real power injection (referred to as Q(P)), power factor control, and the more common voltage based reactive power control (referred to as Q(V)).

In our opinion, solutions at the two ends of this spectrum are more applicable today and should be given a higher priority in research. On one hand, optimal centralized solutions are critical for the purpose of analytical analysis and better understanding of the impact of renewables on the grid. And on the other hand, fully decentralized local control methods are the only approaches available for immediate implementation in today's distribution networks, due to the lack of sufficient telecommunication infrastructure. It is the goal of this thesis to identify some key problems in these two areas and contribute by providing rigorous theoretical basis for further work.

1.5   Thesis overview and contributions

The main body of this thesis is divided into three chapters. In this section, we will summarize each, and highlight the contributions of this dissertation.

1.5.1 Branch Flow Model: relaxations and convexification

In this chapter, we start by providing a general framework for efficiently solving centralized optimization problems in distribution networks. The content is based on the results published in [16, 17, 4, 18]. We propose a branch flow model (BFM) for the analysis and optimization of radial as well as meshed networks. The model is based on the branch power and current flows in addition to nodal voltages, and it leads to a new approach to solving optimal power flow (OPF) problems. It consists of two relaxation steps: the first step eliminates the voltage and current angles and the second step approximates the resulting problem by a conic program that can be solved efficiently. For radial networks, we prove that both relaxation steps are always exact, provided there are no upper bounds on loads. For mesh networks, the conic relaxation is always exact and we provide a simple way to determine if a relaxed solution is globally optimal. We propose a simple method to convexify a mesh network using phase shifters so that both relaxation steps are always exact and OPF for the convexified network can always be solved efficiently for a globally optimal solution. We prove that convexification requires phase shifters only outside a spanning tree of the network graph and their placement depends only on network topology, and not on power flows, generation, loads, or operating constraints. We present simulation results on phase shifter ranges required for the covexification of various IEEE and other test networks.

The proposed relaxation method based on the BFM model has proven to be very reliable and efficient in dealing with distribution system optimization problems. Its success is essentially due to the fact that it explores the radial nature of the distribution networks to improve the computational efficiency of a standard SDP relaxation based methods formulated using the bus injection model (BIM). It reduces the computational complexity from SDP to Conic programming, and avoids the ill-conditioned operations to achieve numerical stability of SDP [12]. These factors are both critical in solving the fast time-sacale optimal inverter var control problem formulated in chapter 3

1.5.2 Voltage control in distribution systems with high PV penetration

In this chapter, a practical viewpoint is adopted and the goal is to apply the theoretical results of the previous chapters to study the distribution system level impacts of high-penetration photovoltaic (PV) integration and propose mitigating solutions. The content of this chapter is based on our published work in [4, 21]

We will start by formulating a volt/var optimization problem in distribution networks and use the relaxation-based algorithm developed in chapter 2 to solve it. We demonstrate, through experimental studies on two real-world distribution feeders on SCE service territory, that the optimal inverter var control algorithms can result in an overall 2%–4% reduction in distribution network energy consumption by carefully flattening the voltage profile curve (using the continuous var control capability of the inverters) and then lowering it. It is important to note that these benefits are achieved at the cost of increasing the internal losses in inverters when they actively participate in volt/var control. Therefore, we include a model to account for this type of loss and weigh it against the overall energy saving benefits in different scenarios. Our findings suggest that, contrary to the common beliefs, there's no simple solution: the optimal inverter var control is a highly non-trivial problem that needs to be properly formulated and rigorously solved. We will see how the additional cost of the internal inverter losses may completely offset the benefits in some scenarios.

1.5.3 Equilibrium and dynamics of local voltage control in distribution networks

This chapter is motivated by lack of sufficient theoretical understanding of the behavior of local voltage control methods in distribution networks. These are the only options available for immediate implementation in today's distribution networks due to scarcity of the information and the lack of sufficient communication infrastructure. The content is based on our published work in [19].

We start by formally modeling inverter-based local volt/var schemes where the

decision on the reactive power at a bus depends only on locally measured bus voltage. These local control algorithms essentially form a closed-loop dynamical system whereby the measured voltage determines the reactive power injection, which in turn affects the voltage. There has been only a limited rigorous treatment of the equilibrium and dynamical properties of such feedback systems. We show that the dynamical system has a unique equilibrium by interpreting the dynamics as a distributed algorithm for solving a certain convex optimization problem whose unique optimal point is the system equilibrium. Moreover, we show that the objective function serves as a Lyapunov function implying global asymptotic stability of the equilibrium. We essentially follow a reverse-engineering approach in this chapter, which not only provides a way to characterize the equilibrium, but also suggests a principled way to engineer the control. We then apply the results to study the parameter setting for the piecewise linear local volt/var control curves proposed in the latest draft of the new IEEE 1547.8 standard document.

1.5.4   Incremental local voltage control algorithms

It has been reported in the literature that in some practical circumstances, the previously studied class of piecewise linear local voltage control curves can lead to undesirable oscillatory behaviors even in the case of a single inverter unit. This motivates us to forward-engineer these commonly adopted non-incremental voltage control algorithms using the results of chapter 4. We first propose an incremental control algorithms that demand less restrictive condition for convergence based on the (sub)gradient method and provide a sufficient condition to ensure convergence. Then, motivated by the shortcomings of this algorithm, we propose a new pseudo-gradient based voltage control algorithm for the distribution network that does not constrain the allowable control functions but admits much lower implementation complexity. We compare these two proposed algorithms against each other and also the original local control dynamic in terms of the convergence condition and the convergence rate. The results are evaluated through simulations using a real-world distribution feeder

in Southern California with multiple large PV generation units. The content is based on our published work in [20, 87].

Chapter 2

Branch Flow Model: Relaxations and Convexification

In this chapter, we propose a branch flow model for the analysis and optimization of mesh as well as radial networks. The model leads to a new approach to solving optimal power flow (OPF) problems that consists of two relaxation steps. The first step eliminates the voltage and current angles and the second step approximates the resulting problem by a conic program that can be solved efficiently. For radial networks, we prove that both relaxation steps are always exact, provided there are no upper bounds on loads. For mesh networks, the conic relaxation is always exact and we provide a simple way to determine if a relaxed solution is globally optimal. We propose a simple method to convexify a mesh network using phase shifters so that both relaxation steps are always exact and OPF for the convexified network can always be solved efficiently for a globally optimal solution. We prove that convexification requires phase shifters only outside a spanning tree of the network graph and their placement depends only on network topology, not on power flows, generation, loads, or operating constraints. We present simulation results on phase shifter ranges required for the covexification of various IEEE and other test networks.

2.1 Background and literature review

The bus injection model is the standard model for power flow analysis and optimization. It focuses on nodal variables such as voltages, current, and power injections,

and does not directly deal with power flows on individual branches. A key advantage is the simple linear relationship $I = YV$ between the nodal current injections I and the bus voltages V through the admittance matrix Y. Instead of nodal variables, the branch flow model focuses on currents and powers on the branches. It has been used mainly for modeling distribution circuits, which tend to be radial, but has received far less attention. In this chapter, we advocate the use of branch flow model for *both* radial and mesh networks, and demonstrate how it can be used for optimizing the design and operation of power systems.

One of the motivations for our work is the optimal power flow (OPF) problem. OPF seeks to optimize a certain objective function, such as power loss, generation cost, and/or user utilities, subject to Kirchhoff's laws, power balance as well as capacity, stability and contingency constraints on the voltages and power flows. There has been a great deal of research on OPF since Carpentier's first formulation in 1962 [22]; surveys can be found in, e.g., [23, 24, 25, 26, 27]. OPF is generally nonconvex and NP-hard, and a large number of optimization algorithms and relaxations have been proposed. A popular approximation is the DC power flow problem, which is a linearization and therefore easy to solve, e.g. [28, 29, 30, 31]. An important observation was made in [32, 33] that the full AC OPF can be formulated as a quadratically constrained quadratic program and therefore can be approximated by a semidefinite program. While this approach is illustrated in [32, 33] on several IEEE test systems using an interior-point method, whether or when the semidefinite relaxation will turn out to be exact is not studied. Instead of solving the OPF problem directly, [12] proposes to solve its convex Lagrangian dual problem and gives a sufficient condition that must be satisfied by a dual solution for the duality gap to be zero and for an optimal OPF solution to be recoverable. Importantly, this provides a way to determine for sure if a power flow solution is globally optimal for the nonconvex problem. This result is extended in [34] to include other variables and constraints and in [35] to exploit the sparsity of power networks and phase shifters for convexification of OPF. In [36, 37], it is proved that the sufficient condition of [12] always holds for a radial (tree) network, provided the bounds on the power flows satisfy a simple pat-

tern. See also [38] for a generalization. These results confirm that radial networks are computationally much simpler. This is important as most distribution systems are radial.

The limitation of semidefinite relaxation for OPF is studied in [39] using mesh networks with 3, 5, and 7 buses. They show that as a line-flow constraint is tightened, the sufficient condition in [12] fails to hold for these examples and the duality gap becomes nonzero. Moreover, the solutions produced by the semidefinite relaxation are physically meaningless in those cases. Indeed, examples of nonconvexity have long been discussed in the literature, e.g., [40, 39, 41]. Hence it is important to develop systematic methods for solving OPF involving mesh networks when convex relaxation fails. See, e.g., [42] for branch-and-bound algorithms for solving OPF when the duality gap is nonzero.

The papers above are all based on the bus injection model. In this chapter, we introduce a branch flow model on which OPF and its relaxations can also be defined. Our model is motivated by a model first proposed by Baran and Wu in [43, 44] for the optimal placement and sizing of switched capacitors in distribution circuits for Volt/VAR control. By recasting their model as a set of linear and quadratic equality constraints, [4, 21] observes that relaxing the quadratic equality constraints to inequality constraints yields a second-order cone program (SOCP). It proves that the SOCP relaxation is exact when there are no upper bounds on the loads. This result is extended here to mesh networks with line limits, and convex, as opposed to linear, objective functions (Theorem 2.1). See also [45, 46] for various convex relaxations of approximations of the Baran-Wu model.

Other branch flow models have also been studied, e.g., in [47, 48, 11], all for radial networks. Indeed, [47] studies a similar model to that in [43, 44], using receiving-end branch powers as variables instead of sending-end branch powers as in [43, 44]. Both [48] and [11] eliminate voltage angles by defining real and imaginary parts of $V_i V_j^*$ as new variables and defining bus power injections in terms of these new variables. This results in a system of linear quadratic equations in power injections and the new variables. While [48] develops a Newton-Raphson algorithm to solve the bus power

injections, [11] solves for the branch flows through an SOCP relaxation for radial networks, though no proof of optimality is provided.

This set of papers [43, 44, 47, 48, 11, 45, 4, 46, 21] all exploit the fact that power flows can be specified by a simple set of linear and quadratic equalities if voltage angles can be eliminated. Phase angles can be relaxed only for radial networks and generally not for mesh networks, as [49] points out for their branch flow model, because cycles in a mesh network impose nonconvex constraints on the optimization variables (similar to the angle recovery condition in our model; see Theorem 2.2 below). For mesh networks, [49] proposes a sequence of SOCP where the nononvex constraints are replaced by their linear approximations and demonstrates the effectiveness of this approach using seven networks. In this chapter we extend the Baran-Wu model from radial to mesh networks and use it to develop a solution strategy for OPF for mesh as well as radial networks, as we now summarize.

2.2 Summary

Our purpose is to develop a formal theory of branch flow model for the analysis and optimization of mesh as well as radial networks. As an illustration, we formulate OPF within this alternative model, propose relaxations, characterize when a relaxed solution is exact, prove that our relaxations are always exact for radial networks when there are no upper bounds on loads but may not be exact for mesh networks, and show how to use phase shifters to convexify a mesh network so that a relaxed solution is always optimal for the convexified network. A similar set of results have been proved in the sequence of papers [12, 36, 37, 35] for the bus injection model, even though the results have distinct characters in each model and the proof techniques are completely different. Indeed, it can be shown that the two models are equivalent and both help deepen our understanding of OPF.

Specifically, we first formulate in Section 2.3 the OPF problem using branch flow equations involving complex bus voltages and complex branch current and power flows. In Section 2.4 we describe our solution approach, which consists of two relax-

ation steps, as illustrated in Figure 2.1:

- *Angle relaxation*: relax OPF by eliminating voltage and current angles from the branch flow equations. This yields the (extended) Baran-Wu model and a relaxed problem OPF-ar which is still nonconvex.

- *Conic relaxation*: relax OPF-ar to a cone program OPF-cr that is convex and hence can be solved efficiently.
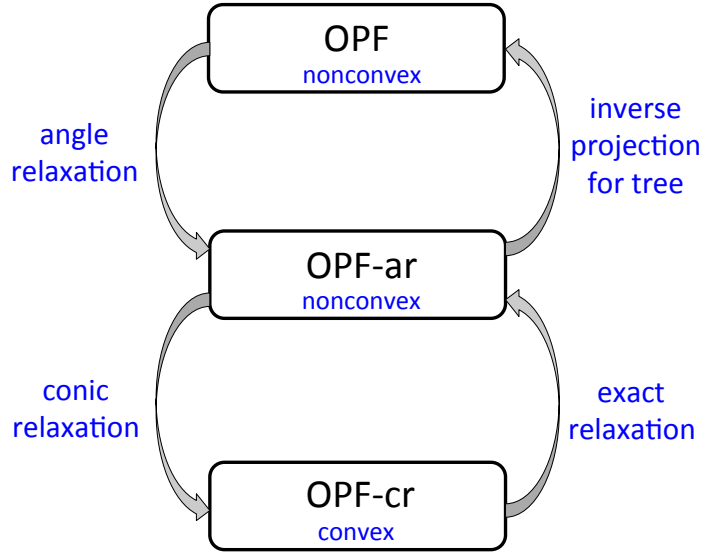
Figure 2.1: Proposed solution strategy for solving OPF.

In Section 2.5 we prove that the conic relaxation OPF-cr is always exact *even for* mesh networks, provided there are no upper bounds on real and reactive loads, i.e., an optimal solution of OPF-cr is also optimal for OPF-ar. Given an optimal solution of OPF-ar, whether we can derive an optimal solution to the original OPF depends on whether we can recover the voltage and current angles correctly from the given OPF-ar solution. In Section 2.6 we characterize the exact condition (the angle recovery condition) under which this is possible, and present two angle recovery algorithms. It turns out that the angle recovery condition always holds for a radial network and hence solving OPF-cr always produces an optimal solution for OPF. For

a mesh network, the angle recovery condition may not hold, and our characterization can be used to check if a relaxed solution yields an optimal solution for OPF.

In Section 2.7 we prove that, by placing phase shifters on some of the branches, *any* relaxed solution of OPF-ar can be mapped to an optimal solution of OPF for the convexified network, with an optimal cost that is no higher than that of the original network. Phase shifters thus convert an NP-hard problem into a simple problem. Our result implies that when the angle recovery condition holds for a relaxed branch flow solution, not only is the solution optimal for the OPF without phase shifters, but the addition of phase shifters cannot further reduce the optimal cost. On the other hand, when the angle recovery condition is violated, then the convexified network may have a strictly lower optimal cost. Moreover, this benefit can be attained by placing phase shifters only outside an *arbitrary* spanning tree of the network graph.

These results suggest an algorithm for solving OPF (2.11)–(2.12) as summarized in Figure 2.1.
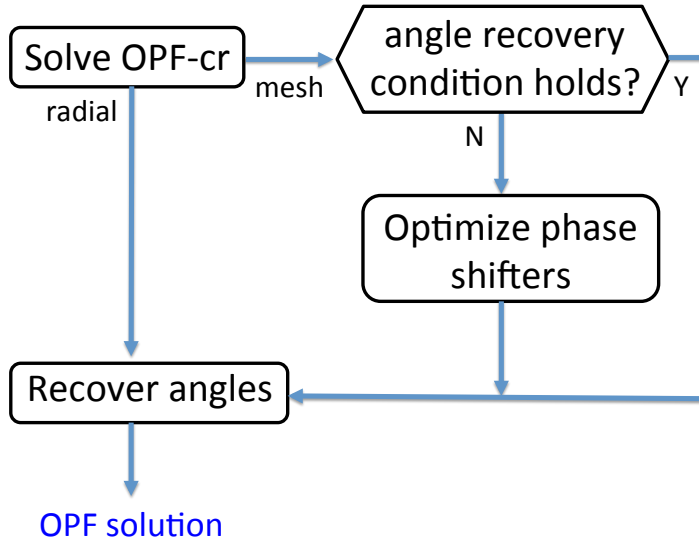
Figure 2.2: Proposed algorithm for solving OPF (2.11)–(2.12). The details are explained in Sections 2.3–2.7.

Since power networks in practice are very sparse, the number of lines not in a spanning tree can be relatively small, as demonstrated in simulations in Section 2.8 using the IEEE test systems with 14, 30, 57, 118, and 300 buses, as well as a

39-bus model of a New England power system and two models of a Polish power system with more than 2,000 buses. Moreover, the placement of these phase shifters depends only on network topology, but not on power flows, generations, loads, or operating constraints. Therefore only one-time deployment cost is required to achieve subsequent simplicity in network operation.

2.3 Branch flow model

Let $\mathbb{R}$ denote the set of real numbers and $\mathbb{C}$ denote the set of complex numbers. A variable without a subscript usually denotes a vector with appropriate components, e.g., $s := (s_i, i = 1, \ldots, n)$, $S := (S_{ij}, (i, j) \in E)$. For a complex scalar or vector a, a^* denotes its complex conjugate. For a vector $a = (a_1, \ldots, a_k)$, a_{-i} denotes $(a_1, \ldots, a_{i-1}, a_{i+1}, a_k)$. For a matrix A, A^t denotes its transpose and A^* its complex conjugate transpose. All angles should be interpreted as modulo (being projected into) $[-\pi, \pi]$.

2.3.1 Branch flow model

Let $G = (N, E)$ be a connected graph representing a power network, where each node in N represents a bus and each link in E represents a line (condition A1). We index the nodes by $i = 0, 1, \ldots, n$. The power network is called *radial* if its graph G is a tree. For a distribution network, which is typically radial, the root of the tree (node 0) represents the substation bus. For a (generally meshed) transmission network, node 0 represents the slack bus. We use node n to represent ground so that if bus i has a shunt impedance, then node i is connected to node n, i.e., $(i, n) \in E$.

We regard G as a directed graph and adopt the following orientation for convenience. Pick *any* spanning tree $T := (N, E_T)$ of G rooted at node 0, i.e., T is connected and $E_T \subseteq E$ has n links. All links in E_T point away from the root. For any link in $E \setminus E_T$ that is not in the spanning tree T, pick an arbitrary direction. Denote a link by (i, j) if it points from node i to node j. We will use e and (i, j) interchangeably to refer to a link in E. We write $i \sim j$ if i and j are connected, i.e.,

if either $(i, j) \in E$ or $(j, i) \in E$ (but not both). For each link $(i, j) \in E$, we will call node i the *parent* of node j and j the *child* of i. Let $\pi(j) \subseteq N$ be the set of all parents of node j and $\delta(i) \subseteq N$ the set of all children of node i. Henceforth we will assume without loss of generality that G and T are directed graphs as described above[1].

The basic variables of interest can be defined in terms of G. For each $(i, j) \in E$, let I_{ij} be the complex current from buses i to j and $S_{ij} = P_{ij} + \mathbf{i}Q_{ij}$ be the *sending-end* complex power from buses i to j. For each node $i \in N$, let V_i be the complex voltage on bus i. Let s_i be the net complex power, which is load minus generation on bus i. For power flow analysis, we assume s_i are given. For optimal power flow, VAR control, or demand response, s_i are control variables. We use s_i to denote both the complex number $p_i + \mathbf{i}q_i$ and the pair (p_i, q_i) depending on the context. Finally, let $z_{ij} = r_{ij} + \mathbf{i}x_{ij}$ be the complex impedance on the line connecting buses i and j. Recall that z_{in} represents the shunt impedance on bus i.

Then these quantities satisfy the Ohm's law:

$$V_i - V_j = z_{ij}I_{ij}, \qquad \forall(i, j) \in E \tag{2.1}$$

the definition of branch power flow:

$$S_{ij} = V_iI_{ij}^*, \qquad \forall(i, j) \in E \tag{2.2}$$

and power balance at each bus:

$$\sum_{i \in \pi(j)} \left(S_{ij} - z_{ij}|I_{ij}|^2\right) - \sum_{k \in \delta(j)} S_{jk} = s_j, \quad \forall j \tag{2.3}$$

We will refer to (2.1)–(2.3) as the *branch flow model/equations*. As customary, we assume that the complex voltage V_0 is given and the corresponding complex net load s_0 is a variable. Recall that the cardinality $|N| = n + 1$ and let $m := |E|$. The branch flow equations (2.1)–(2.3) specify $2m + n + 1$ nonlinear equations in $2m + n + 1$

---

[1]The orientation of G and T are different for different spanning trees T, but we often ignore this subtlety in this chapter.

complex variables $(S, I, V, s_0) := (S_{ij}, I_{ij}, (i, j) \in E, V_i, i = 1, \dots, n, s_0)$, when other bus power injections $s := (s_i, i = 1, \dots, n)$ are specified.

We will call a solution of (2.1)–(2.3) a *branch flow solution* with respect to a given s, and denote it by $x(s) := (S, I, V, s_0)$. Let $\mathbb{X}(s) \subseteq \mathbb{C}^{2m+n+1}$ be the set of all branch flow solutions with respect to a given s:

$$\mathbb{X}(s) := \{x := (S, I, V, s_0) \mid x \text{ solves (2.1)–(2.3) given } s\}$$

$$(2.4)$$

and let $\mathbb{X}$ be the set of all branch flow solutions:

$$\mathbb{X} := \bigcup_{s \in \mathbb{C}^n} \mathbb{X}(s) \tag{2.5}$$

For simplicity of exposition, we will often abuse notation and use $\mathbb{X}$ to denote either the set defined in (2.4) or that in (2.5), depending on the context. For instance, $\mathbb{X}$ is used to denote the set in (2.4) for a fixed s in Section 2.6 for power flow analysis, and to denote the set in (2.5) in Section 2.5 for optimal power flow where s itself is also an optimization variable. Similarly for other variables such as x for $x(s)$.

2.3.2 Optimal power flow

Consider the optimal power flow problem where, in addition to (S, I, V, s_0), each $s_i = (p_i, q_i)$, $i = 1, \dots, n$, is also an optimization variable. Let $p_i := p_i^c - p_i^g$ and $q_i := q_i^c - q_i^g$ where p_i^c and q_i^c are the real and reactive power consumption at node i, and p_i^g and q_i^g are the real and reactive power generation at node i. The active and reactive power generation and consumption at each node can be either positive or zero depending on whether the node represents a generator, a load, a shunt capacitor, or a storage device, etc. For instance, [43, 44] formulate a Volt/VAR control problem for a distribution circuit where q_i^g represent the placement and sizing of shunt capacitors. In addition to (2.1)–(2.3), we impose the following constraints on power generation:

for $i = 0, 1, \ldots, n$,

$$\underline{p}_i^g \leq p_i^g \leq \overline{p}_i^g, \quad \underline{q}_i^g \leq q_i^g \leq \overline{q}_i^g \tag{2.6}$$

In particular, any of p_i^g, q_i^g can be a fixed constant by specifying that $\underline{p}_i^g = \overline{p}_i^g$ and/or $\underline{q}_i^g = \overline{q}_i^g$. For instance, in the inverter-based VAR control problem of [4], p_i^g are the fixed (solar) power outputs and the reactive power q_i^g are the control variables. For power consumption, we require, for $i = 0, 1, \ldots, n$,

$$\underline{p}_i^c \leq p_i^c, \quad \underline{q}_i^c \leq q_i^c \tag{2.7}$$

i.e., there cannot be upper bounds on p_i^c, q_i^c for our proof below to work[2]. The voltage magnitudes must be maintained in a tight range: for $i = 1, \ldots, n$,

$$\underline{v}_i \quad \leq \quad |V_i|^2 \quad \leq \quad \overline{v}_i \tag{2.8}$$

Finally, we impose line flow limits: for all $(i, j) \in E$,

$$|S_{ij}| \quad \leq \quad \overline{S}_{ij} \tag{2.9}$$

We allow any objective function that is convex and does not depend on the angles $\angle V_i, \angle I_{ij}$ of voltages and currents nor on consumptions p_i^c, q_i^c. For instance, suppose we aim to minimize real power losses $r_{ij}|I_{ij}|^2$, minimize real power generation costs $c_i p_i^g$, and maximize energy savings through conservation voltage reduction (CVR). Then the objective function takes the form (see [4])

$$\sum_{(i,j)\in E} r_{ij}|I_{ij}|^2 + \sum_{i\in N} c_i p_i^g + \sum_{i\in N} \alpha_i |V_i|^2 \tag{2.10}$$

for some given constants $c_i, \alpha_i \geq 0$. We also allow the cost to be quadratic in real power as is commonly assumed.

---

[2]This is equivalent to the "over-satisfaction of load" condition in [12, 36]. As we show in the simulations below, this condition is sufficient but not necessary for the conic relaxation OPF-cr to be exact with respect to OPF-ar. See [50] for exact conic relaxation of OPF-cr for radial networks where the "over-satisfaction" assumption is replaced with an alternative set of assumptions.

To simplify notation, let $\ell_{ij} := |I_{ij}|^2$ and $v_i := |V_i|^2$. Let $s^g := (s_i^g, i = 1, \ldots, n) = (p_i^g, q_i^g, i = 1, \ldots, n)$ be the power generations, and $s^c := (s_i^c, i = 1, \ldots, n) = (p_i^c, q_i^c, i = 1, \ldots, n)$ the power consumptions. Let s denote either $s^c - s^g$ or (s^c, s^g) depending on the context. Given a branch flow solution $x := x(s) := (S, I, V, s_0)$ with respect to a given s, let $\hat{y} := \hat{y}(s) := (S, \ell, v, s_0)$ denote the projection of x that have phase angles $\angle V_i, \angle I_{ij}$ eliminated. This defines a projection function $\hat{h}$ such that $\hat{y} = \hat{h}(x)$, to which we will return in Section 2.4. Then our objective function is $f\left(\hat{h}(x), s^g\right)$. We assume $f(\hat{y}, s^g)$ is convex (condition A2); in addition, we assume f is strictly increasing in $\ell_{ij}, (i, j) \in E$ (condition A3). Finally, let

$$\mathbb{S} \;:=\; \{\, (v, s_0, s) \,|\, (v, s_0, s) \text{ satisfies } (2.6) - (2.9) \,\}$$

All quantities are optimization variables except V_0, which is given.

The optimal power flow problem is

OPF:

$$\min_{x,s} \quad f\left(\hat{h}(x), s^g\right) \tag{2.11}$$

$$\text{subject to} \quad x \in \mathbb{X}, \quad (v, s_0, s) \in \mathbb{S} \tag{2.12}$$

where $\mathbb{X}$ is defined in (2.5). To avoid triviality, we assume the problem is feasible (condition A4).

The feasible set is specified by the nonlinear branch flow equations and hence OPF (2.11)–(2.12) is in general nonconvex and hard to solve. The goal of this chapter is to propose an efficient way to solve OPF by exploiting the structure of the branch flow model.

2.3.3   Notations and assumptions

The main variables and assumptions are summarized in Table 2.1 and below for ease of reference:

Table 2.1: Notations.

G, T	(directed) network graph G and a spanning tree T of G
B, B_T	reduced (and transposed) incidence matrix of G and the submatrix corresponding to T
V_i, v_i	complex voltage on bus i with $v_i := |V_i|^2$
$s_i = p_i + \mathbf{i}q_i$	net complex load power on bus i
$p_i = p_i^c - p_i^g$	net real power equals load minus generation;
$q_i = q_i^c - q_i^g$	net reactive power equals load minus generation
I_{ij}, ℓ_{ij}	complex current from buses i to j with $\ell_{ij} := |I_{ij}|^2$
$S_{ij} = P_{ij} + \mathbf{i}Q_{ij}$	complex power from buses i to j (sending-end)
$\mathbb{X}$	set of all branch flow solutions that satisfy (2.1)–(2.3) either for some s, or for a given s (sometimes denoted more accurately by $\mathbb{X}(s)$);
$\hat{\mathbb{Y}}$	set of all relaxed branch flow solutions that satisfy (2.13)–(2.16) either for a given s or for some s;
$\overline{\mathbb{Y}}$	convex hull of $\hat{\mathbb{Y}}$, i.e., solutions of (2.13)–(2.15) and (2.24);
$\overline{X}, \overline{X}_T$	set of branch flow solutions that satisfy (2.3), (2.43), (2.2), for some phase shifter angles ϕ and for some $\phi \in T^\perp$;
$x = (S, I, V, s_0) \in \mathbb{X}$	vector x of power flow variables
$\hat{y} = (S, \ell, v, s_0) \in \hat{\mathbb{Y}}$	and its projection $\hat{y}$;
$\hat{y} = \hat{h}(x); \quad x = h_\theta(\hat{y})$	projection mapping $\hat{y}$ and an inverse h_θ
$z_{ij} = r_{ij} + \mathbf{i}x_{ij}$	impedance on line connecting buses i and j
f	objective function of OPF, of the form $f\left(\hat{h}(x), s^g\right)$

A1 The network graph G is connected.

A2 The cost function $f(\hat{y}, s^g)$ for optimal power flow is convex.

A3 The cost function $f(\hat{y}, s^g)$ is strictly increasing in $\ell_{ij}, (i, j) \in E$.

A4 The optimal power flow problem OPF (2.11)–(2.12) is feasible.

These assumptions are standard and realistic. For instance, the objective function in (2.10) satisfies conditions A2–A3. A3 holds if the cost function is increasing in power loss in the lines.

2.4 Relaxations and solution strategy

We now describe our solution approach.

2.4.1 Relaxed branch flow model

Substituting (2.2) into (2.1) yields $V_j = V_i - z_{ij} S_{ij}^* / V_i^*$. Taking the magnitude squared, we have $v_j = v_i + |z_{ij}|^2 \ell_{ij} - (z_{ij} S_{ij}^* + z_{ij}^* S_{ij})$. Using (2.3) and (2.2) and in terms of real variables, we therefore have

$$p_j = \sum_{i \in \pi(j)} (P_{ij} - r_{ij}\ell_{ij}) - \sum_{k \in \delta(j)} P_{jk}, \quad \forall j \tag{2.13}$$

$$q_j = \sum_{i \in \pi(j)} (Q_{ij} - x_{ij}\ell_{ij}) - \sum_{k \in \delta(j)} Q_{jk}, \quad \forall j \tag{2.14}$$

$$v_j = v_i - 2(r_{ij}P_{ij} + x_{ij}Q_{ij}) + (r_{ij}^2 + x_{ij}^2)\ell_{ij}$$
$$\forall (i,j) \in E \tag{2.15}$$

$$\ell_{ij} = \frac{P_{ij}^2 + Q_{ij}^2}{v_i}, \qquad \forall (i,j) \in E \tag{2.16}$$

Branch flow variables are shown in figure 2.3. We will refer to (2.13)–(2.16) as the *relaxed (branch flow) model/equations* and a solution a *relaxed (branch flow) solution*. These equations were first proposed in [43, 44] to model radial distribution circuits. They define a system of equations in the variables $(P, Q, \ell, v, p_0, q_0) :=$ $(P_{ij}, Q_{ij}, \ell_{ij}, (i,j) \in E, \ v_i, i = 1, \ldots, n, \ p_0, q_0)$. We often use (S, ℓ, v, s_0) as a short-
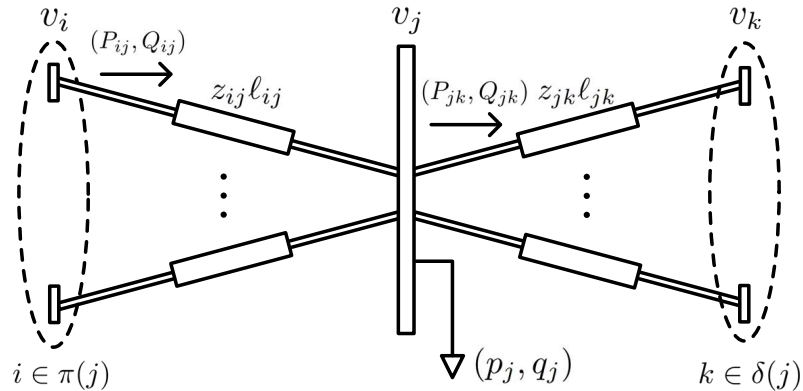
Figure 2.3: Illustration of the branch flow variables

hand for $(P, Q, \ell, v, p_0, q_0)$. Since we assume the original branch flow model has a solution, the relaxed model also has a solution.

In contrast to the original branch flow equations (2.1)–(2.3), the relaxed equations (2.13)–(2.16) specifies $2(m + n + 1)$ equations in $3m + n + 2$ real variables $(P, Q, \ell, v, p_0, q_0)$, for a given s. For a radial network, i.e., G is a tree, $m = |E| = |N| - 1 = n$. Hence the relaxed system (2.13)–(2.16) specifies $4n + 2$ equations in $4n + 2$ real variables. It is shown in [51] that there are generally multiple solutions, but for practical networks where $V_0 \simeq 1$ and r_{ij}, x_{ij} are small p.u., the solution of (2.13)–(2.16) is unique. Exploiting structural properties of the Jacobian matrix, efficient algorithms have also been proposed in [52] to solve the relaxed branch flow equations.

For a connected mesh network, $m = |E| > |N| - 1 = n$, in which case there are more variables than equations for the relaxed model (2.13)–(2.16), and therefore the solution is generally nonunique. Moreover, some of these solutions may be spurious, i.e., they do not correspond to a solution of the original branch flow equations (2.1)–(2.3).

Indeed, one may consider (S, ℓ, v, s_0) as a projection of (S, I, V, s_0) where each variable I_{ij} or V_i is relaxed from a point in the complex plane to a circle with a radius equal to the distance of the point from the origin. It is therefore not surprising that a relaxed solution of (2.13)–(2.16) may not correspond to any solution of (2.1)–(2.3). The key is whether, given a relaxed solution, we can recover the angles $\angle V_i, \angle I_{ij}$ correctly from it. It is then remarkable that, when G is a tree, indeed the solutions of (2.13)–(2.16) coincide with those of (2.1)–(2.3). Moreover for a general network, (2.13)–(2.16) together with the angle recovery condition in Theorem 2.2 below are indeed equivalent to (2.1)–(2.3), as explained in Section 2.6.

To understand the relationship between the branch flow model and the relaxed model and formulate our relaxations precisely, we need some notations. Fix an s. Given a vector $(S, I, V, s_0) \in \mathbb{C}^{2m+n+1}$, define its projection $\hat{h} : \mathbb{C}^{2m+n+1} \to \mathbb{R}^{3m+n+2}$

by $\hat{h}(S, I, V, s_0) = (P, Q, \ell, v, p_0, q_0)$ where

$$P_{ij} = \text{Re } S_{ij}, \qquad Q_{ij} = \text{Im } S_{ij}, \quad \ell_{ij} = |I_{ij}|^2 \qquad (2.17)$$

$$p_i = \text{Re } s_i, \qquad q_i = \text{Im } s_i, \qquad v_i = |V_i|^2 \qquad (2.18)$$

Let $\mathbb{Y} \subseteq \mathbb{C}^{2m+n+1}$ denote the set of all $y := (S, I, V, s_0)$ whose projections are the
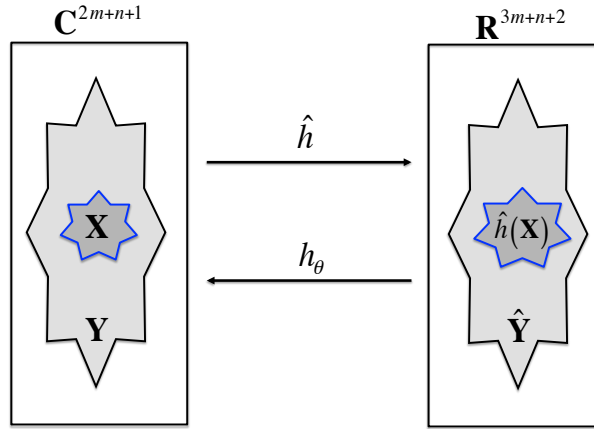
Figure 2.4: $\mathbb{X}$ is the set of branch flow solutions and $\hat{\mathbb{Y}} = \hat{h}(\mathbb{Y})$ is the set of relaxed solutions. The inverse projection h_θ is defined in Section V.

relaxed solutions[3]:

$$\mathbb{Y} := \left\{ y := (S, I, V, s_0) \,|\, \hat{h}(y) \text{ solves } (2.13)–(2.16) \right\} \qquad (2.19)$$

Define the projection $\hat{\mathbb{Y}} := \hat{h}(\mathbb{Y})$ of $\mathbb{Y}$ onto the space $\mathbb{R}^{2m+n+1}$ as

$$\hat{\mathbb{Y}} \;\; := \;\; \{ \; \hat{y} := (S, \ell, v, s_0) \,|\, \hat{y} \text{ solves } (2.13)–(2.16) \; \}$$

Clearly

$$\mathbb{X} \subseteq \mathbb{Y} \;\; \text{and} \;\; \hat{h}(\mathbb{X}) \subseteq \hat{h}(\mathbb{Y}) = \hat{\mathbb{Y}}$$

---

[3]As mentioned earlier, the set defined in (2.19) is strictly speaking $\mathbb{Y}(s)$ with respect to a fixed s. To simplify exposition, we abuse notation and use $\mathbb{Y}$ to denote both $\mathbb{Y}(s)$ and $\bigcup_{s \in \mathbb{C}^n} \mathbb{Y}(s)$, depending on the context. The same applies to $\hat{\mathbb{Y}}$ and $\overline{\mathbb{Y}}$ etc.

Their relationship is illustrated in Figure 2.4.

2.4.2 Two relaxations

Consider the OPF with angles relaxed:

OPF-ar:

$$\min_{x,s} \quad f\left(\hat{h}(x), s^g\right) \tag{2.20}$$

$$\text{subject to} \quad x \in \mathbb{Y}, \quad (v, s_0, s) \in \mathbb{S} \tag{2.21}$$

Clearly, this problem provides a lower bound to the original OPF problem since $\mathbb{Y} \supseteq \mathbb{X}$. Since neither $\hat{h}(x)$ nor the constraints in $\mathbb{Y}$ involves angles $\angle V_i, \angle I_{ij}$, this problem is equivalent to the following

OPF-ar:

$$\min_{\hat{y},s} \quad f\left(\hat{y}, s^g\right) \tag{2.22}$$

$$\text{subject to} \quad \hat{y} \in \hat{\mathbb{Y}}, \quad (v, s_0, s) \in \mathbb{S} \tag{2.23}$$

The feasible set of OPF-ar is specified by a system of linear-quadratic equations. Hence OPF-ar is in general still nonconvex and hard to solve directly. The key to our solution is the observation that the only source of nonconvexity is the quadratic equalities in (2.16). Relax them to inequalities:

$$\ell_{ij} \quad \geq \quad \frac{P_{ij}^2 + Q_{ij}^2}{v_i}, \qquad (i,j) \in E \tag{2.24}$$

and define the convex hull $\overline{\mathbb{Y}} \subseteq \mathbb{R}^{2m+n+1}$ of $\hat{\mathbb{Y}}$ as

$$\overline{\mathbb{Y}} := \{\hat{y} := (S, \ell, v, s_0) \,|\, \hat{y} \text{ solves } (2.13)–(2.15) \text{ and } (2.24)\}$$

Consider the following relaxation of OPF-ar:

OPF-cr:

$$\min_{\hat{y},s} \quad f\left(\hat{y}, s^g\right) \tag{2.25}$$

$$\text{subject to} \quad \hat{y} \in \overline{\mathbb{Y}}, \quad (v, s_0, s) \in \mathbb{S} \tag{2.26}$$

Clearly OPF-cr provides a lower bound to OPF-ar since $\overline{\mathbb{Y}} \supseteq \hat{\mathbb{Y}}$.

2.4.3   Solution strategy

In the rest of this chapter, we will prove the following results:

1. OFP-cr is convex. Moreover the conic relaxation is exact so that *any* optimal solution $(\hat{y}_{cr}, s_{cr})$ of OPF-cr is also optimal for OPF-ar (Section 2.5, Theorem 2.1).

2. Given a solution $(\hat{y}_{ar}, s_{ar})$ of OPF-ar, if the network is radial, then we can always recover the phase angles $\angle V_i, \angle I_{ij}$ uniquely to obtain an optimal solution (x_*, s_*) of the original OPF (2.11)–(2.12) through an inverse projection (Section 2.6, Theorems 2.2 and 2.3).

3. For a mesh network, an inverse projection may not exist to map the given $(\hat{y}_{ar}, s_{ar})$ to a feasible solution of OPF. In that case, however, the network can be convexified so that $(\hat{y}_{ar}, s_{ar})$ can indeed be mapped to an optimal solution of OPF for the convexified network. Moreover, convexification requires phase shifters only on lines outside an arbitrary spanning tree of the network graph (Section 2.7, Theorem 2.4 and Corollary 2).

These results motivate the algorithm in Figure 2.1.

2.5   Exact conic relaxation

Our first key result says that OPF-cr is exact.

Theorem 2.1. *OPF-cr is convex. Moreover, it is exact, i.e., any optimal solution of OPF-cr is also optimal for OPF-ar.*

Proof. The feasible set is convex since the nonlinear inequalities in $\overline{\mathbb{Y}}$ can be written as the following second order cone constraint:

$$\left\| \begin{array}{c} 2P_{ij} \\ 2Q_{ij} \\ \ell_{ij} - v_i \end{array} \right\|_2 \leq \ell_{ij} + v_i$$

Since the objective function is convex, OPF-cr is a conic optimization[4]. To prove that the relaxation is exact, it suffices to show that any optimal solution of OPF-cr attains equality in (2.24).

Assume for the sake of contradiction that $(\hat{y}_*, s_*) := (S_*, \ell_*, v_*, s^g_{*0}, s^c_{*0}, s^g_*, s^c_*)$ is optimal for OPF-cr, but a link $(i,j) \in E$ has strict inequality, i.e., $[v_*]_i [\ell_*]_{ij} > [P_*]_{ij}^2 + [Q_*]_{ij}^2$. For some $\varepsilon > 0$ to be determined below, consider another point $(\tilde{y}, \tilde{s}) = (\tilde{S}, \tilde{\ell}, \tilde{v}, \tilde{s}^g_0, \tilde{s}^c_0, \tilde{s}^g, \tilde{s}^c)$ defined by:

$$\tilde{v} = v_*, \qquad \tilde{s}^g = s^g_*$$

$$\tilde{\ell}_{ij} = [\ell_*]_{ij} - \varepsilon, \qquad \tilde{\ell}_{-ij} = [\ell_*]_{-ij}$$

$$\tilde{S}_{ij} = [S_*]_{ij} - z_{ij}\varepsilon/2, \qquad \tilde{S}_{-ij} = [S_*]_{-ij}$$

$$\tilde{s}^c_i = [s^c_*]_i + z_{ij}\varepsilon/2, \qquad \tilde{s}^c_j = [s^c_*]_j + z_{ij}\varepsilon/2$$

$$\tilde{s}^c_{-(i,j)} = [s^c_*]_{-(i,j)}$$

where a negative index means excluding the indexed element from a vector. Since $\tilde{\ell}_{ij} = [\ell_*]_{ij} - \varepsilon$, $(\tilde{y}, \tilde{s})$ has a strictly smaller objective value than $(\hat{y}_*, s_*)$ because of assumption A3. If $(\tilde{y}, \tilde{s})$ is a feasible point, then it contradicts the optimality of $(\hat{y}_*, s_*)$.

---

[4]If the objective function is linear, such as (2.10), then OPF-cr is an SOCP. This is the case proved in [4] for radial networks. This result is extended here to mesh networks with line limits and convex objective functions.

It suffices then to check that there exists an $\varepsilon > 0$ such that $(\tilde{y}, \tilde{s})$ satisfies (2.6)–(2.9), (2.13)–(2.15) and (2.24), and hence is indeed a feasible point. Since $(\hat{y}_*, s_*)$ is feasible, (2.6)–(2.9) hold for $(\tilde{y}, \tilde{s})$ too. Similarly, $(\tilde{y}, \tilde{s})$ satisfies (2.13)–(2.14) at all nodes $k \neq i, j$ and (2.15), (2.24) across all links $(k, l) \neq (i, j)$. We now show that $(\tilde{y}, \tilde{s})$ satisfies (2.13)–(2.14) also at nodes i, j, and (2.15), (2.24) across link (i, j):

- Proving (2.13)–(2.14) is equivalent to proving (2.3). At node i, we have

$$
\begin{aligned}
\tilde{s}_i \;=\; \tilde{s}_i^c - \tilde{s}_i^g \;&=\; [s_*^c]_i + z_{ij}\varepsilon/2 - [s_*^g]_i \\
&=\; \sum_{k \in \pi(i)} ([S_*]_{ki} - z_{ki}[\ell_*]_{ki}) - \sum_{j' \in \delta(i), j' \neq j} [S_*]_{ij'} \\
&\qquad - [S_*]_{ij} + z_{ij}\varepsilon/2 \\
&=\; \sum_{k \in \pi(i)} \left(\tilde{S}_{ki} - z_{ki}\tilde{\ell}_{ki} \right) - \sum_{j' \in \delta(i), j' \neq j} \tilde{S}_{ij'} \\
&\qquad - \left(\tilde{S}_{ij} + z_{ij}\varepsilon/2 \right) + z_{ij}\varepsilon/2 \\
&=\; \sum_{k \in \pi(i)} \left(\tilde{S}_{ki} - z_{ki}\tilde{\ell}_{ki} \right) - \sum_{j' \in \delta(i)} \tilde{S}_{ij'}
\end{aligned}
$$

At node j, we have

$$
\begin{aligned}
\tilde{s}_j \;=\; \tilde{s}_j^c - \tilde{s}_j^g \;&=\; [s_*^c]_j + z_{ij}\varepsilon/2 - [s_*^g]_j \\
&=\; \sum_{i' \in \pi(j), i' \neq i} ([S_*]_{i'j} - z_{i'j}[\ell_*]_{i'j}) + [S_*]_{ij} \\
&\qquad - z_{ij}[\ell_*]_{ij} - \sum_{k \in \delta(j)} [S_*]_{jk} + z_{ij}\varepsilon/2 \\
&=\; \sum_{i' \in \pi(j), i' \neq i} \left(\tilde{S}_{i'j} - z_{i'j}\tilde{\ell}_{i'j} \right) + \tilde{S}_{ij} + z_{ij}\varepsilon/2 \\
&\qquad - z_{ij}(\tilde{\ell}_{ij} + \varepsilon) - \sum_{k \in \delta(j)} \tilde{S}_{jk} + z_{ij}\varepsilon/2 \\
&=\; \sum_{i' \in \pi(j)} \left(\tilde{S}_{i'j} - z_{i'j}\tilde{\ell}_{i'j} \right) - \sum_{k \in \delta(j)} \tilde{S}_{jk}
\end{aligned}
$$

Hence (2.13)–(2.14) hold at nodes i, j.

- For (2.9) across link (i, j), we have $|\tilde{S}_{ij}|^2 = |S_{ij}|^2 - \frac{\varepsilon}{4}\left(2(z_{ij}^* S_{ij} + z_{ij} S_{ij}^*) - \varepsilon|z_{ij}|^2 \right) \leq$

$|S_{ij}|^2 \leq \overline{S}_{ij}^2$ for small enough $\varepsilon > 0$.

- For (2.15) across link (i, j), we have

$$
\begin{aligned}
\tilde{v}_j &= [v_*]_i - 2(r_{ij}[P_*]_{ij} + x_{ij}[Q_*]_{ij}) \\
&\quad + (r_{ij}^2 + x_{ij}^2)[\ell_*]_{ij} \\
&= \tilde{v}_i - 2(r_{ij}\tilde{P}_{ij} + x_{ij}\tilde{Q}_{ij}) + (r_{ij}^2 + x_{ij}^2)\tilde{\ell}_{ij}
\end{aligned}
$$

- For (2.24) across link (i, j), we have

$$
\begin{aligned}
&\tilde{v}_i \tilde{\ell}_{ij} - \tilde{P}_{ij}^2 - \tilde{Q}_{ij}^2 \\
&= [v_*]_i \left([\ell_*]_{ij} - \varepsilon\right) - \left([P_*]_{ij} - r_{ij}\varepsilon/2\right)^2 \\
&\qquad - \left([Q_*]_{ij} - x_{ij}\varepsilon/2\right)^2 \\
&= \left([v_*]_i[\ell_*]_{ij} - [P_*]_{ij}^2 - [Q_*]_{ij}^2\right) \\
&\qquad - \varepsilon \left([v_*]_i - r_{ij}[P_*]_{ij} - x_{ij}[Q_*]_{ij}\right. \\
&\qquad + \varepsilon(r_{ij}^2 + x_{ij}^2)/4\Big)
\end{aligned}
$$

Since $[v_*]_i[\ell_*]_{ij} - [P_*]_{ij}^2 - [Q_*]_{ij}^2 > 0$, we can choose an $\varepsilon > 0$ sufficiently small such that $\tilde{\ell}_{ij} \geq (\tilde{P}_{ij}^2 + \tilde{Q}_{ij}^2)/\tilde{v}_i$.

This completes the proof. $\qquad\qquad\qquad\qquad\qquad\qquad\qquad\qquad\qquad\qquad\square$

Remark 2.1. *Assumption A3 is used in the proof here to contradict the optimality of $(\hat{y}_*, s_*^g)$. Instead of A3, if $f(\hat{y}, s^g)$ is nondecreasing in ℓ, the same argument shows that, given an optimal $(\hat{y}_*, s_*^g)$ with a strict inequality $[v_*]_i[\ell_*]_{ij} > [P_*]_{ij}^2 + [Q_*]_{ij}^2$, one can choose $\varepsilon > 0$ to obtain another optimal point $(\tilde{y}, \tilde{s}^g)$ that attains equality and has a cost $f(\tilde{y}, \tilde{s}^g) \leq f(\hat{y}_*, s_*^g)$. This implies that, in the absence of A3, there is always an optimal solution of OPF-cr that is also optimal for OPF-ar, even though it is possible that the convex relaxation OPF-cr may also have other optimal points with strict inequality that are infeasible for OPF-ar. This is the case for semidefinite relaxation in the bus injection model, e.g., in [34, 36, 38], i.e., the relaxation generally*

may also have optimal solutions that are infeasible for the original OPF problem.

2.6   Angle relaxation

Theorem 2.1 justifies solving the convex problem OPF-cr for an optimal solution of OPF-ar. Given a solution $(\hat{y}, s)$ of OPF-ar, when and how can we recover a solution (x, s) of the original OPF (2.11)–(2.12)? The issue boils down to whether we can recover a solution x to the branch flow equations (2.1)–(2.3) from $\hat{y}$, given any nodal power injections s.

Hence, for the rest of this section, we fix an s. We abuse notation in this section and write $x, \hat{y}, \theta, \mathbb{X}, \mathbb{Y}, \hat{\mathbb{Y}}$ instead of $x(s), \hat{y}(s), \theta(s), \mathbb{X}(s), \mathbb{Y}(s), \hat{\mathbb{Y}}(s)$, respectively.

2.6.1   Angle recovery condition

Fix a relaxed solution $\hat{y} := (S, \ell, v, s_0) \in \hat{\mathbb{Y}}$. Define the $(n+1) \times m$ incidence matrix C of G by

$$C_{ie} = \begin{cases} 1 & \text{if link } e \text{ leaves node } i \\ -1 & \text{if link } e \text{ enters node } i \\ 0 & \text{otherwise} \end{cases} \tag{2.27}$$

The first row of C corresponds to node 0, the reference bus with a given $V_0 = |V_0| e^{\mathbf{i}\theta_0}$. In this chapter we will only work with the $m \times n$ *reduced* incidence matrix B obtained from C by removing the first row (corresponding to V_0) and taking the transpose, i.e., for $e \in E, i = 1, \ldots, n$,

$$B_{ei} = \begin{cases} 1 & \text{if link } e \text{ leaves node } i \\ -1 & \text{if link } e \text{ enters node } i \\ 0 & \text{otherwise} \end{cases},$$

Since G is connected, $m \geq n$ and $\text{rank}(B) = n$ [53]. Fix any spanning tree $T = (N, E_T)$ of G. We can assume without loss of generality (possibly after re-labeling some of the links) that E_T consists of links $e = 1, \ldots, n$. Then B can be partitioned into

$$B = \begin{bmatrix} B_T \\ B_\perp \end{bmatrix} \tag{2.28}$$

where the $n \times n$ submatrix B_T corresponds to links in T and the $(m-n) \times n$ submatrix $B_\perp$ corresponds to links in $T^\perp := G \setminus T$.

Let $\beta := \beta(\hat{y}) \in [-\pi, \pi]^m$ be defined in terms of the given $\hat{y}$ by

$$\beta_{ij} := \angle \left(v_i - z_{ij}^* S_{ij} \right), \qquad (i, j) \in E \tag{2.29}$$

Write β as

$$\beta = \begin{bmatrix} \beta_T \\ \beta_\perp \end{bmatrix} \tag{2.30}$$

where β_T is $n \times 1$ and $\beta_\perp$ is $(m-n) \times 1$.

Recall the projection mapping $\hat{h} : \mathbb{C}^{2m+n+1} \to \mathbb{R}^{3m+n+2}$ defined in (2.17)–(2.18). For each $\theta := (\theta_i, i = 1, \ldots, n) \in [-\pi, \pi]^n$, define the inverse projection $h_\theta : \mathbb{R}^{3m+n+2} \to \mathbb{C}^{2m+n+1}$ by $h_\theta(P, Q, \ell, v, p_0, q_0) = (S, I, V, s_0)$ where

$$S_{ij} := P_{ij} + \mathbf{i}Q_{ij} \tag{2.31}$$

$$I_{ij} := \sqrt{\ell_{ij}}\, e^{\mathbf{i}(\theta_i - \angle S_{ij})} \tag{2.32}$$

$$V_i := \sqrt{v_i}\, e^{\mathbf{i}\theta_i} \tag{2.33}$$

$$s_0 := p_0 + \mathbf{i}q_0 \tag{2.34}$$

These mappings are illustrated in Figure 2.4.

By definition of $\hat{h}(\mathbb{X})$ and $\hat{\mathbb{Y}}$, a branch flow solution in $\mathbb{X}$ can be recovered if a given relaxed solution $\hat{y}$ is in $\hat{h}(\mathbb{X})$ and cannot be recovered if $\hat{y}$ is in $\hat{\mathbb{Y}} \setminus \hat{h}(\mathbb{X})$. In

other words, $\hat{h}(\mathbb{X})$ consists of exactly those points $\hat{y} \in \hat{\mathbb{Y}}$ for which there exist θ such that their inverse projections $h_\theta(\hat{h})$ are in $\mathbb{X}$. Our next key result characterizes the exact condition under which such an inverse projection exists, and provides an explicit expression for recovering the phase angles $\angle V_i, \angle I_{ij}$ from the given $\hat{y}$.

A *cycle c* in G is a set $\{i_1, \ldots, i_k\}$ of nodes in V such that $i_j \sim i_{j+1}$ and $i_k \sim i_1$, i.e., nodes i_j, i_{j+1} is in c if either $(i_j, i_{j+1}) \in E$ or $(i_{j+1}, i_j) \in E$ (but not both). We write $e \in c$ when $e = (i_j \sim i_{j+1})$ or $e = (i_k \sim i_1)$. Let $\tilde{\beta}$ be the extension of β from directed links to undirected links: if $(i, j) \in E$ then $\tilde{\beta}_{ij} := \beta_{ij}$ and $\tilde{\beta}_{ji} := -\beta_{ij}$.

Theorem 2.2. *Let T be any spanning tree of G. Consider a relaxed solution $\hat{y} \in \hat{\mathbb{Y}}$ and the corresponding β defined by (2.29)–(2.30) in terms of $\hat{y}$.*

1. *There exists a unique $\theta_* \in [-\pi, \pi]^n$ such that $h_{\theta_*}(\hat{y})$ is a branch flow solution in $\mathbb{X}$ if and only if*

$$B_\perp B_T^{-1} \beta_T = \beta_\perp \qquad (2.35)$$

2. *The angle recovery condition (2.35) holds if and only if for every cycle c in G*

$$\sum_{e \in c} \tilde{\beta}_e = 0 \qquad (2.36)$$

3. *If (2.35) holds then $\theta_* = B_T^{-1} \beta_T$.*[5]

Remark 2.2. *Given a relaxed solution $\hat{y} := (S, \ell, v, s_0)$, Theorem 2.2 prescribes a way to check if a branch flow solution can be recovered from it, and if so, the required computation. The angle recovery condition (2.35) is a condition on $\hat{y}$ and depends only on the network topology through the reduced incidence matrix B. The choice of spanning tree T corresponds to choosing n linearly independent rows of B to form B_T and does not affect the conclusion of the theorem.*

Remark 2.3. *When it holds, the angle recovery condition (2.36) has a familiar interpretation (due to Lemma 1 below): the voltage angle differences (implied by $\hat{y}$) sum*

---

[5]Recall that all angles should be interpreted as modulo (being projected into) $[-\pi, \pi]^n$.

to zero around any cycle.

Remark 2.4. *A direct consequence of Theorem 2.2 is that the relaxed branch flow model (2.13)–(2.16) together with the angle recovery condition (2.35) is equivalent to the original branch flow model (2.1)–(2.3). That is, x satisfies (2.1)–(2.3) if and only if $\hat{y} = \hat{h}(x)$ satisfies (2.13)–(2.16) and (2.35).*

The proof of Theorem 2.2 relies on the following important lemma that describes when any arbitrary inverse projection $h_\theta(\hat{y})$ is a branch flow solution in $\mathbb{X}$.

Lemma 1. *Given $\hat{y} := (S, \ell, v, s_0)$ in $\hat{\mathbb{Y}}$ and $\theta \in [-\pi, \pi]^n$, the vector $h_\theta(\hat{y})$ defined by (2.31)–(2.34) is in $\mathbb{X}$ if and only if θ satisfies*

$$\theta_i - \theta_j \;=\; \angle\left(v_i - z_{ij}^* S_{ij}\right), \qquad (i,j) \in E \tag{2.37}$$

Moreover such a θ, if it exists, is unique.

Proof. It is necessary since, from (2.1) and (2.2), we have $V_i V_j^* = |V_i|^2 - z_{ij}^* S_{ij}$, yielding $\theta_i - \theta_j = \angle(v_i - z_{ij}^* S_{ij})$.

For sufficiency, we need to show that (2.13)–(2.16) together with (2.31)–(2.34) and (2.37) implies (2.1)–(2.3). Now (2.13) and (2.14) are equivalent to (2.3). Moreover (2.16) and (2.31)–(2.33) imply (2.2). To prove (2.1), we can substitute (2.2) into (2.37) to get

$$\theta_i - \theta_j \;=\; \angle\left(v_i - z_{ij}^* V_i I_{ij}^*\right) \;=\; \angle\, V_i \left(V_i - z_{ij} I_{ij}\right)^*$$

Hence

$$\angle V_j \;=\; \theta_j \;=\; \angle\left(V_i - z_{ij} I_{ij}\right) \tag{2.38}$$

From (2.15) and (2.2), we have

$$
\begin{aligned}
|V_j|^2 &= |V_i|^2 + |z_{ij}|^2|I_{ij}|^2 - (z_{ij}S_{ij}^* + z_{ij}^*S_{ij}) \\
&= |V_i|^2 + |z_{ij}|^2|I_{ij}|^2 - (z_{ij}V_i^*I_{ij} + z_{ij}^*V_iI_{ij}^*) \\
&= |V_i - z_{ij}I_{ij}|^2
\end{aligned}
$$

This together with (2.38) implies $V_j = V_i - z_{ij}I_{ij}$ which is (2.1).

The condition (2.37) implies that a branch flow solution can be recovered from a relaxed solution if and only if there exist θ that solves

$$
B\theta = \beta \tag{2.39}
$$

Since G is connected, $m \geq n$ and $\mathrm{rank}(A) = n$ and hence (2.39) has at most one solution. $\qquad\square$

Proof of Theorem 2.2. Since $m \geq n$ and $\mathrm{rank}(B) = n$, we can always find n linearly independent rows of B to form a basis. The choice of this basis corresponds to choosing a spanning tree of G, which always exists since G is connected [54, Chapter 5]. Assume without loss of generality that the first n rows is such a basis so that B and β are partitioned as in (2.28) and (2.30), respectively. Then Lemma 1 implies that there exists a unique $\theta_* \in [-\pi, \pi]^n$ such that $h_{\theta_*}(\hat{y})$ is a branch flow solution in $\mathbb{X}$ if and only if θ_* solves (2.39), i.e.,

$$
\begin{bmatrix} B_T \\ B_\perp \end{bmatrix} \theta = \begin{bmatrix} \beta_T \\ \beta_\perp \end{bmatrix} \tag{2.40}
$$

Since T is a spanning tree, the $n \times n$ submatrix B_T has a full rank and hence is invertible. Therefore, $\theta_* = B_T^{-1}\beta_T$. Moreover, (2.40) has a unique solution if and only if $B_\perp \theta_* = B_\perp B_T^{-1}\beta_T = \beta_\perp$.

We are left to prove the equivalence of (2.35) and (2.36). Recall that the spanning tree T defines the orientation of all links in T to be directed away from the root node

0. Let $T(i \rightsquigarrow j)$ denote the unique path from node i to node j in T; in particular, $T(0 \rightsquigarrow j)$ consists of links all with the same orientation as the path and $T(j \rightsquigarrow 0)$ of links all with the opposite orientation. Then it can be verified directly that B_T^{-1} is defined by [54, Chapter 5]

$$\left[B_T^{-1}\right]_{ei} := \begin{cases} -1 & \text{if link } e \text{ is in } T(0 \rightsquigarrow i) \\ 0 & \text{otherwise} \end{cases}$$

Then $B_T^{-1}\beta_T$ represents the (negative of the) sum of angle differences on the path $T(0 \rightsquigarrow i)$ for each node $i \in T$:

$$\left[B_T^{-1}\beta_T\right]_i = \sum_e \left[B_T^{-1}\right]_{ie} [\beta_T]_e = -\sum_{e \in T(0 \rightsquigarrow i)} [\beta_T]_e$$

Hence $B_\perp B_T^{-1}\beta_T$ is the sum of voltage angle differences from node i to node j along the unique path in T, for every link $(i, j) \in E \setminus E_T$ not in the tree T. To see this, we have, for each link $e := (i, j) \in E \setminus E_T$,

$$\left[B_\perp B_T^{-1}\beta_T\right]_e = \left[B_T^{-1}\beta_T\right]_i - \left[B_T^{-1}\beta_T\right]_j$$
$$= \sum_{e' \in T(0 \rightsquigarrow j)} [\beta_T]_{e'} - \sum_{e' \in T(0 \rightsquigarrow i)} [\beta_T]_{e'}$$

Since

$$\sum_{e' \in T(0 \rightsquigarrow j)} [\beta_T]_{e'} = -\sum_{e' \in T(j \rightsquigarrow 0)} \left[\tilde{\beta}_T\right]_{e'}$$

the angle recovery condition (2.35) is equivalent to

$$\sum_{e' \in T(0 \rightsquigarrow i)} [\beta_T]_{e'} + [\beta_\perp]_{ij} + \sum_{e' \in T(j \rightsquigarrow 0)} \left[\tilde{\beta}_T\right]_{e'}$$
$$= \sum_{e' \in c(i,j)} \tilde{\beta}_{e'} = 0$$

where $c(i,j)$ denotes the unique basis cycle (with respect to T) associated with each link (i,j) not in T [54, Chapter 5]. Hence (2.35) is equivalent to (2.36) on all basis cycles, and therefore it is equivalent to (2.36) on all cycles.

□

2.6.2 Angle recovery algorithms

Theorem 2.2 suggests a centralized method to compute a branch flow solution from a relaxed solution.

Algorithm 1: centralized angle recovery. Given a relaxed solution $\hat{y} \in \hat{\mathbb{Y}}$,

1. Choose *any* n basis rows of B and form B_T and $B_\perp$.

2. Compute β from $\hat{y}$ and check if $B_\perp B_T^{-1} \beta_T = \beta_\perp$.

3. If not, then $\hat{y} \notin \hat{h}(\mathbb{X})$; stop.

4. Otherwise, compute $\theta_* = B_T^{-1} \beta_T$.

5. Compute $h_{\theta_*}(\hat{y}) \in \mathbb{X}$ through (2.31)–(2.34).

Theorem 2.2 guarantees that $h_{\theta_*}(\hat{y})$, if it exists, is the unique branch flow solution of (2.1)–(2.3) corresponding to (whose projection is) $\hat{y}$.

The relations (2.2) and (2.37) motivate an alternative iterative procedure to compute the angles $\angle I_{ij}$, $\angle V_i$, and hence a branch flow solution. This procedure is more amenable to a distributed implementation.

Algorithm 2: distributed angle recovery. Given a relaxed solution $\hat{y} \in \hat{\mathbb{Y}}$,

1. Choose *any* spanning tree T of G rooted at node 0.

2. For $j = 0, 1, \ldots, n$ (i.e., as index j ranges over the tree T, starting from the root and in the order of breadth-first search), for all descendents $k \in \delta(j)$, set

$$\angle I_{jk} := \angle V_j - \angle S_{jk} \tag{2.41}$$

$$\angle V_k := \angle V_j - \angle(v_j - z_{jk}^* S_{jk}) \tag{2.42}$$

3. For each link $(j, k) \in E \setminus E_T$ not in the spanning tree, node j is an additional parent of k in addition to k's parent in the spanning tree from which $\angle V_k$ has already been computed in Step 2.

   (a) Compute current angle $\angle I_{jk}$ using (2.41).

   (b) Compute a new voltage angle θ_k^j using the new parent j and (2.42). If $\theta_k^j \neq \angle V_k$, then angle recovery has failed and $\hat{y}$ is spurious.

If the angle recovery procedure succeeds in Step 3, then $\hat{y}$ together with these angles $\angle V_k, \angle I_{jk}$ are indeed a branch flow solution. Otherwise, a link (j, k) not in the tree T has been identified where condition (2.36) is violated over the basis cycle $c(j, k)$ associated with link (j, k).

2.6.3   Radial networks

Recall that all relaxed solutions in $\hat{\mathbb{Y}} \setminus \hat{h}(\mathbb{X})$ are spurious. Our next key result shows that, for radial network, $\hat{h}(\mathbb{X}) = \hat{\mathbb{Y}}$ and hence angle relaxation is always exact in the sense that there is always a unique inverse projection that maps any relaxed solution $\hat{y}$ to a branch flow solution in $\mathbb{X}$ (even though $\mathbb{X} \neq \mathbb{Y}$).

Theorem 2.3. *Suppose $G = T$ is a tree. Then*

1. *$\hat{h}(\mathbb{X}) = \hat{\mathbb{Y}}$.*

2. *given any $\hat{y}$, $\theta_* := B^{-1}\beta$ always exists and is the unique phase angle vector such that $h_{\theta_*}(\hat{y}) \in \mathbb{X}$.*

Proof. When $G = T$ is a tree, $m = n$ and hence $B = B_T$ and $\beta = \beta_T$. Moreover B is $n \times n$ and of full rank. Therefore $\theta_* = B^{-1}\beta$ always exists and, by Theorem 2.2, $h_{\theta_*}(\hat{y})$ is the unique branch flow solution in $\mathbb{X}$ whose projection is $\hat{y}$. Since this holds for any arbitrary $\hat{y} \in \hat{\mathbb{Y}}$, $\hat{\mathbb{Y}} = \hat{h}(\mathbb{X})$. $\square$

A direct consequence of Theorem 2.1 and Theorem 2.3 is that, for a radial network, OPF is equivalent to the convex problem OPF-cr in the sense that we can obtain an optimal solution of one problem from that of the other.

Corollary 1. *Suppose G is a tree. Given any optimal solution $(\hat{y}_*, s_*)$ of OPF-cr, there exists a unique θ_* such that $(h_{\theta_*}(\hat{y}_*), s_*)$ is an optimal solution of the original OPF.*

2.7 Convexification of mesh network

For mesh networks a relaxed solution may be spurious if it does not satisfy the angle recovery condition in Theorem 2.2. In this section, we explain how to use phase shifters to convexify a mesh network so that *any* relaxed solution can be mapped to a valid branch flow solution of the convexified network. As a consequence, the OPF for the convexified network can always be solved efficiently (in polynomial time).

2.7.1 Branch flow model with phase shifters

In this section we study power flow solutions and hence we fix an s. All quantities, such as $x, \hat{y}, \mathbb{X}, \hat{\mathbb{Y}}, \overline{X}, \overline{X}_T$, are with respect to the given s, even though that is not explicit in the notation. In the next section, s is also an optimization variable and the sets $\mathbb{X}, \hat{\mathbb{Y}}, \overline{X}, \overline{X}_T$ are for any s; c.f. the more accurate notation in (2.4) and (2.5).

Phase shifters can be traditional transformers or FACTS (Flexible AC Transmission Systems) devices. They can increase transmission capacity and improve stability and power quality [55, 56]. In this chapter, we consider an idealized phase shifter that only shifts the phase angles of the sending-end voltage and current across a line, and has no impedance nor limits on the shifted angles. Specifically, consider an idealized phase shifter parametrized by ϕ_{ij} across line (i, j), as shown in Figure 2.5. As before, let V_i denote the sending-end voltage. Define I_{ij} to be the *sending-end* current leaving node i towards node j. Let k be the point between the phase shifter ϕ_{ij} and line impedance z_{ij}. Let V_k and I_k be the voltage at k and current from k to j, respectively. Then the effect of the idealized phase shifter is summarized by the following modeling assumption:

$$V_k = V_i \, e^{\mathbf{i}\phi_{ij}} \quad \text{and} \quad I_k = I_{ij} \, e^{\mathbf{i}\phi_{ij}}$$
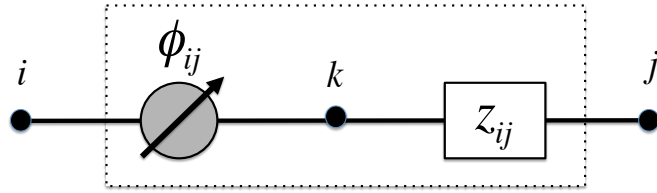
Figure 2.5: Model of a phase shifter in line (i, j).

The power transferred from nodes i to j is still (defined to be) $S_{ij} := V_i I_{ij}^*$, which, as expected, is equal to the power $V_k I_k^*$ from nodes k to j since the phase shifter is assumed to be lossless. Applying Ohm's law across z_{ij}, we define the *branch flow model with phase shifters* as the following set of equations:

$$z_{ij} I_{ij} = V_i - V_j\, e^{-\mathbf{i}\phi_{ij}} \tag{2.43}$$

$$S_{ij} = V_i I_{ij}^* \tag{2.44}$$

$$s_j = \sum_{i \in \pi(j)} \left(S_{ij} - z_{ij} |I_{ij}|^2 \right) - \sum_{k \in \delta(j)} S_{jk} \tag{2.45}$$

Without phase shifter ($\phi_{ij} = 0$), (2.43) reduces to (2.1).

Recall the set $\mathbb{X}$ of branch flow solutions defined in (2.4) (and (2.5)). The inclusion of phase shifters modifies the network and enlarges the solution set of the (new) branch flow equations. Formally, let

$$\overline{\mathbb{X}} := \{x \,|\, x \text{ solves } (2.43)–(2.45) \text{ for some } \phi\} \tag{2.46}$$

Here and henceforth, $\phi \in [-\pi, \pi]^m$. For any spanning tree T of G, let "$\phi \in T^{\perp}$" stands for "$\phi_{ij} = 0$ for all $(i, j) \in T$", i.e., ϕ involves only phase shifters in branches not in the spanning tree T. Define

$$\overline{\mathbb{X}}_T := \{x \,|\, x \text{ solves } (2.43)–(2.45) \text{ for some } \phi \in T^{\perp}\} \tag{2.47}$$

Since (2.43) reduces to (2.1) when $\phi = 0$, $\mathbb{X} \subseteq \overline{\mathbb{X}}_T \subseteq \overline{\mathbb{X}}$.

From (2.43) and (2.44), we have

$$S_{ij} \;=\; V_i \frac{V_i^* - V_j^* \, e^{\mathbf{i}\phi_{ij}}}{z_{ij}^*}$$

leading to $V_i V_j^* \, e^{\mathbf{i}\phi_{ij}} = v_i - z_{ij}^* S_{ij}$, and hence $\theta_i - \theta_j = \beta_{ij} - \phi_{ij}$. This changes the angle recovery condition from whether there exists θ that solves $B\theta = \beta$ in (2.39) to whether there exists (θ, ϕ) that solves

$$B\theta \;=\; \beta - \phi \qquad\qquad (2.48)$$

The condition (2.39) for the case without phase shifter corresponds to setting $\phi = 0$. The voltage angles are $\theta = B_T^{-1}(\beta_T - \phi_T)$, and the angle recovery condition (2.35) becomes

$$B_\perp B_T^{-1}(\beta_T - \phi_T) \;=\; \beta_\perp - \phi_\perp \qquad\qquad (2.49)$$

which can always be satisfied by appropriate (nonunique) choices of ϕ.

A similar argument to the proof of Theorem 2.2.2 leads to the following interpretation of (2.49). For any link $(i, j) \in E$, (2.48) says that the phase angle difference from node i to node j is β_{ij} and consists of the voltage angle difference $\theta_i - \theta_j = \beta_{ij} - \phi_{ij}$ and the phase shifter angle ϕ_{ij}. Fix any link $(i, j) \in E \setminus E_T$ not in tree T. The left-hand side $\left[B_\perp B_T^{-1}(\beta_T - \phi_T)\right]_{ij}$ of (2.49) represents the sum of the voltage angle differences from node i to node j along the unique path in T, *not* including the phase shifter angles along the path. This must be equal to the voltage angle difference $[\beta_\perp - \phi_\perp]_{ij}$ across (the non-tree) link (i, j), *not* including the phase shifter angle across (i, j). Therefore the sum $\left[B_\perp B_T^{-1}\phi_T\right]_{ij}$ of phase shifter angles from node i to node j along the unique path in T must equal the phase shifter angle $[\phi_\perp]_{ij}$ across (the non-tree) link (i, j).

Our next key result implies that, given a relaxed solution $\hat{y} := (S, \ell, v, s_0) \in \hat{\mathbb{Y}}$, we can always recover a branch flow solution $x := (S, I, V, s_0) \in \overline{\mathbb{X}}$ of the convexified network. Moreover it suffices to use phase shifters in branches only outside a spanning

tree. It extends Theorem 2.2 to the case with phase shifters.

Theorem 2.4. *Let T be any spanning tree of G. Consider a relaxed solution $\hat{y} \in \hat{\mathbb{Y}}$ and the corresponding β defined by (2.29)–(2.30) in terms of $\hat{y}$.*

1. *There exists a unique solution (θ_*, ϕ_*) of (2.48) with $\phi_* \in T^\perp$. Specifically*

$$\theta_* = B_T^{-1}\beta_T$$

$$\phi_* = \begin{bmatrix} 0 \\ \beta_\perp - B_\perp B_T^{-1}\beta_T \end{bmatrix}$$

2. *$h_{\theta_*}(\hat{y}) \in \overline{\mathbb{X}}_T$, i.e., $h_{\theta_*}(\hat{y})$ is a branch flow solution of the convexified network.*

3. *$\mathbb{Y} = \overline{\mathbb{X}} = \overline{\mathbb{X}}_T$ and hence $\hat{\mathbb{Y}} = \hat{h}(\overline{X}) = \hat{h}(\overline{\mathbb{X}}_T)$.*

Proof.   1. Write $\phi = [\phi_T^t \ \ \phi_\perp^t]^t$ and set $\phi_T = 0$. Then (2.48) becomes

$$\begin{bmatrix} B_T \\ B_\perp \end{bmatrix} \theta = \begin{bmatrix} \beta_T \\ \beta_\perp \end{bmatrix} - \begin{bmatrix} 0 \\ \phi_\perp \end{bmatrix}$$

The same argument as in the proof of Theorem 2.2 shows that a solution (θ_*, ϕ_*) to (2.48), with $\theta_* \in T^\perp$, exists and is unique if and only if

$$B_\perp B_T^{-1}\beta_T = \beta_\perp - \phi_\perp$$

i.e., iff $\phi_\perp = \beta_\perp - B_\perp B_T^{-1}\beta_T$. Hence the (θ_*, ϕ_*) given in the theorem solves (2.48).

2. Theorem 2.2 then implies $h_{\theta_*}(S, \ell, v, s_0) \in \overline{\mathbb{X}}_T$ with $\phi_* \in T^\perp$ given in assertion 1.

3. This follows from assertions 1 and 2.

□

Remark 2.5. *More generally, consider a network with phase shifters on an arbitrary subset of links. Given a relaxed solution $\hat{y}$, under what condition does there exist a*

θ such that the inverse projection $h_\theta(\hat{y})$ is a branch flow solution in $\mathbb{X}$? If there is a spanning tree T such that all links outside T have phase shifters, then Theorem 2.4 says that such a θ always exists, with an appropriate choice of phase shifter angles on non-tree links. Suppose no such spanning tree exists, i.e., given any spanning tree T, there is a set $E_{\perp'} \subseteq E \setminus E_T$ of links that contain no phase shifters. Let $B_{\perp'}$ and $\beta_{\perp'}$ denote the submatrix of B and subvector of β, respective, corresponding to these links. Then a necessary and sufficient condition for angle recovery is as follows: there exists a spanning tree T such that

$$B_{\perp'} B_T^{-1} \beta_T \;\; = \;\; \beta_{\perp'}$$

This condition reduces to (2.35) if there are no phase shifters in the network ($E_{\perp'} = E \setminus E_T$) and is always satisfied if every link outside any spanning tree has a phase shifter ($E_{\perp'} = \emptyset$).

Remark 2.6. *The expression for ϕ_* in Theorem 2.4.1, in particular,*

$$B_\perp B_T^{-1} \beta_T + [\phi_*]_\perp \;\; = \;\; \beta_\perp \tag{2.50}$$

is a special case of (2.49). It says that, for any link $(i,j) \in E \setminus E_T$ not in T, the sum $\left[B_\perp B_T^{-1} \beta_T\right]_{ij}$ of the voltage angle differences (since there is no phase shifter in T) from node i to node j along the unique path in T plus the phase shifter angle across link (i,j) must equal $[\beta_\perp]_{ij}$, the angle difference across link (i,j) implied by the relaxed solution $\hat{y}$. If $[\beta_\perp]_{ij} = [\theta_*]_i - [\theta_*]_j$, then the sum of voltage angle differences around the (unique) basis cycle defined by (i,j) is zero, and $[\phi_*]_{ij} = 0$; this is the case in Theorem 2.2.2 for link (i,j). Otherwise, a nonzero phase shifter angle $[\phi_*]_{ij}$ is required to compensate for the angle difference.

Theorem 2.4 implies that given any relaxed solution $\hat{y}$, there exists a $\phi \in T^\perp$ such that its inverse projection $x := h_\theta(\hat{y})$ is a branch flow solution, i.e., (x, ϕ) satisfies (2.43)–(2.45). We now give an alternative direct construction of such a solution (x, ϕ) from any given branch flow solution $\tilde{x}$ and phase shifter setting $\tilde{\phi}$ that may

have nonzero angles on some links in T. It exhibits how the effect of phase shifters in a tree is equivalent to changes in voltage angles.

Fix any spanning tree T. Given any $(\tilde{x}, \tilde{\phi})$, partition $\tilde{\phi}^t = [\tilde{\phi}_T \quad \tilde{\phi}_\perp]$ with respect to T. Define $\alpha \in [-\pi, \pi]^n$ by $B_T \alpha = \tilde{\phi}_T$ or $\alpha := B_T^{-1} \tilde{\phi}_T$. Then define the mapping $(x, \phi) = g(\tilde{x}, \tilde{\phi})$ by

$$V_i := \tilde{V}_i e^{\mathbf{i}\alpha_i}, \quad I_{ij} := \tilde{I}_{ij} e^{\mathbf{i}\alpha_i}, \quad S_{ij} := \tilde{S}_{ij} \tag{2.51}$$

and

$$\phi_{ij} := \begin{cases} 0 & \text{if } (i, j) \in E_T \\ \tilde{\phi}_{ij} - (\alpha_i - \alpha_j) & \text{if } (i, j) \in E \setminus E_T \end{cases} \tag{2.52}$$

i.e., ϕ is nonzero only on non-tree links. It can be verified that $\alpha_i - \alpha_j = \sum_{e \in T(i \rightsquigarrow j)} \tilde{\phi}_e$ where $T(i \rightsquigarrow j)$ is the unique path in tree T from node i to node j. Note that $|V_i| = |\tilde{V}_i|$, $|I_{ij}| = |\tilde{I}_{ij}|$ and $S = \tilde{S}$. Hence if $h(\tilde{x})$ is a relaxed branch flow solution, so is $h(x)$. Moreover, the effect of phase shifters in T is equivalent to adding α_i to the phases of V_i and I_{ij}.

Theorem 2.5. *Fix any tree T. If $(\tilde{x}, \tilde{\phi})$ is a solution of (2.43)–(2.45), so is $(x, \phi) = g(\tilde{x}, \tilde{\phi})$ defined in (2.51)–(2.52).*

Proof. Since $|V_i| = |\tilde{V}_i|$, $|I_{ij}| = |\tilde{I}_{ij}|$ and $S = \tilde{S}$, (x, ϕ) satisfies (2.44)–(2.45). For any link $(i, j) \in E_T$ in tree T, (2.51)–(2.52) imply

$$\begin{aligned} V_i - V_j e^{-\mathbf{i}\phi_{ij}} &= \left(\tilde{V}_i - \tilde{V}_j e^{-\mathbf{i}(\alpha_i - \alpha_j)} \right) e^{\mathbf{i}\alpha_i} \\ &= \left(\tilde{V}_i - \tilde{V}_j e^{-\mathbf{i}\tilde{\phi}_{ij}} \right) e^{\mathbf{i}\alpha_i} \end{aligned}$$

where the second equality follows from $B_T \alpha = \tilde{\phi}_T$. For any link $(i, j) \in E \setminus E_T$ not in T, (2.51)–(2.52) imply

$$V_i - V_j e^{-\mathbf{i}\phi_{ij}} = \left(\tilde{V}_i - \tilde{V}_j e^{-\mathbf{i}\tilde{\phi}_{ij}} \right) e^{\mathbf{i}\alpha_i}$$

But $\left(\tilde{V}_i - \tilde{V}_j \, e^{-\mathbf{i}\tilde{\phi}_{ij}}\right) = \tilde{I}_{ij}$ since $(\tilde{x}, \tilde{\phi})$ satisfies (2.43). Therefore $V_i - V_j \, e^{-\mathbf{i}\phi_{ij}} = I_{ij}$, i.e., (x, ϕ) satisfies (2.43) on every link. $\qquad \square$

Remark 2.7. *A less direct proof of Theorem 2.5 is as follows: by (2.49), we must have*

$$B_\perp B_T^{-1}(\beta_T - \tilde{\phi}_T) \;\; = \;\; \beta_\perp - \tilde{\phi}_\perp$$

where $\beta := \beta(h(\tilde{x})) = \beta(h(x))$ *is defined by (2.29) and the relaxed solutions* $h(\tilde{x})$ *and* $h(x)$ *are identical. Substituting* $\alpha = B_T^{-1}\tilde{\phi}_T$ *and rearranging, this becomes (using (2.52))*

$$B_\perp B_T^{-1}\beta_T \;\; = \;\; \beta_\perp - (\tilde{\phi}_\perp - B_\perp \alpha) \;\; = \;\; \beta_\perp - \phi_\perp$$

This is simply the necessary and sufficient condition for (x, ϕ) *to satisfy (2.48).*

2.7.2 Optimal power flow

Theorem 2.4 suggests using phase shifters to convexify a mesh network so that *any* solution of OPF-ar can be mapped into an optimal solution of OPF of the convexified network. Convexification thus modifies a NP-hard problem into a simple problem without loss in optimality; moreover this requires an one-time deployment cost for subsequent operational simplicity, as we now show.

We will compare four OPF problems: the original OPF (2.11)–(2.12), OPF-ar (2.20)–(2.21), the following problem where there is a phase shifter on every line ($\phi \in [-\pi, \pi]^m$):

OPF-ps:

$$\min_{x, s, \phi} \quad f\left(\hat{h}(x), s^g\right)$$
$$\text{subject to} \quad x \in \overline{\mathbb{X}}, \; (v, s_0, s) \in \mathbb{S}$$

and the problem where, given any spanning tree T, there are phase shifters only

outside T:

OPF-ps(T):

$$
\begin{aligned}
\min_{x,s,\phi} \quad & f\left(\hat{h}(x), s^g\right) \\
\text{subject to} \quad & x \in \overline{\overline{\mathbb{X}}}_T, \ (v, s_0, s) \in \mathbb{S}, \ \phi \in T^{\perp}
\end{aligned}
$$

Let the optimal values of OPF, OPF-ar, OPF-ps, and OPF-ps(T) be f_*, f_{ar}, f_{ps}, and f_T, respectively.

Theorem 2.4 implies that $\mathbb{X} \subseteq \mathbb{Y} = \overline{\mathbb{X}} = \overline{\overline{\mathbb{X}}}_T$ for any spanning tree T. Hence we have

Corollary 2. *For any spanning tree T, $f_* \geq f_{ar} = f_{ps} = f_T$, with equality if there is a solution $(\hat{y}_{ar}, s_{ar}^g)$ of OPF-ar that satisfies (2.35).*

Corollary 2 has several important implications:

1. Theorem 2.1 implies that we can solve OPF-ar efficiently through conic relaxation to obtain a relaxed solution $(\hat{y}_{ar}, s_{ar})$. An optimal solution of OPF may or may not be recoverable from it. If $\hat{y}_{ar}$ satisfies the angle recovery condition (2.35) with respect to s_{ar}, then Theorem 2.2 guarantees a unique θ_* such that the inverse projection $(\hat{h}_{\theta_*}(\hat{y}_{ar}), s_{ar})$ is indeed optimal for OPF.

2. In this case, Corollary 2 implies that adding any phase shifters to the network cannot further reduce the cost since $f_* = f_{ar} = f_{ps}$.

3. If (2.35) is not satisfied, then $\hat{y}_{ar} \notin \hat{h}(\mathbb{X})$ and there is no inverse projection that can recover an optimal solution of OPF from $(\hat{y}_{ar}, s_{ar})$. In this case, $f_* \geq f_{ar}$. Theorem 2.4 implies that if we allow phase shifters, we can always attain $f_{ar} = f_{ps}$ with the relaxed solution $(\hat{y}_{ar}, s_{ar})$, with potentially strict improvement over the network without phase shifters (when $f_* > f_{ar}$).

4. Moreover, Corollary 2 implies that such benefit can be achieved with phase shifters only in branches outside an arbitrary spanning tree T.

2.8 Simulations

For radial networks, Theorem 2.3 guarantees that both the angle relaxation and the conic relaxation are exact. For mesh networks, the angle relaxation may be inexact and phase shifters may be needed to implement a solution of the conic relaxation. We now explore through numerical experiments the following questions:

- How many phase shifters are typically needed to convexify a mesh network?

- What are typical phase shifter angles to implement an optimal solution for the convexified network?

Test cases. We explore these questions using the IEEE benchmark systems with 14, 30, 57, 118, and 300 buses, as well as a 39-bus model of a New England power system and two models of a Polish power system with 2,383 and 2,737 buses. The data for all the test cases were extracted from the library of built-in models of the MATPOWER toolbox [57] in Matlab. The test cases involve constraints on bus voltages as well as limits on the real and reactive power generation at every generator bus. The New England and the Polish power systems also involve MVA limits on branch power flows. All of these systems are mesh networks, but very sparse.

Objectives. We solve the test cases for two scenarios:

- *Loss minimization.* In this scenario, the objective is to minimize the total active power loss of the circuit given constant load values, which is equivalent to minimizing the total active power generation. The results are shown in Table 2.2.

- *Loadability maximization.* In this scenario, the objective is to determine the maximum possible load increase in the system while satisfying the generation, voltage and line constraints. We have assumed all real and reactive loads grow uniformly, i.e., by a constant multiplicative factor called the *max loadability* in Table 2.3.

Test cases	# links	No PS	With phase shifters (PS)				
		Min loss	Min loss	# required PS	# active PS	Angle range (°)	Angle/loop size (°)
	(m)	(OPF, MW)	(OPF-cr, MW)	$(m-n)$	$\|\phi_i\| > 0.1°$	$[\phi_{\min}, \phi_{\max}]$	$[\phi_{\min}, \phi_{\max}]$
IEEE 14-Bus	20	0.546	0.545	7 (35%)	2 (10%)	$[-2.09,\ 0.58]$	$[-0.70,\ 0.02]$
IEEE 30-Bus	41	1.372	1.239	12 (29%)	3 (7%)	$[-0.2,\ 4.47]$	$[-0.03,\ 0.50]$
IEEE 57-Bus	80	11.302	10.910	24 (30%)	19 (24%)	$[-3.47,\ 3.15]$	$[-0.58,\ 0.38]$
IEEE 118-Bus	186	9.232	8.728	69 (37%)	36 (19%)	$[-1.95,\ 2.03]$	$[-0.39,\ 0.28]$
IEEE 300-Bus	411	211.871	197.387	112 (27%)	101 (25%)	$[-13.27,\ 9.40]$	$[-3.96,\ 1.68]$
New England 39-Bus	46	29.915	28.901	8 (17%)	7 (15%)	$[-0.26,\ 1.83]$	$[-0.04,\ 0.26]$
Polish (case2383wp)	2,896	433.019	385.894	514 (18%)	373 (13%)	$[-19.99,\ 16.82]$	$[-1.68,\ 0.93]$
Polish (case2737sop)	3,506	130.145	109.905	770 (22%)	395 (11%)	$[-10.88,\ 11.98]$	$[-0.93,\ 0.71]$

Table 2.2: Loss minimization. Min loss without phase shifters (PS) was computed using SDP relaxation of OPF; min loss with phase shifters was computed using SOCP relaxations OPF-cr of OPF-ar. The "(%)" indicates the number of PS as a percentage of #links.

Test cases	No PS	With phase shifters (PS)				
	Max loadability	Max loadability	# required PS	# active PS	Angle range (°)	Simulation time
	(OPF)	(OPF-cr)	$(m-n)$	$\|\phi_i\| > 0.1°$	$[\phi_{\min}, \phi_{\max}]$	(seconds)
IEEE 14-Bus	195.0%	195.2%	7 (35%)	6 (30%)	$[-0.5,\ 1.4]$	1.92
IEEE 30-Bus	156.7%	158.7%	12 (29%)	9 (22%)	$[-0.4,\ 12.4]$	3.86
IEEE 57-Bus	108.2%	118.3%	24 (30%)	24 (30%)	$[-13.1,\ 23.2]$	7.13
IEEE 118-Bus	203.7%	204.9%	69 (37%)	64 (34%)	$[-16.5,\ 22.3]$	15.96
IEEE 300-Bus	106.8%	112.8%	112 (27%)	103 (25%)	$[-15.0,\ 16.5]$	34.6
New England 39-Bus	109.1%	114.8%	8 (17%)	5 (11%)	$[-6.3,\ 10.6]$	2.82
Polish (case2383wp)	101.4%	106.6%	514 (18%)	435 (15%)	$[-19.6,\ 19.4]$	434.5
Polish (case2737sop)	127.6%	132.5%	770 (22%)	420 (12%)	$[-16.7,\ 17.0]$	483.7

Table 2.3: Loadability maximization. Max loadability without phase shifters (PS) was computed using SDP relaxation of OPF; max loadability with phase shifters was computed using SOCP relaxations OPF-cr of OPF-ar. The "(%)" indicates the number of PS as a percentage of #links.

Solution methods. We use the "SEDUMI" solver in Matlab [58]. We first solved the SOCP relaxation OPF-cr for a solution $(\hat{y}, s)$ of OPF-ar. In all test cases, equality was attained in (2.24) at optimality, and hence OPF-cr was exact, as Theorem 2.1 would suggest. Recall however that the load values were constants in all the test cases. Even though this violated our condition that there are no upper bounds on the loads, OPF-cr turned out to be exact with respect to OPF-ar in all cases. This confirms that the no-upper-bound condition is sufficient but not necessary for the conic relaxation to be exact.

Using the solution $(\hat{y}, s)$ of OPF-ar, we checked if the angle recovery condition in Theorem 2.2 was satisfied. In all test cases, the angle recovery condition failed and hence no $(h_\theta(\hat{y}), s)$ was feasible for OPF without phase shifters. We computed

the phase shifter angles $\phi \in T^\perp$ and the corresponding unique $(h_\theta(\hat{y}), s)$ that was an optimal solution of OPF for the convexified network.

To place the phase shifters, we have used a minimum spanning tree of the network where the weights on the lines are their reactance values. In Tables 2.2 and 2.3, we report the number $m - n$ of phase shifters potentially required, the number of active phase shifters (i.e., those with a phase angles greater than $0.1°$), the range of the phase angles at optimality, the range of phase angles per link around the associated basis cycles (Table 2.2), and the simulation time on an Intel 1.8 GHz Core i5 CPU (Table 2.3).

We also report the optimal objective values of OPF with and without phase shifters in Tables 2.2 and 2.3. The optimal values of OPF without phase shifters were obtained by implementing the SDP formulation and relaxation proposed in [36] for solving OPF. In all test cases, the solution matrix was of rank one and hence the SDP relaxation was exact. Therefore the values reported here are indeed optimal for OPF.

The SDP relaxation requires the addition of small resistances (10^{-6} pu) to every link that has a zero resistance in the original model, as suggested in [34]. This addition is, on the other hand, not required for the SOCP relaxation: OPF-cr is tight with respect to OPF-ar with or without this addition. For comparison, we report the results where the same resistances are added for both the SDP and SOCP relaxations.

Summary. From Tables 2.2 and 2.3:

1. Across all test cases, the convexified networks have higher performance (lower minimum loss and higher maximum loadability) than the original networks. More important than the modest performance improvement, convexification is design for simplicity: it guarantees an efficient solution for optimal power flow.

2. The networks are (mesh but) very sparse, with the ratios $m/(n + 1)$ of the number of lines to the number of buses varying from 1.2 to 1.6 (Table 2.2). The numbers $m - n$ of phase shifters potentially required on every link outside a spanning tree for convexification vary from 17% of the numbers m of links to 37%.

3. The numbers of active phase shifters in the test cases vary from 7% of the numbers m of links to 25% for loss minimization, and 11% to 34% for loadability maximization. The phase angles required at optimality is no more than 20° in magnitude. Moreover the phase angle per link around a cycle is much smaller.

4. The simulation times range from a few sec to mins. This is much faster than SDP relaxation. Furthermore the simulation time appears to be linear with the network size.

2.9   Extensions

In [50], we prove a variety of sufficient conditions under which the conic relaxation proposed here is exact for radial networks. The main difference from Theorem 2.1 below is that [50] allows upper bounds on the loads, i.e., it replaces the load over-satisfaction assumption in this chapter with a different set of assumptions.

Both the bus injection model and the branch flow model are descriptions of the Kirchhoff laws. It is shown in [59] that there is a one-one correspondence between the semidefinite relaxation in the bus injection model and the relaxations proposed here in the branch flow model. As a consequence, the various conditions on radial networks proved in [36, 37, 35, 38] for the exactness of semidefinite relaxation imply immediately the exactness of the relaxations proposed here. Conversely, the condition in [50] for the conic relaxation immediately implies that the matrix solution of the semidefinite relaxation in [36, 37, 35, 38] has rank 1. This is useful because some results may be easier to formulate and prove in one model than in the other.

2.10   Conclusion

We have presented a branch flow model that focuses on branch current and power flows instead of nodal injections, and demonstrated how it can be used for the analysis and optimization of mesh as well as radial networks. Our results confirm that radial networks are computationally much simpler than mesh networks and we should exploit

this advantage whenever we can. For mesh networks, we have proposed a simple way to convexify them using phase shifters that will render them as computationally simple as radial networks for power flow solution and optimization.

We have proposed a solution strategy for OPF that consists of two steps:

1. Compute a relaxed solution of OPF-ar by solving its conic relaxation OPF-cr.

2. Recover from a relaxed solution an optimal solution of the original OPF using an angle recovery algorithm.

We have proved that, for radial networks, both steps are always exact so this strategy guarantees a globally optimal solution. For mesh networks the angle recovery condition can be used to check if a given relaxed solution is globally optimal.

Since power networks in practice are very sparse, the number of required phase shifters may be relatively small. Moreover, the placement of these phase shifters depends only on network topology, but not on power flows, generations, loads, or operating constraints. Therefore only one-time deployment cost is required to achieve the subsequent simplicity in network operation, market operation, and investment decisions.

2.11 Appendix

2.11.1 OPF-ar has zero duality gap

Theorem 2.6. *Suppose OPF-cr has a finite optimal value and a strictly feasible point. Then both OPF-cr and OPF-ar have zero duality gap.*

Proof. Recall that the original OPF is feasible by assumption. Hence OPF-ar and OPF-cr are both feasible. In particular the optimal value of OPF-cr is either finite or $-\infty$. We assume without loss of generality that, for all i, $\underline{p}_i^g < \overline{p}_i^g$, $\underline{q}_i^g < \overline{q}_i^g$ in (2.6) and $\underline{v}_i < \overline{v}_i$ in (3.5) so that $\mathbb{S}$ has a nonempty interior[6].

Let f_{cr}, d_{cr} denote the optimal primal and dual value of OPF-ar and f_{ar}, d_{ar} those of OPF-ar. The weak duality theorem and Theorem 2.1 imply

$$d_{cr} \leq f_{cr} \quad = \quad f_{ar} \geq d_{ar}$$

We will prove strong duality first for OPF-cr and then for OPF-ar.

Theorem 2.1 implies that OPF-cr is a convex program. By assumption its optimal value f_{cr} is finite and Slater's condition is satisfied, i.e., there exists an $(\hat{y}, s)$ in the relative interior of the feasible set such that

$$\ell_{ij} \quad > \quad \frac{P_{ij}^2 + Q_{ij}^2}{v_i} \tag{2.53}$$

Hence OPF-cr has a zero duality gap [60, Chapter 5.3.1]. We then have

$$d_{cr} = f_{cr} \quad = \quad f_{ar} \geq d_{ar} \tag{2.54}$$

To prove that OPF-ar has zero duality gap, it suffices to prove that $d_{ar} \geq d_{cr}$. Notice that the dual variables corresponding to the inequality constraints (2.24) in OPF-cr are restricted to be non-negative whereas the dual variables corresponding to the equality constraints (2.16) are unconstrained. The dual problems of OPF-cr and

---

[6]Otherwise some of these quantities are constants and can be eliminated from the optimization variables.

OPF-ar are otherwise identical. Hence $d_{ar} \geq d_{cr}$ and (2.54) completes the proof.

$\square$

2.11.2 $\hat{h}$ is injective on $\mathbb{X}$

The uniqueness of the θ in Theorem 2.2 for each $\hat{y}$ implies that the projections into $\hat{\mathbb{Y}}$ of two branch flow solutions in $\mathbb{X}$ must be distinct. Clearly this does not hold for points in $\mathbb{Y} \setminus \mathbb{X}$ that are not branch flow solutions. Formally,

Fact 2.7. *The mapping $\hat{h}$ is one-to-one on $\mathbb{X}$, i.e., if $x, x' \in \mathbb{X}$ and $x \neq x'$, then $\hat{h}(x) \neq \hat{h}(x')$.*

Proof. Suppose not and there are x and x' in $\mathbb{X}$ such that $\hat{h}(x) = \hat{h}(x') = \hat{y}$. Let $\beta = \beta(\hat{y})$ be the vector defined by $\hat{y}$ through (2.29). Theorem 2.2 implies that there is a unique θ_* such that $h_{\theta_*}(\hat{y})$ is the only branch flow solution in $\mathbb{X}$ whose projection is $\hat{y}$. Hence $x = x' = h_{\theta_*}(\hat{y})$. $\square$

To visualize this, we identify $\mathbb{C}^{2m+n+1}$ with $\mathbb{R}^{3m+n+2} \times [-\pi, \pi]^n$. Then $(S, I, V, s_0) \in \mathbb{C}^{2m+n+1}$ and $(S, \ell, v, s_0; \theta) \in \mathbb{R}^{3m+n+2} \times [-\pi, \pi]^n$ refer to the same vector if

$$h_\theta(S, \ell, v, s_0) \;=\; (S, I, V, s_0)$$

and we use them interchangeably in that case. Then an equivalent description of $\mathbb{Y}$ is

$$\mathbb{Y} \;:=\; \{ (S, \ell, v, s_0; \theta) \,|\, (S, \ell, v, s_0) \text{ solves } (2.13)\text{--}(2.16),$$
$$\theta \in [-\pi, \pi]^n \}$$

Clearly $\mathbb{X} \subseteq \mathbb{Y}$ and $\hat{h}(\mathbb{X}) \subseteq \hat{h}(\mathbb{Y}) = \hat{\mathbb{Y}}$. Their relationship is illustrated in Figure 2.6.

2.11.3 Optimization Reference

Quadratic constrained quadratic program (QCQP) is the following problem:
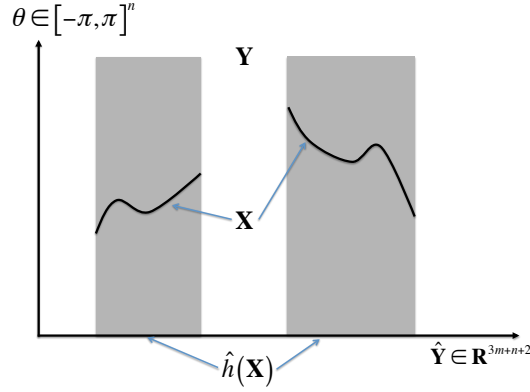
Figure 2.6: Fact 2.7: $\hat{h}$ is injective on $\mathbb{X}$. $\mathbb{X}$ can be represented by curves in the space $\mathbb{R}^{3m+n+2} \times [-\pi, \pi]^n$, and $\mathbb{Y}$ by the shaded areas (higher dimensional).

$$\min_{x \in \mathbb{C}^n} \quad x^H C_0 x \tag{2.55}$$

$$\text{subj. to} \quad x^H C_m x \leq b_m, \ m = 1, \ldots, M \tag{2.56}$$

where, for $m = 0, \ldots, M, C_m \in \mathbb{S}^n$ (so that $x^H C_m x$ are real) and $b_m \in \mathbb{R}$ are given. If $C_m, m = 0, \ldots, M$, are positive semidefinite then this is a convex QCQP. Otherwise it is generally nonconvex.

Any psd rank-1 matrix X has a unique spectral decomposition $X = xx^H$. Using $x^H C_m x = \text{tr } C_m xx^H = \text{tr } C_m X$ we can rewrite a QCQP as the following equivalent problem where the optimization is over Hermitian matrices:

$$\min_{x \in \mathbb{S}^n} \quad \text{tr } C_0 X \tag{2.57}$$

$$\text{subj. to} \quad \text{tr } C_m X \leq b_m, \ m = 1, \ldots, M \tag{2.58}$$

$$X \succeq 0, \ \text{rank } X = 1 \tag{2.59}$$

The objective function and the constraints (2.58) are linear in X and $X \succeq 0$ is a convex constraint ($\mathbb{S}^n_+$ is a convex set). The rank constraint in (2.59) is the only nonconvex constraint and the only source of computational difficulty.

Removing this constraint results in a semidefinite program (SDP):

$$\min_{x \in \mathbb{S}^n} \quad \text{tr } C_0 X \tag{2.60}$$

$$\text{subj. to} \quad \text{tr } C_m X \leq b_m, \ m = 1, \dots, M \tag{2.61}$$

$$X \succeq 0 \tag{2.62}$$

A special case of SDP is a second-order cone program (SOCP) in the following rotated form:

$$\min_{x \in \mathbb{C}^n} \quad c_0^H x \tag{2.63}$$

$$\text{subj. to} \quad ||C_m x + b_m||^2 \leq (c_m^H x + d_m)(\hat{c}_m^H x + \hat{d}_m), \ m = 1, \dots, M \tag{2.64}$$

2.11.4   A remark on the case of negative impedance values

Negative impedances have long been studied in power system analysis. It is well-known that the conventional method of modeling three-winding transformers and two-winding tap-changing transformers, as well as the presence of series capacitors, can lead to negative resistance and reactance values. Therefore, it is important to note that the adverse effect of negative impedances is not limited to OPF studies. It has been shown that negative impedances can cause instability of transient simulations and also divergence of some steady-state power flow analysis methods. For instance, there's a large literature on how negative impedance values can cause Gauss-Seidel steady state method to diverge for systems on which Newton-Raphson can easily converge.

Negative impedances can easily induce inexactness of the conic relaxation of OPF problems. For instance, this happens in the case of the Polish 3375-bus system used in the simulation section of this chapter, which has 10 lines with negative impedance values. This inability is not specific to conic relaxations of the OPF problem, as it applies to other OPF solutions methods, such as the SDP relaxation of [34] as

well. One simple remedy in these cases is to go back to the simplified model of the transformers and avoid negative reactance values in the first place.

Chapter 3

Voltage Control in Distribution Systems with High PV Penetration

In this chapter we study the potential benefits of fast timescale inverter VAR control in saving energy and improving voltage regulation, in the presence of losses in DC/AC conversion. In this chapter, we first propose a model that augments the traditional volt/var control through switched controllers on a slow timescale, with inverter control on a fast timescale. This model is motivated by the need to mitigate rapid and large voltage fluctuations in power distribution systems with high penetration of renewable generation. Our approach is to formulate a radial optimal power flow (OPF) problem to minimize the sum of line and inverter losses and energy consumption at loads, subject to constraints on voltage magnitudes. The resulting optimization problem is non-convex and therefore hard to solve. We adopt the Branch Flow Model and the proposed relaxation method described in previous chapter to efficiently solve this problem to better study the structure of optimal inverter var injection and their net benefit. We demonstrate that the optimal reactive power injection of the inverters is not necessarily monotone with respect to their real power output, but depends on a nontrivial trade-off between line loss, inverter losses, load models, and on the circuit topology and its loading condition. Simulations of two real-world distribution circuits from the Southern California Edison (SCE) company illustrates that the proposed inverter control achieves significant improvement over the current unity power factor standard of the IEEE 1547 in terms of power quality and power savings.

3.1   Introduction

The connection of large amounts of highly intermittent solar power at the distribution level presents a number of technical issues to our existing operation and control methods, and necessitates design of more advanced and much faster monitoring and control systems. These challenges include protection impacts of bi-directional power flow, low voltage ride-through, load following, resource adequacy for contingencies, stability (given loss of system inertia), line capacity, short circuit contribution, distribution system planning and operation (load rolling), and volt/voltage control. The latter is the focus of this chapter.

3.1.1   Volt/var control high PV penetration scenarios

Regulating the voltage in distribution circuits within the acceptable range specified in ANSI C84.1 is an important responsibility of utility companies. Traditionally voltage profile and reactive power flow in distribution feeders has been locally controlled using switched devices such as shunt capacitor banks, On-Load Tap Changers (OLTCs), and voltage regulators. These devices are expected to switch only a few times a day to accommodate relatively slow variation in load, which might not be sufficient to cope with the rapid fluctuations in renewable generation.

When a large solar generator is interconnected to a distribution circuit, the real power it injects tends to cause a local voltage rise due primarily to the substation bus voltage and the resistance of the circuit back to the substation. In some cases this rise might be large, and due to variable output may cause adverse voltage fluctuations for other connected customers. These fluctuations may also cause traditional voltage regulating elements such as line regulators and capacitors to operate too frequently. The higher voltage will also work against Conservation Voltage Reduction (CVR) strategies. Since 1976, California has required utilities to provide voltage in the lower half of the ANSI C84.1 range (114 to 120 Volts) for CVR purposes. Significant energy savings are attainable by better regulation of customer supply voltage, and Southern California Edison has pursued closed loop capacitor control methods for this purpose

for many years [4].

Among the means being considered to mitigate these voltage effects is the use of the inverter's inherent reactive power capability to offset its real power effect. An inverter will often have a KVA size on the order of 110% of its maximum KW output. This leaves 46% of its capacity for reactive power even at full real power output. Since voltage rise as a function of KVAR on a typical distribution circuit is 2 to 3 time that as a function of KW significant voltage regulation is possible. However, according to the current IEEE 1547, the standard for integration of Distributed Energy Resources (DERs), "inverters should not actively participate in the voltage and var regulation". This limitation may have been appropriate for low levels of penetration, but as we move towards higher penetration of renewables, it will be essential to exploit the advanced control capability of inverter interfaces to the grid.

In this chapter we show how the reactive power capability of the solar plant inverters can be optimally used to regulate voltage. In particular, we seek to determine voltage regulation operation that minimizes power losses considering (1) CVR effects, (2) line losses, and (3) inverter losses due to reactive power injection. Maintaining customer voltage within ANSI C84.1 and reactive power flow limits are treated as hard constraints.

Literature Review: Volt/var control in a distribution system has been extensively studied in the literature. Most effort focus on finding optimal switching schedules for shunt capacitors and Under Load Tap Changer (ULTCs) to minimize system losses [44, 61, 62]. Inverter control has been considered in some recent works, e.g., [63, 64]. In [63], the authors consider centralized reactive power flow control of inverters and use DC power flow approximations. Although recent studies show that deployment of conservation voltage reduction plans on distribution feeders of United States can provide a 3.04% reduction in the annual national energy consumption [65], almost all existing VVC solutions in the literature ignore this and only aim to minimize systems losses.

3.1.2 High PV penetration cases in Southern California

California, as one of the leading states driving America's clean energy boom, has embarked on several initiatives to reach its ambitious goals in increasing the share of renewable energy in its total energy mix. California Solar Initiative (CSI) aims to create 3,000 megawatts of new solar generation by 2016. As a result distribution planners of the electric utilities are facing a rapidly increasing number of integration request for small size residential PV as well as large scale commercial PV systems. In particular, under the Solar Photovoltaic Program (SPVP) 500 MW of warehouse rooftop and ground mounted commercial generation in the 1 to 10 MW range are being deployed in Southern California Edison's (SCE) service territory, one of the nation's largest utility companies. These large scale plants have already created a number of distribution circuits with very high penetration of PV generation. This chapter adopts the Branch Flow Model (BFM) framework and a two time-scale control scheme to study these distribution circuits.

One such example is a 12 rural 12KV feeder with a 5 MW generator near the end of the circuit to explore the use of the generator inverter's reactive power capability to control voltage. This circuit is particularly interesting because of its low loading, high generation, long distance of the generator from the substation, and large reverse power flow. Figure 3.1, shows the feeder current data measured at the substation, taken from the SCADA system of SCE. In this plot, a positive current shows a reverse power flow back to the substation. Note that this feeder has a peak reverse flow of more than 3MW. We have chosen four typical days in November 2011 to represent the four class of solar radiation behavior introduced in [66], i.e., clear, cloudy, intermittent clear, and intermittent cloudy days. The later type is the worst case in terms of voltage fluctuations.
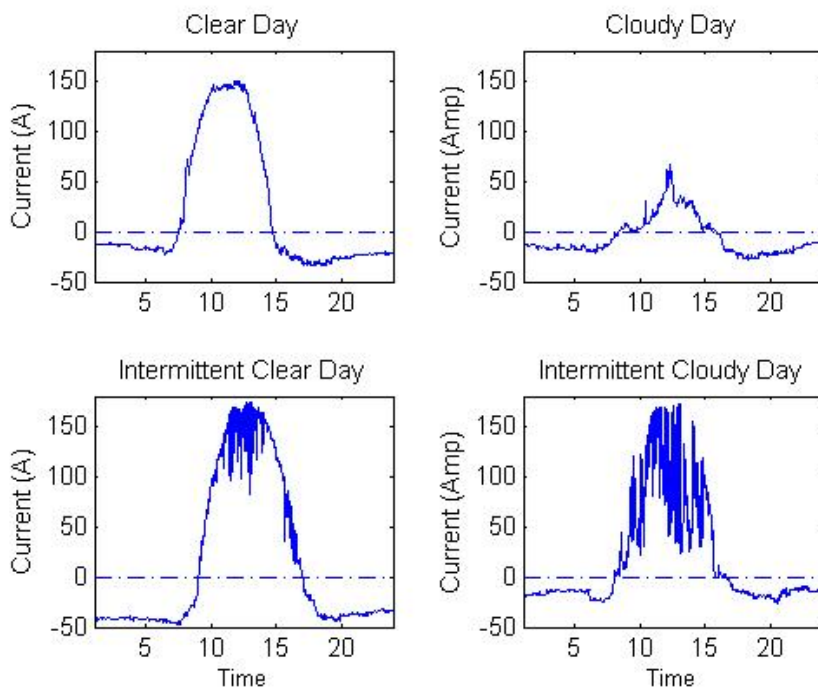
Figure 3.1: Line current measurement at the substation for one of SCE's lightly loaded 12KV feeders with 5MW of PV installed almost at the end of the line. A positive current represents reverse power flow into the substation and a negative current shows real power flowing into the feeder. The plots are from SCADA data of SCE for 4 days in Nov 2011.

3.2   Problem Formulation

In this section, we will describe our two time-scale control model and formulate the optimal volt/var control problem using the branch flow model.

3.2.1   Two time-scale control

As mentioned earlier, there are two types of control devices with two different control timescales: shunt capacitors and the voltage controllers that are controlled on a slow timescale of, say, hourly, and inverters that can be controlled on a fast timescale, say, minutes. In practice, the switched controllers are typically re-configured only a few times each day due to their limited life cycle. As the aggregate load changes slowly, the slow timescale control has been sufficient to provide voltage support. As renewable penetration such as solar PV and wind generation increases, fast timescale

control of the inverters will become indispensable in order to adapt to the large, rapid, and random fluctuations of their output.

Hence, in our model, we divide each day into M slots and index these slots by T. Each of these M slots is further divided into N slots indexed by t, as shown in Figure 3.2. For instance, we can choose each T-slot to be an hour and each t-slot a minute, i.e., $M = 24, N = 60$. We will assume that the state of the network (the voltages, real and reactive power at each bus), and the input to the network (real and reactive power generated or consumed at each bus) remain unchanged within each t-slot, and may change only from t to $t+1$. As we will explain below, the inverter control will be applied for each t to match renewable output fluctuations, and the configuration of the shunt capacitors and the substation voltage will be adjusted for each T-slot to match load fluctuations.

3.2.2 Power flow equations and constraints

Let $G(\{0\} \cup V, E)$ be a graph representing a radial distribution circuit. Each node in $\{0\} \cup V$ is a bus and each link in E is a line. We index the nodes by $i = 0, 1, \ldots, |V|$. Node 0 denotes the substation bus and other nodes in V denote branch buses. Let $v_i(t)$, $i \geq 0$ denote the *square* of the voltage magnitude at node i at time t. Node 0 is special in that its voltage v_0 is adjusted on the slow timescale T while other voltages $v_i(t)$, $i \geq 1$, are adjusted every t.

There are two types of nodes in V that generate reactive power. Let V_c be the set of nodes with switched shunt capacitors that are controlled at the slow timescale T, and the remaining nodes in $V \setminus V_c$ have inverters that are controlled at the fast
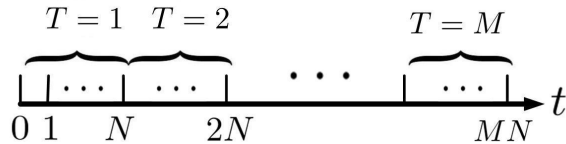
Figure 3.2: Two-timescale discretization of a day for switched controllers and inverters.

timescale t. For notational simplicity only, we assume without loss of generality that each node can have either a shunt capacitor or an inverter, but not both nor neither. Let $p_i^g(t)$ and $q_i^g(t)$ be the real and reactive power generation, respectively, at node i at time t. For nodes $i \in V \setminus V_c$, $p_i^g(t)$ represent real power generated by renewable sources such as solar PV that are connected to the grid via inverters. For nodes $i \in V_c$ that has (only) switched shunt capacitors, $p_i^g(t) \equiv 0$ for all t. For each $i \in V$, let $p_i^c(t)$ and $q_i^c(t)$ be the real and reactive power demand, respectively, at time t. If there is no load at node i, we assume $p_i^c(t) \equiv q_i^c(t) \equiv 0$ for all t. Here, $p_i^c(t), q_i^c(t)$, and $p_i^g(t)$ are assumed to be given quantities, whereas the reactive power generated $q_i^g(t)$ are the control variables.

The shunt capacitor and inverter settings $q_i^g(t)$, $i \geq 1$, and the substation voltage $v_0(t)$, together with the inputs $(p_i^c(t), p_i^g(t), q_i^c(t))$ determine the voltages and real and reactive power flows on the network. Let $P_{ij}(t)$ and $Q_{ij}(t)$ be the real and reactive power flows from nodes i to j over link (i,j). Then, from [44], these variables satisfy the following recursion (Dist-Flow equations): for each link (i,j) in the distribution circuit,

$$
\begin{aligned}
P_{ij}(t) &= \sum_{k:(j,k) \in E} P_{jk}(t) + r_{ij} \frac{P_{ij}^2(t) + Q_{ij}^2(t)}{v_i(t)} \\
&\quad + p_j^c(t) - p_j^g(t) \tag{3.1} \\
Q_{ij}(t) &= \sum_{k:(j,k) \in E} Q_{jk}(t) + x_{ij} \frac{P_{ij}^2(t) + Q_{ij}^2(t)}{v_i(t)} \\
&\quad + q_j^c(t) - q_j^g(t) \tag{3.2} \\
v_j(t) &= v_i(t) - 2(r_{ij} P_{ij}(t) + x_{ij} Q_{ij}(t)) \\
&\quad + (r_{ij}^2 + x_{ij}^2) \frac{P_{ij}^2(t) + Q_{ij}^2(t)}{v_j(t)} \tag{3.3}
\end{aligned}
$$

The end points of the feeder can be modeled through the boundary condition that there is zero power flow downstream from them. For this purpose, all the leaf nodes in our model $G = (\{0\} \cup V, E)$ and the edges incident on these leaf nodes are actually artificial nodes and edges added to each leaf node (bus) in the real distribution circuit.

Denote by $V' \subset V$ the set of leaf nodes. The the boundary constraints will force the real and reactive power flows to be zero on each edge incident to V': for all t

$$\forall (i,j) \in E \text{ with } j \in V': \qquad P_{ij}(t) = Q_{ij}(t) = 0 \tag{3.4}$$

The primary purpose of VVC on distribution circuits is to maintain voltages in an acceptable range at customer level without creating excessive var demand on transmission and subtransmission systems under all operating conditions. This is formulated as constraints on the voltage variables v_i: for all $i \notin V'$ for all t,

$$\underline{v} \quad \leq \quad v_i(t) \quad \leq \quad \overline{v} \tag{3.5}$$

The total reactive power demand on the feeder may also be constrained within limits set by operators for different seasons and even sometimes for different times of a day considering transmission var emergency cases, but this is outside the scope of this chapter. For our purpose, we assume these limits are given

$$\underline{Q}_0(t) \quad \leq \quad \sum_{j:(0,j)\in E} Q_{0j}(t) \quad \leq \quad \overline{Q}_0(t) \tag{3.6}$$

3.2.3 Inverter limits

Besides the slow timescale control, nodes $i \in V \setminus V_c$ have inverters that are controlled at the fast timescale t. We use the inverter model of [63, 67]. For our purposes, the main implication is that the magnitude of the reactive power $q_i^g(t)$ generated at an inverter is upper bounded by a quantity that depends on the real power generated at node i: for all $i \in V \setminus V_c$,

$$|q_i^g(t)| \quad \leq \quad \overline{q}_i(t) \tag{3.7}$$

where the upper bound

$$\overline{q}_i(t) := \sqrt{s_i^2 - (p_i^g(t))^2} \tag{3.8}$$
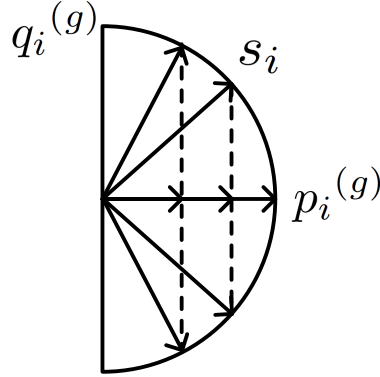
Figure 3.3: In order to regulate the voltage, inverters can quickly dispatch reactive power limited by $|q_i^g(t)| \leq \sqrt{s_i^2 - (p_i^g(t))^2}$.

is assumed given for each t^1. Here s_i represents the rated apparent power capacity of PV panel at bus i and $p_i^g(t)$ is the real power generated at time t. As illustrated in figure 3.3, the real power generation of the PV panel approaches its capacity, s_i, when the range of available reactive power reduces to zero.

3.2.4 Inverter losses

DC-AC inverters are not perfect, they have losses. The real power loss in an inverter can be approximated by a quadratic function of its apparent power [68]:

$$P_i^{\text{loss}}(t) \quad = \quad c_s + c_v \sqrt{(p_i^g(t))^2 + (q_i^g(t))^2} + c_r \left((p_i^g(t))^2 + (q_i^g(t))^2\right) \qquad (3.9)$$

where c_s models the inverter's standby losses, c_v is the voltage dependent losses over the power electronic components which is proportional to its current, I, c_r is the ohmic losses proportional to I^2, and $\sqrt{(p_i^g(t))^2 + (q_i^g(t))^2}$ is the magnitude of the apparent power injection of the inverter. Clearly, even though optimal inverter var control can reduce the line losses and the energy consumption as measured by the CVR term, its deviation from unity power factor also increases the inverter real power loss.

---

[1]There is no loss of generality by assuming all nodes not in V_c have inverters, because if node i has neither shunt capacitors nor inverter, we can assume $i \in V \setminus V_c$ with $\bar{q}_i(t) = 0$ for all t.

3.2.5 Voltage dependent load model

We will now approximate total real power consumption of loads as a function of voltage on the feeder to model the conservation energy reduction (CVR) term. Recall that v_i represents the *square* of the voltage magnitude at node i. A model of a voltage-dependent load p_i^c is the following: for $0 \leq n \leq 2$

$$p_i^c(t) = p_i^c \cdot (v_i(t))^{n_i/2} \tag{3.10}$$

$$q_i^c(t) = q_i^c \cdot (v_i(t))^{n_i/2} \tag{3.11}$$

where $\sqrt{v_i}(t)$ is the per unit value of the load's voltage magnitude at time t, and the constants p_i^c and q_i^c are the real and reactive power consumed by the load at the reference voltage, assumed given[2]. Three special cases are of particular interest: $n = 0$ for constant power loads, $n = 1$ for constant current loads, and $n = 2$ for constant impedance loads.

The real power consumption at a load at per unit voltage $v_i(t)$ can be approximated as: $p_i^c \cdot (v_i(t))^{n_i/2} \approx p_i^c \left(1 + \frac{n_i}{2}(v_i(t) - 1)\right) = \sum_i \alpha_i v_i + \text{constant}$, where $\alpha_i = (n_i/2)p_i^c$ and the constant can be neglected in the power consumption minimization (see below). Here we have used the fact that for all loads, $v_i(t) \approx 1$. It is also common to model a load as a combination of above three models:

$$p_i^c(t) = p_i^c \left(a_i^0 + a_i^1 \sqrt{v_i(t)} + a_i^2 v_i(t)\right)$$
$$q_i^c(t) = q_i^c \left(a_i^0 + a_i^1 \sqrt{v_i(t)} + a_i^2 v_i(t)\right)$$

where $a_i^0 + a_i^1 + a_i^2 = 1$. The real power consumption of such a load can again be approximated as $\sum_i \alpha_i v_i + \text{constant}$, where $\alpha_i = p_i^c \left(a_i^1/2 + a_i^2\right)$. Hence for our purposes, minimizing real power consumption, i.e. the CVR term, is equivalent to minimizing a weighted sum of the v_i values over all voltage dependent loads.

---

[2] If there is no load at node i, then $p_i^c = q_i^c = 0$.

3.2.6 Switched controllers

Let us now include switched shunt capacitors and substation Under Load Tap Changer (ULTC) in our two time-scale volt/var control scheme. Shunt capacitors generate reactive power when they are on. Since shunt capacitor settings are changed on slow timescale for each T, we represent this by

$$q_i^g(t) \;=\; c_i(T)q_i \qquad \forall i \in V_c, t \in T$$

where $c_i(T) \in \{0, 1\}$ is the switching control for period T. That is, the capacitor at node i generates reactive power of q_i if it is on and no reactive power if it is off. The substation ULTC regulates the voltage $v_0(T)$ at the substation bus in discrete steps corresponding to different tap levels. It is also controlled at the slow timescale.

Let S denote the set of possible states for the discrete controllers $(v_0(T), c_i(T), \forall i \in V_c)$. With k number of taps for the substation's ULTC and m number of switched capacitors, we will have $|S| = k \times 2^m$ different states. Let $s(T) := (v_0(T), c(T)) := (v_0(T), c_i(t), i \in V_c)$ be the control at time T. Then $s(T) \in S$. The traditional volt/var control is to choose $s(T)$ so as to minimize a certain cost function of the form $J(s) + C(s', s)$, where $C(s', s)$ represents the cost of switching from the configuration s' in the previous time period to the new configuration s in the current period, and $J(s)$ represents the cost in the new state s, e.g., the loss in the distribution circuit. Hence, the slow timescale control can be formulated as the following optimization problem

$$\min_{s(T) \in S} \sum_{T=1,\ldots,M} \{J(s(T)) + C(s(T-1), s(T))\} \qquad (3.12)$$

Given the cost functions J and C, this can be solved using dynamic programming. Typically each distribution feeder has a small number of capacitors and hence searching through the state space for the optimal setting of the discrete controllers should be computationally tractable at the slow timescale. The idea is illustrated in

figure 3.4 for the case of a distribution feeder with 4 switched capacitors. [3]
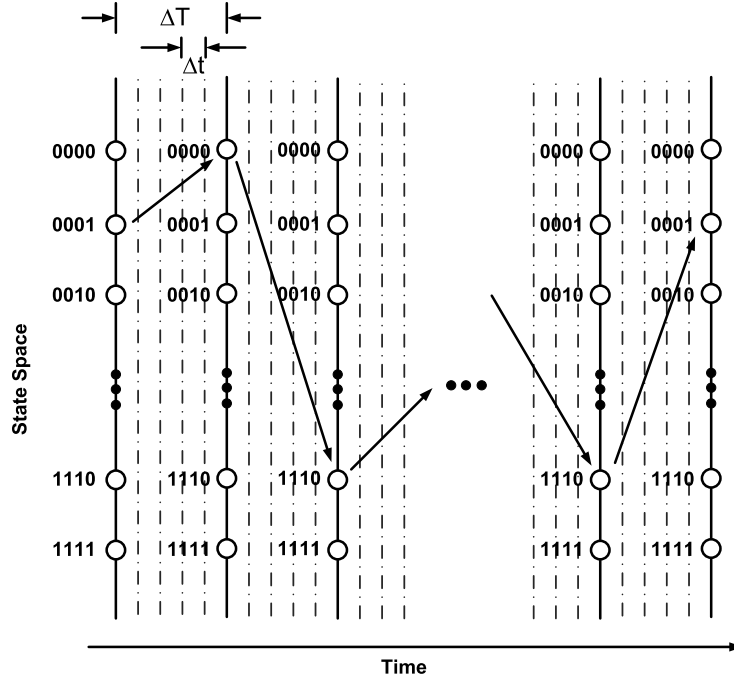
Figure 3.4: Illustration of the dynamic programming approach to solve the slow time-scale voltage control problem in a distribution feeder with 4 on/off switched capacitors.

3.2.7 VVC optimization problem

We are now ready to state the the VVC optimization problem. As explained in Section 3.2.6, the switched controllers are controlled at the timescale T. Within each period T, the control $s(T)$ is fixed and the reactive power $q_i^g(t), i \in V \setminus V_c$ generated by inverters is adjusted at the fast timescale $t \in T$. The daily operation is then represented by a hierarchical optimization problem, where the slow timescale control solves

$$\min_{s(T) \in S} \sum_{T=1,...,M} \{J(s(T)) + C(s(T-1), s(T))\} \tag{3.13}$$

---

[3] An alternative option, particularly when dealing with a large number of discrete controllers, is to consider reactive power injection of capacitors and the substation voltage as continuous variables, find the optimal solution of the resulting optimization problem and then determine On/Off and tap setting for the switched capacitors and substation ULTC by projecting the solution to the discrete state space using thresholding.

and the cost $J(s(T))$ in period T is the sum of cost $J(s(T), t)$ in each period $t \in T$ under the fast timescale control:

$$J(s(T)) = \sum_{t \in T} J(s(T), t)$$

Here, for each t, the optimal cost $J(s(T), t)$ is the sum of the loss in the distribution circuit and the weighted voltages as explained in Section 3.2.5: given the switched control $s(T) = (v_0(T), c(T))$. If we denote the set of the nodes with DC-AC inverters with I, then the overall fast time-scale inverter var control problem can be formulated as follows:

$$J(S_T, t) = \min \sum_{(i,j) \in E} r_{ij} \frac{P_{ij}^2(t) + Q_{ij}^2(t)}{v_i(t)} + \sum_i \alpha_i v_i(t) + \sum_{i \in I} P_i^{\text{loss}}(t) \tag{3.14}$$

$$\text{subject to} \quad (3.1)\text{--}(3.9) \tag{3.15}$$

$$v_0(t) = v_0(T) \tag{3.16}$$

$$q_i^g(t) = c_i(T)q_i, \qquad i \in V_c \tag{3.17}$$

$$\text{over} \quad P(t), Q(t), v(t), q^g(t) \tag{3.18}$$

3.3 Fast-timescale control: inverter optimization

In this section, we focus on the fast timescale inverter control, i.e., we assume a given $s(T)$ and consider solving (3.14)–(3.18) for a fixed $t \in T$. For the sake of simplicity, we drop time dependency labels t from the fast time-scale control problem. Now let us introduce the following new variables for every bus and every line, respectively,

$$\nu_i := |V_i|^2 \tag{3.19}$$

$$\ell_{ij} := |I_{ij}|^2 \tag{3.20}$$

and also the following new variables for every bus with an inverter, i.e. $i \in I$,

$$s_i := \sqrt{(p_i^g)^2 + (q_i^g)^2} \tag{3.21}$$

$$t_i := s_i^2 = (p_i^g)^2 + (q_i^g)^2 \tag{3.22}$$

In order to remove the nonlinear equality constraints as the source of nonconvexity and cast this problem into a Second Order Cone Program (SOCP), we follow the relaxation step introduced in chapter 2:

$$\forall (i,j) \in E : \quad \ell_{ij} \geq \frac{P_{ij}^2 + Q_{ij}^2}{\nu_i} \tag{3.23}$$

This is equivalent to relaxing the magnitude of currents on all links, and the hope is to find these inequalities to be tight the optimal solution. Note that relaxed constraints (3.23) represent second order cones with respect to (P, Q, ν, ℓ_{ij}). Now consider the following relaxed SOCP program to solve the fast time-scale inverter var control problem,

$$\min \qquad \sum_{(i,j)\in E} r_{ij}\ell_{ij} + \sum_i \alpha_i \nu_i + \sum_{i\in I}(c_v s_i + c_r t_i) \qquad (3.24)$$

$$\text{s. t.} \qquad P_{ij} = \sum_{k:(j,k)\in E} P_{jk} + r_{ij}\ell_{ij} + p_j^c - p_j^g \qquad (3.25)$$

$$Q_{ij} = \sum_{k:(j,k)\in E} Q_{jk} + x_{ij}\ell_{ij} + q_j^c - q_j^g - q_j^c \nu_j \qquad (3.26)$$

$$\nu_j = \nu_i - 2(r_{ij}P_{ij} + x_{ij}Q_{ij}) + (r_{ij}^2 + x_{ij}^2)\ell_{ij} \qquad (3.27)$$

$$\forall (i,j) \in E: \quad \ell_{ij} \geq \frac{P_{ij}^2 + Q_{ij}^2}{\nu_i} \qquad (3.28)$$

$$\forall i \in I: s_i \geq \sqrt{(p_i^g)^2 + (q_i^g)^2} \qquad (3.29)$$

$$\forall i \in I: t_i \geq (p_i^g)^2 + (q_i^g)^2 \qquad (3.30)$$

$$\forall i \in I: |q_i^g| \leq \bar{q}_i^g \qquad (3.31)$$

$$\underline{V}_i^2 \leq \nu_i \leq \overline{V}_i^2 \qquad (3.32)$$

$$\underline{p}_i^c \leq p_i^c \ , \quad \underline{q}_i^c \leq q_i^c \qquad (3.33)$$

$$\text{over} \qquad X := (P, Q, p^g, p^c, q^g, q^c, \nu, \ell, s, t) \qquad (3.34)$$

Using relaxations (3.29), (3.30) is the typical method of linearizing the Euclidean norms and quadratic terms in the objective function and casting them as second order cone constraints. It is easy to see that these inequalities will be tight in the solution. We have also made two other relaxations in the problem formulation. First the nonlinear equalities in the original problem are relaxed to inequalities (3.28). Second, in (3.33), we have used the over-satisfaction of active and reactive loads (see chapter 2) . The result is

Theorem 3.1. *The volt/var control problem (3.24)–(3.34) is convex. Moreover, it is exact, i.e., any optimal solution of (3.24)–(3.34) achieves equality in (3.28), (3.29),(3.30), and therefore specifies valid and optimal inverter reactive generation q_i^g and voltage magnitudes $|V_i|$.*

Proof. A slightly simpler version of this theorem was proved in the previous chapter.

The only difference here is the addition of more linear terms due to inverter losses in the objective function and more second order cone constraints in (3.29), (3.30). However, the same proof would still apply since the active and reactive power generation variables are not involved in the proof steps. □

Remark 3.1. *Theorem 3.1 implies that the original nonconvex optimal inverter control problem can be efficiently solved using the above SOCP relaxation. This opens the way to implement efficient volt/var control in real time to cope with random, rapid, and large fluctuations of solar generation.*

3.4 Case study: reverse power flow with a single large solar PV

In this section we evaluate the proposed solution using data from one of SCE's distribution circuits with a large 5MW solar PV installed at at the end of a distribution rural feeders. We use historical SCADA data for load and PV generation to illustrate the ideas and to estimate the net benefits of optimal inverter var control. The following is a very lightly loaded rural distribution feeder (less than 1MW) in which a 5MW PV has been integrated almost 6 miles away from the substation. The circuit diagram of the distribution system is shown Figure 3.5 and the various parameters are given in Table 5.1. The load data in Table 5.1 are peak values. Historical data shows a typical day time loading of around 20% of the peak with a typical power factor of 0.9. In the simulation results discussed below, the voltage magnitude of bus 1 at the substation is fixed at 1 pu. The voltage magnitude bounds at all other buses are assumed to be 0.97 pu and 1.03 pu.

Figure 3.6 shows the voltage magnitude at bus 45, i.e., the Point of Common Coupling (PCC), as a function of solar output, when the inverter provides no var control, i.e., unity power factor with $q_i^g = 0$, according IEEE 1547. The load is in percentage of peak load. The figure shows that the range of voltage fluctuation can
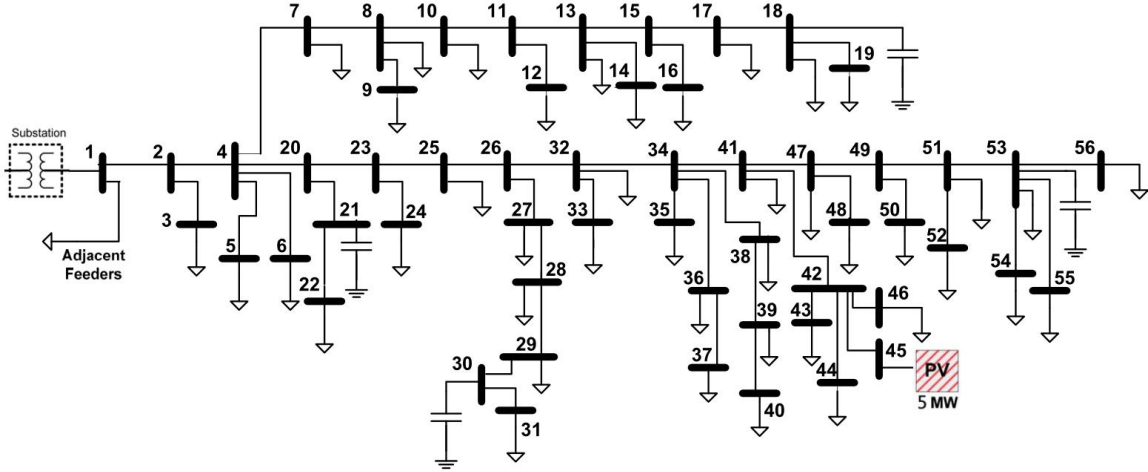
Figure 3.5: Circuit diagram for SCE distribution system.

Table 3.1: Line impedances, peak spot load KVA, capacitors and PV generation's nameplate ratings for the distribution circuit in Figure 3.5.

Network Data																
Line Data				Line Data				Line Data				Load Data		Load Data		Load Data
From Bus.	To Bus.	R (Ω)	X (Ω)	From Bus.	To Bus.	R (Ω)	X (Ω)	From Bus.	To Bus.	R (Ω)	X (Ω)	Bus No.	Peak MVA	Bus No.	Peak MVA	Bus No.	Peak MVA
1	2	0.160	0.388	20	21	0.251	0.096	39	40	2.349	0.964	3	0.057	29	0.044	52	0.315
2	3	0.824	0.315	21	22	1.818	0.695	34	41	0.115	0.278	5	0.121	31	0.053	54	0.061
2	4	0.144	0.349	20	23	0.225	0.542	41	42	0.159	0.384	6	0.049	32	0.223	55	0.055
4	5	1.026	0.421	23	24	0.127	0.028	42	43	0.934	0.383	7	0.053	33	0.123	56	0.130
4	6	0.741	0.466	23	25	0.284	0.687	42	44	0.506	0.163	8	0.047	34	0.067	Shunt Cap	
4	7	0.528	0.468	25	26	0.171	0.414	42	45	0.095	0.195	9	0.068	35	0.094	Bus	MVAR
7	8	0.358	0.314	26	27	0.414	0.386	42	46	1.915	0.769	10	0.048	36	0.097	19	0.6
8	9	2.032	0.798	27	28	0.210	0.196	41	47	0.157	0.379	11	0.067	37	0.281	21	0.6
8	10	0.502	0.441	28	29	0.395	0.369	47	48	1.641	0.670	12	0.094	38	0.117	30	0.6
10	11	0.372	0.327	29	30	0.248	0.232	47	49	0.081	0.196	14	0.057	39	0.131	53	0.6
11	12	1.431	0.999	30	31	0.279	0.260	49	50	1.727	0.709	16	0.053	40	0.030	Photovoltaic	
11	13	0.429	0.377	26	32	0.205	0.495	49	51	0.112	0.270	17	0.057	41	0.046	Bus	Capacity
13	14	0.671	0.257	32	33	0.263	0.073	51	52	0.674	0.275	18	0.112	42	0.054		
13	15	0.457	0.401	32	34	0.071	0.171	51	53	0.070	0.170	19	0.087	43	0.083	45	5MW
15	16	1.008	0.385	34	35	0.625	0.273	53	54	2.041	0.780	22	0.063	44	0.057		
15	17	0.153	0.134	34	36	0.510	0.209	53	55	0.813	0.334	24	0.135	46	0.134	$V_{\text{base}} = 12\text{KV}$	
17	18	0.971	0.722	36	37	2.018	0.829	53	56	0.141	0.340	25	0.100	47	0.045	$S_{\text{base}} = 1\text{MVA}$	
18	19	1.885	0.721	34	38	1.062	0.406					27	48	48	0.196	$Z_{\text{base}} = 144\Omega$	
4	20	0.138	0.334	38	39	0.610	0.238					28	38	50	0.045		
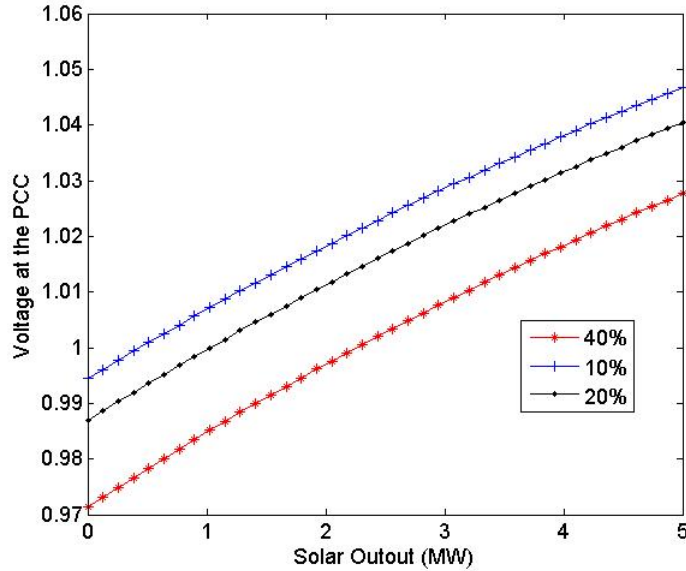
Figure 3.6: Voltage magnitude at the point of common coupling (PCC) vs solar output.

exceed 5% as solar output varies from 0 to 5 MW (its nameplate capacity). It clearly demonstrates the need for fast timescale inverter var control for voltage support to cope with random, rapid, and large solar output fluctuations.

3.4.1 Inverter var control trade-offs

In this subsection we examine the inverter var injection q_i^{g*} at the PV bus under the proposed optimal control, as solar output varies and as load varies. Multiple factors interact to determine the optimal inverter var injection. As illustrated in figure 3.7, there is trade-off between the line loss term and the CVR term in the objective function: a higher voltage magnitude reduces line loss but increases energy consumption in the CVR term. The optimal trade-off is determined by the solar output and the total load, and the constraints (3% tolerance) on the voltage magnitude. Intuitively, one should increase var injection (more positive) either when the voltage magnitude is low in order to keep it above its lower bound, or when the solar is high so as to minimize the line losses in transferring power from the PV bus towards the substation. Conversely, one should decrease var injection (more negative) either when the
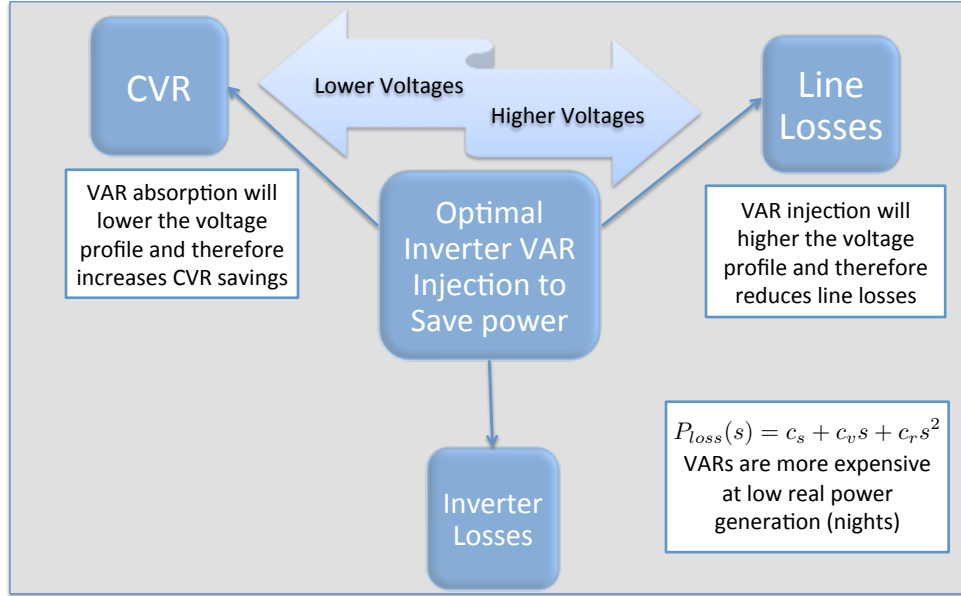
Figure 3.7: Illustration of trade-offs in optimal inverter volt/var control problem.

voltage magnitude is high in order to keep it below its upper bound or when the load is high in order to decrease energy consumption due to the CVR term in the objective function.

We now take a closer look at these interactions, as solar output and as load varies. Figures 3.8 and 3.9 show the optimal inverter var injection as a function of solar output for a fixed total load. At low load (Figure 3.8), as solar output increases, the optimal inverter var injection q_i^{g*} initially increases so as to minimize line losses in transferring power from the PV bus towards the substation. Eventually, as the solar output continues to rise above a threshold the optimal inverter var injection q_i^{g*} decreases (absorbs var) in order to maintain a voltage magnitude within its upper bound. The opposite effect dominates at high load (Figure 3.9) when the voltage magnitude is typically well below the upper bound. As solar output increases, the optimal inverter var injection q_i^{g*} decreases so as to reduce the energy consumption due to the CVR term in the objective function. We can also see the transition between these two phenomena in these Figures.

Figure 3.10 shows the optimal inverter var injection as a function of total load for a fixed solar output. At low solar output, optimal inverter var injection decreases
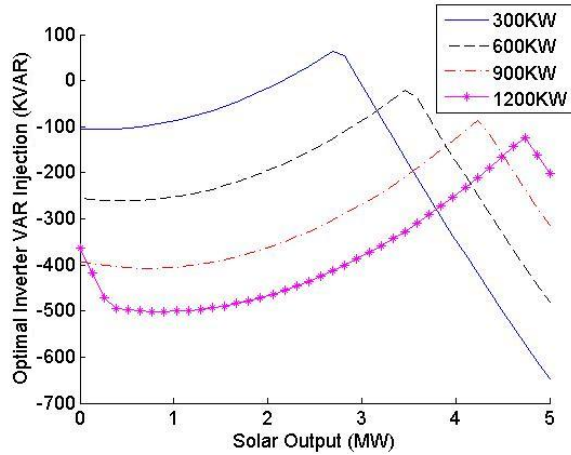
Figure 3.8: Optimal inverter reactive power (in KVAR) vs PV output when load is low.
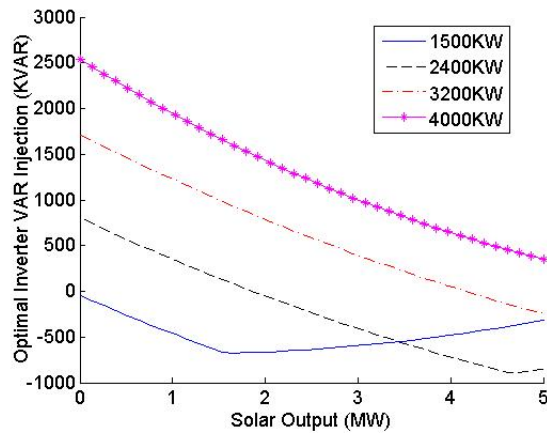
Figure 3.9: Optimal inverter reactive power (in KVAR) vs PV output when load is high.
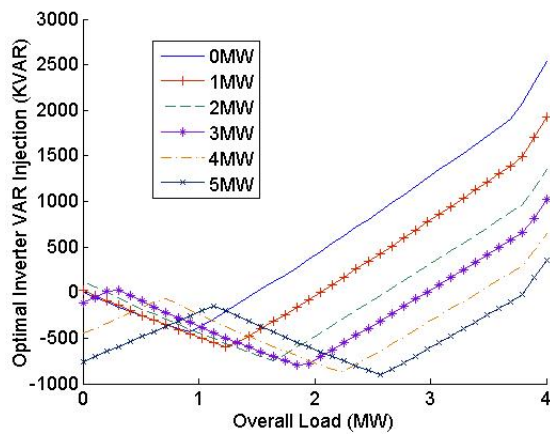
Figure 3.10: Optimal inverter reactive power (in KVAR) vs total load.

as load initially increases to as to reduce the energy consumption in the CVR term, until the load reaches a threshold that reduces the voltages to near the lower bounds. Beyond that threshold, the optimal inverter var injection increases as load increases so as to maintain the voltage magnitudes above the lower bounds. At high solar output, on the other hand, the above behavior is preceded by a section where the line losses term dominates over the CVR term. Then the optimal inverter var injection increases as load initially increases from zero in order to reduce line losses.

3.4.2   Net benefits of optimal inverter var control

We implemented the proposed convex relaxation of the radial OPF problem and solved it using CVX optimization toolbox [69] in Matlab. In all our simulations, we checked the inequality constraint in condition (3.28) for optimal solutions of the relaxed problem and confirmed that the inequality constraints were all active, i.e., equality holds at the optimal solutions.

We will assess the benefit of the proposed optimal inverter var control in two ways. First, when inverters do not participate in var control (i.e., unity power factor as specified in the current IEEE 1547 standard), the voltage magnitudes may violate the specified limits when the total load is low and solar power is high. This represents an undesirable operation mode. The proposed optimal inverter var control should help maintain the voltage magnitudes within their specified limits and thus enlarge the region of desirable operation mode.

Second, the net cost is the sum of line losses and energy consumption, as expressed in (3.24), plus the real power loss in the inverter. We have used typical loss model parameters from [68] for an inverter with maximum efficiency of 96% to evalue the total cost. Table 3.4 summarizes these two benefits using the distribution circuit specified in Table 5.1. First, when inverters do not participate in var control, the feeder spends a significant amount of time (e.g., 1,214 hours per year with 3% voltage drop tolerance) outside the feasibility region where voltage magnitudes violate their specified limits. Under the proposed optimal inverter var control, this undesirable

Table 3.2: Simulation Results For Some Voltage Tolerance Thresholds

Voltage Drop Tolerance	Annual Hours Saved Spending Outside Feasibility Region	Average Power Saving
3%	1,214h	2.04%
4%	223h	2.24%
5%	37h	2.53%

operation mode is completely eliminated. Second, the optimal control yields significant savings (above 2 %), as measured by the total cost that includes the inverter real power loss. Note that the savings in total cost are calculated only for times where both the unity power factor control and the optimal control are feasible. As the voltage drop tolerance decreases, the unity power factor control becomes infeasible more often while the optimal control remains feasible, but the corresponding savings are excluded in the calculation.

3.5 Case study: multiple inverter interactions

We investigate the interactions of multiple solar PV inverters in voltage regulation on a different feeder of Southern California Edison. The Fontana feeder is a 12 kV distribution system about one mile from the local substation. The entire length of the interconnected distribution circuit is 7.8 miles including all mainline and branch circuits. Voltage regulation of the circuit is accomplished by switched capacitor banks placed along the length of the mainline of the distribution circuit. The capacitors are controlled using a time schedule with a voltage override. The voltage override operating set points are adjusted automatically if the ambient temperature, measured at the capacitor bank controller, is above 90 F. Voltage regulation at the substation is also accomplished using switched capacitors located at the substation. The capacitors at the substation are operated to both regulate the voltage at the substation bus bars and compensate var flows in the subtransmission system.
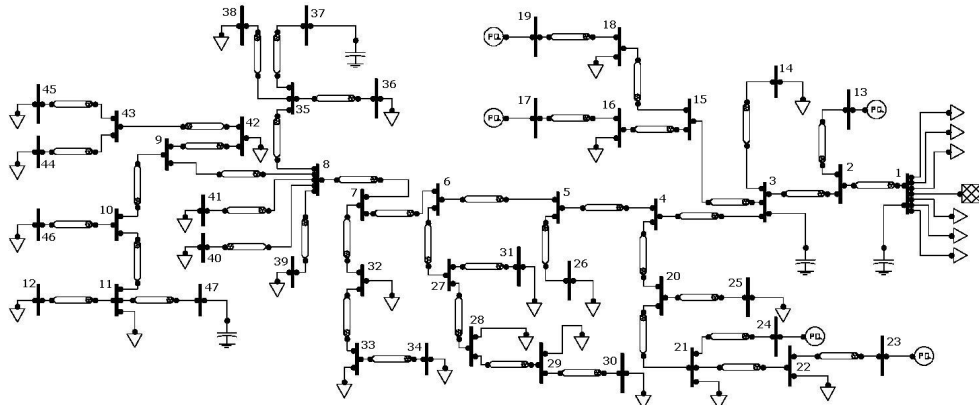
Figure 3.11: Schematic diagram of a distribution feeder with high penetration of Photovoltaics. Bus No. 1 is the substation bus and the 6 loads attached to it model other feeders on this substation.

Table 3.3: Network of Fig. 3.11: Line impedances, peak spot load KVA, capacitors, and PV generation's nameplate ratings.

Network Data																	
Line Data				Line Data				Line Data				Load Data		Load Data		PV Generators	
From Bus.	To Bus.	R (Ω)	X (Ω)	From Bus.	To Bus.	R (Ω)	X (Ω)	From Bus.	To Bus.	R (Ω)	X (Ω)	Bus No.	Peak MVA	Bus No.	Peak MVAR	Bus No.	Nameplate Capacity
1	2	0.259	0.808	8	41	0.107	0.031	21	22	0.198	0.046	1	30	34	0.2		
2	13	0	0	8	35	0.076	0.015	22	23	0	0	11	0.67	36	0.27	13	1.5MW
2	3	0.031	0.092	8	9	0.031	0.031	27	31	0.046	0.015	12	0.45	38	0.45	17	0.4MW
3	4	0.046	0.092	9	10	0.015	0.015	27	28	0.107	0.031	14	0.89	39	1.34	19	1.5 MW
3	14	0.092	0.031	9	42	0.153	0.046	28	29	0.107	0.031	16	0.07	40	0.13	23	1 MW
3	15	0.214	0.046	10	11	0.107	0.076	29	30	0.061	0.015	18	0.67	41	0.67	24	2 MW
4	20	0.336	0.061	10	46	0.229	0.122	32	33	0.046	0.015	21	0.45	42	0.13	Shunt Capacitors	
4	5	0.107	0.183	11	47	0.031	0.015	33	34	0.031	0	22	2.23	44	0.45	Bus No.	Nameplate Capacity
5	26	0.061	0.015	11	12	0.076	0.046	35	36	0.076	0.015	25	0.45	45	0.2	1	6000 KVAR
5	6	0.015	0.031	15	18	0.046	0.015	35	37	0.076	0.046	26	0.2	46	0.45	3	1200 KVAR
6	27	0.168	0.061	15	16	0.107	0.015	35	38	0.107	0.015	28	0.13	Base Voltage (KV) = 12.35		37	1800 KVAR
6	7	0.031	0.046	16	17	0	0	42	43	0.061	0.015	29	0.13	Base KVA = 1000		47	1800 KVAR
7	32	0.076	0.015	18	19	0	0	43	44	0.061	0.015	30	0.2	Substation Voltage = 12.35			
7	8	0.015	0.015	20	21	0.122	0.092	43	45	0.061	0.015	31	0.07				
8	40	0.046	0.015	20	25	0.214	0.046					32	0.13				
8	39	0.244	0.046	21	24	0	0					33	0.27				

Figure 3.12: Joint distribution of the normalized solar output level and the normalized load level

3.5.1 Simulation setup

In this section we present an example to illustrate the effectiveness of our fast-timescale VVC control, compared with the current PV integration standards IEEE 1547 which require all the inverters to operate at unity power factor and not participate in VAR control of the distribution circuit [67].

We use the 47-bus distribution feeder shown in Fig. 3.11 in our simulations. This circuit is a simplified model of an industrial distribution feeder of SCE with high penetration of renewables, integrated with 5 large PV plants. The network data, including line impedances, peak MVA demand of loads, and the nameplate capacity of the shunt capacitors and the PV generations, are listed in table 3.3. For all the loads in this industrial area, we assume a constant power factor of 0.8.

To focus on the fast-timescale control, we fix the trajectory of slow-timescale control $(v_0(T), c(T),$

$T = 1, \ldots, M)$ to be the settings used in practice, and only solve problem (3.14)–(3.15) for each time t. We use real data for load and solar generation over the course of a year. Using minute based data for one year, the empirical joint probability
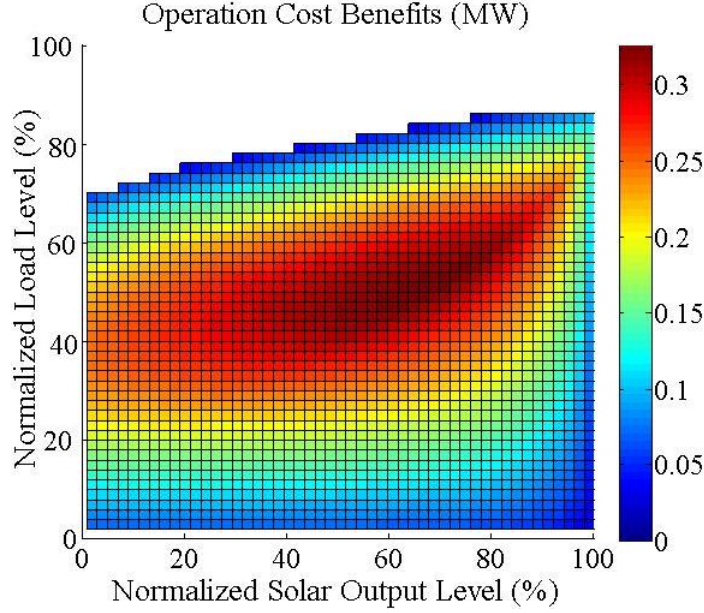
Figure 3.13: Overall power savings in MW, for different load and solar output levels assuming a 3% voltage drop tolerance.

distribution of the load and solar output levels is shown in Figure 3.12. We have used a hot color scale, with hotter colors representing a higher probability for the system to spend time in. The axes are scaled to the peak power demand and total capacity of installed PV generation, respectively. We assume $n_i = 1$ for all loads, corresponding to a constant current load model for this feeder. We further constrain the reactive power flow through the substation bus to be less than 2MVAR at all times. To compare the cost of the operation under the IEEE 1547 standard and our proposed algorithm, we choose a fixed voltage drop tolerance.

We implemented the proposed convex relaxation of the original VVC optimization problem and solved it using CVX optimization toolbox [69] in Matlab. In all our simulations, we checked the inequality constraint in condition (3.28) for optimal solutions of the relaxed problem and confirmed that the inequality constraints were all active. Figure 3.13 shows the difference in the objective function between current standard IEEE 1547 standard and our proposed solution for different load and solar output levels, given a 3% voltage drop tolerance. This can be interpreted as the overall power savings achieved by optimal control of inverter's VAR dispatch. Interestingly, in typi-

Table 3.4: Simulation Results For Some Voltage Tolerance Thresholds

Voltage Drop Tolerance	Annual Hours Saved Spending Outside Feasibility Region	Average Power Saving
3%	842.9h	3.93%
4%	160.7h	3.67%
5%	14.5h	3.62%

cal loading conditions, optimal inverter control can save more than 200KW in overall power consumption, even at night. The missing region in Figure 3.13 is the set of the infeasible settings of load and solar for the IEEE 1547 operation mode in the relaxed problem formulation, and is therefore also infeasible for the original problem. The feasible operation region for the proposed method is considerably a superset of that of IEEE 1547 operation mode. This demonstrates significant power quality benefits achieved by optimal inverter control. Table 3.4 summarizes the overall time that the feeder can save not spending outside the feasible region, and the overall operation cost benefits for the whole year, for different voltage drop tolerances. The results show more than 3% savings achieved by optimal reactive power dispatch for the inverters.

3.6   Conclusion

We discussed a general framework for optimal reactive power dispatch of inverters and switched controllers in radial networks by considering different time scale of variations in load and the output of intermittent renewable sources. Our proposed centralized solution for the fast time-scale subproblem demonstrated the benefits of inverter var control to mitigate rapid and large voltage fluctuations due to high penetration of photovoltaic generation and the resulting reverse power flow. We have formulated the fast time-scale subproblem as a radial OPF problem that minimizes line losses, internal inverter losses, and energy consumption (CVR term), subject to operational constraints on voltage magnitudes and var injections. We adopt the SOCP relaxation of the BFM model discussed in the previous chapter to solve the resulting nonconvex problem efficiently. Finally, we illustrated the improvement in both reliability and

efficiency under the optimal inverter var control on two cases of SCE's distribution feeders with very high PV penetration.

Chapter 4

Equilibrium and Dynamics of Local Voltage Control in Distribution Networks

4.1 Introduction

As previously discussed, traditionally voltages in a primary distribution system fluctuate slowly due to changes in demand which are relatively mild and predictable. Capacitor banks and under load tap changers (ULTC) are reconfigured a few times a day to stabilize voltages around their nominal values; see, e.g., [70, 44, 51]. The continued proliferation of distributed generation such as photovoltaic will introduce frequent, rapid, and random fluctuations in supply and voltages in a primary distribution system. Capacitor banks and ULTC alone may not be adequate to stabilize voltages in such an environment. Distributed energy resources such as photovoltaic systems are connected to the grid through inverters. Even though the current IEEE Standard 1547 requires unity power factor at the output of an inverter, the inverter hardware can easily optimize its reactive power output to help stabilize voltages. Indeed the IEEE Standards group is actively exploring a new inverter-based volt/var control. Unlike the capacity banks or ULTC, inverters can push and pull reactive power much faster, in a much finer granularity, and with low operation costs; see, e.g., [2, 3, 4]. They will enable the realtime distributed volt/var control that is needed for the future power grid.

The literature on inverter-based volt/var control in distribution systems can be divided into the following three main categories: (i) approaches that propose a centralized control scheme by solving a global optimal power flow (OPF) problem. These methods implicitly assume an underlying complete two-way communication system between a central computing authority and the controlled nodes [4, 11, 12]; (ii) distributed message-passing algorithms in which communications are limited to neighboring nodes [5, 13, 12, 14]; (iii) local control methods that require no communications and rely only on local measurements and computations [3, 6, 15]. These include reactive power control based on local real power injection (referred to as Q(P)), power factor control, and the more common voltage based reactive power control (referred to as Q(V)). Although the methods proposed in the first two categories are critical for theoretical analysis and better understanding the impact of renewables on the grid, lack of sufficient telecommunication infrastructure discourages practical implementation of these methods in most practical scenarios.

Inverter-based local volt/var control is a closed-loop dynamical system whereby the measured voltage determines the reactive power injection, which in turn affects the voltage. There has been only a limited theoretical treatment of the equilibrium and dynamic properties of such feedback systems; see, e.g., [17, 71, 72]. In this chapter we study these local volt/var control schemes that are motivated by the proposed 1547.8 standard [73]. We use a linear branch flow model similar to the *Simplified DistFlow equations* introduced in [43]. The linear branch flow model and the local volt/var control form a closed loop dynamical system (Section 4.2). We show that the dynamical system has a unique equilibrium point and characterize it as the unique optimal solution of a certain convex optimization problem (Section 4.3). The optimization problem has a simple interpretation: the local volt/var control tries to achieve an optimal tradeoff between minimizing the cost of voltage deviations and minimizing the cost of reactive power provisioning. Moreover, the objective of the optimization problem serves as a Lyapunov function of the dynamical system under local volt/var control, implying global asymptotic stability of the equilibrium. We further provide a sufficient condition under which the dynamical system yields a con-

traction mapping, implying that it converges exponentially fast to the equilibrium. We apply these results to study the inverter-based volt/var control in IEEE 1547.8 standard[73], and discuss how to set the parameters for the proposed control functions (Section 4.4). The optimization-based model not only provides a way to characterize the equilibrium and establish the convergence of the local volt/var control, but also suggests a principled way to engineer the control. New design goals such as fairness and economic efficiency can be revised by engineering the global objective function in the optimization problem; and new control schemes with better dynamical properties can be designed based on various optimization algorithms, e.g., the gradient algorithms.

4.2   Network model and local voltage control

Consider a tree graph $G = \{\mathcal{N} \cup \{0\}, \mathcal{L}\}$ that represents a radial distribution network consisting of $n + 1$ buses and a set $\mathcal{L}$ of lines between these buses. Bus 0 is the substation bus and is assumed to have a fixed voltage. Let $\mathcal{N} := \{1, \ldots, n\}$. For each bus $i \in \mathcal{N}$, denote by $\mathcal{L}_i \subseteq \mathcal{L}$ the set of lines on the unique path from bus 0 to bus i, p_i^c and p_i^g the real power consumption and generation, and q_i^c and q_i^g the reactive power consumption and generation, respectively. Let v_i be the magnitude of the complex voltage (phasor) at bus i. For each line $(i, j) \in \mathcal{L}$, denote by r_{ij} and x_{ij} its resistance and reactance, and P_{ij} and Q_{ij} the real and reactive power from bus i to bus j, respectively. Let ℓ_{ij} denote the squared magnitude of the complex branch current (phasor) from bus i to bus j. These notations are summarized in Table 4.1. Note that a quantity without subscript is usually a vector with appropriate components defined earlier, e.g., $v := (v_i, i \in \mathcal{N}), q^g := (q_i^g, i \in \mathcal{N})$.

Table 4.1: Notations.

t	time index, $t \in \mathcal{T} := \{1, \ldots, T\}$
$\mathcal{N}$	set of buses excluding bus 0, $\mathcal{N} := \{1, \ldots, n\}$
$\mathcal{L}$	set of power lines
$\mathcal{L}_i$	set of the lines form bus 0 to bus i
p_i^c, q_i^c	real, reactive power consumption at bus i
p_i^g, q_i^g	real, reactive power generation at bus i
P_{ij}, Q_{ij}	real and reactive power flow from i to j
r_{ij}, x_{ij}	resistance and reactance of line (i, j)
V_i	complex voltage at bus i
v_i	$v_i := |V_i|^2, \quad i \in \mathcal{N}$
I_{ij}	complex current from i to j
ℓ_{ij}	$\ell_i := |I_{ij}|^2, \quad (i, j) \in \mathcal{L}$
$\beta(j) \subset \mathcal{N}$	Set of all descendants of bus j, $\beta(j) = \{i | \mathcal{L}_j \subseteq \mathcal{L}_i\}$
x^+	positive part, $x^+ = max\{0, x\}$
$[x]_a^b$	$[x]_a^b = x + (a - x)^+ - (x - b)^+$
λ_{max}	the maximum eigenvalue

4.2.1 Linearized branch flow model

We adopt the following branch flow model introduced in [44, 70] (called *DistFlow equations* there) to model a *radial* distribution system:

$$P_{ij} = p_j^c - p_j^g + \sum_{k:(j,k)\in\mathcal{L}} P_{jk} + r_{ij}\ell_{ij}, \tag{4.1a}$$

$$Q_{ij} = q_j^c - q_j^g + \sum_{k:(j,k)\in\mathcal{L}} Q_{jk} + x_{ij}\ell_{ij}, \tag{4.1b}$$

$$v_j^2 = v_i^2 - 2(r_{ij}P_{ij} + x_{ij}Q_{ij}) + (r_{ij}^2 + x_{ij}^2)\ell_{ij}, \tag{4.1c}$$

$$\ell_{ij}v_i = P_{ij}^2 + Q_{ij}^2. \tag{4.1d}$$

Following [43] we assume $\ell_{ij} = 0$ for all $(i, j) \in \mathcal{L}$ in (4.1). This approximation neglects the higher order real and reactive power loss terms. Since losses are typically much smaller than power flows P_{ij} and Q_{ij}, it only introduces a small relative error, typically on the order of 1%. We further assume that $v_i \approx 1$ so that we can set $v_j^2 - v_i^2 = 2(v_j - v_i)$ in equation (4.1c). This approximation introduces a small relative error of at most 0.25% (1%) if there is a 5% (10%) deviation in voltage magnitude.

With the above approximations the model (4.1) simplifies to the following linear model [43]:

$$P_{ij} = \sum_{k \in \beta(j)} \left(p_k^c - p_k^g \right),$$

$$Q_{ij} = \sum_{k \in \beta(j)} \left(q_j^c - q_j^g \right),$$

$$v_i - v_j = r_{ij} P_{ij} + x_{ij} Q_{ij}$$

where $\beta(j)$ is the set of all descendants of node j including node j itself, i.e., $\beta(j) = \{i | \mathcal{L}_j \subseteq \mathcal{L}_i\}$. This yields an explicit solution for v_i in terms of v_0 (which is given and fixed):

$$v_0 - v_i = \sum_{(j,k) \in \mathcal{L}_i} r_{jk} P_{jk} + \sum_{(j,k) \in \mathcal{L}_i} x_{jk} Q_{jk}$$

$$= \sum_{(j,k) \in \mathcal{L}_i} r_{jk} \left(\sum_{h \in \beta(k)} \left(p_h^c - p_h^g \right) \right) + \sum_{(j,k) \in \mathcal{L}_i} x_{jk} \left(\sum_{h \in \beta(k)} \left(q_h^c - q_h^g \right) \right)$$

$$= \sum_{j \in \mathcal{N}} \left(p_j^c - p_j^g \right) \left(\sum_{(h,k) \in \mathcal{L}_i \cap \mathcal{L}_j} r_{hk} \right) + \sum_{j \in \mathcal{N}} \left(q_j^c - q_j^g \right) \left(\sum_{(h,k) \in \mathcal{L}_i \cap \mathcal{L}_j} x_{hk} \right)$$

$$= \sum_{j \in \mathcal{N}} R_{ij} \left(p_j^c - p_j^g \right) + \sum_{j \in \mathcal{N}} X_{ij} \left(q_j^c - q_j^g \right)$$

where

$$R_{ij} := \sum_{(h,k) \in \mathcal{L}_i \cap \mathcal{L}_j} r_{hk},$$

$$X_{ij} := \sum_{(h,k) \in \mathcal{L}_i \cap \mathcal{L}_j} x_{hk} \tag{4.2}$$

Figure 4.1 gives an illustration of $\mathcal{L}_i \cap \mathcal{L}_j$ for two arbitrary buses i and j in
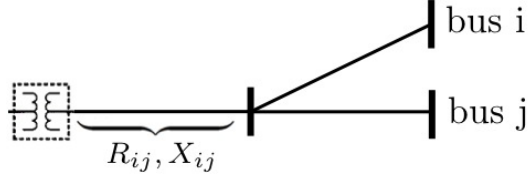
Figure 4.1: $\mathcal{L}_i \cap \mathcal{L}_j$ for two arbitrary buses i, j in the network and the corresponding mutual voltage-to-power-injection sensitivity factors R_{ij}, X_{ij}

a radial network and the corresponding R_{ij} and X_{ij}[1]. Define a resistance matrix $R = [R_{ij}]_{n \times n}$ and a reactance matrix $X = [X_{ij}]_{n \times n}$. Both matrices are symmetric. Using the matrices R and X the linearized branch flow model can be summarized compactly as

$$v = \overline{v}_0 + R(p^g - p^c) + X(q^g - q^c),$$

where $\overline{v}_0 = (v_0, \ldots, v_0)$ is an n-dimensional vector. In this chapter we assume that $\overline{v}_0, p^c, p^g, q^c$ are given constants. The only variables are (column) vectors $v := (v_1, \ldots, v_n)$ of squared voltage magnitudes and $q^g := (q_1^g, \ldots, q_n^g)$ of reactive powers. Let $\tilde{v} = \overline{v}_0 + R(p^g - p^c) - Xq^c$, which is a constant vector. For notational simplicity in the rest of the chapter we will ignore the superscript in q^g and write q instead. Then the linearized branch flow model reduces to the following simple form:

$$v = Xq + \tilde{v}. \tag{4.3}$$

The following result is important for the rest of this chapter.

Lemma 2. *The matrices R and X are positive definite.*

Proof. The proof will use the fact that the values of resistances and reactances of power lines in the network are all positive. Here we give a proof for the reactance matrix X, and exactly the same argument applies to the resistance matrix R.

---

[1]Since

$$R_{ij} = \frac{dv_i}{dp_j^g} = -\frac{dv_i}{dp_j^c},$$
$$X_{ij} = \frac{dv_i}{dq_j^g} = -\frac{dv_i}{dq_j^c},$$

we refer to R_{ij}, X_{ij} as the mutual voltage-to-power-injection sensitivity factors.

We prove by induction on the number k of buses in the network, excluding bus 0 (the root bus). The base case of $k = 1$ corresponds to a two-bus network with one line. Here X is obviously a positive scalar that is equal to the reactance of the line connecting the two buses.

Suppose that the theorem holds for all $k \leq n$. For the case of $k = n + 1$ we consider two possible network topologies as shown in Figure 4.2:

(a) Case1: degree of bus 0 is greater than 1

(b) Case 2: degree of bus 0 is 1
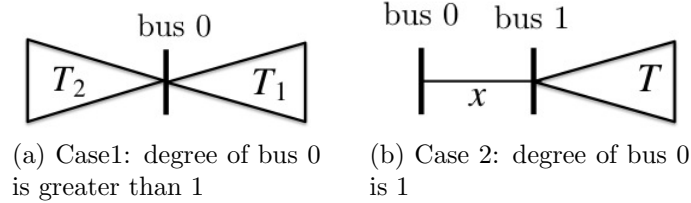
Figure 4.2: Two possible network structures

Case 1: bus 0 is of degree greater than 1. Split the network into two different trees rooted at bus 0, denoted by T_1 and T_2, each of which has no more than n buses excluding bus 0. Denote by Y and Z, respectively, the reactance matrices of T_1 and T_2. By induction assumption Y and Z are positive definite. Note that the set $\mathcal{L}_i$ of lines on the unique path from bus 0 to bus i must completely lie inside either T_1 or T_2, for all i. Therefore, by definition (4.2), the reactance matrix X of the network has the following block-diagonal form:

$$
X_{ij} = \begin{cases} Y_{ij}, & i, j \in T_1 \\ Z_{ij}, & i, j \in T_2 \\ 0, & \text{otherwise} \end{cases} \quad \Rightarrow \quad X = \begin{bmatrix} Y & 0 \\ 0 & Z \end{bmatrix}.
$$

Since Y and Z are positive definite, so is X.

Case2: bus 0 is of degree 1. Suppose without loss of generality that bus 0 is connected to bus 1. Denote by x the reactance of the line connecting buses 0 and 1, and T the tree rooted at bus 1. Tree T has $n - 1$ buses excluding bus 1 (i.e., its root bus). Denote by Y the reactance matrix of T, and by induction assumption, Y is positive definite. Note that, for all nodes i in the network, the set $\mathcal{L}_i$ includes the

single line that connects buses 0 and 1. Therefore, by definition (4.2), the reactance matrix X has the following form:

$$X_{ij} = \begin{cases} Y_{ij} + x, & i, j \in T^- \\ x, & \text{otherwise} \end{cases} \Rightarrow X = \begin{bmatrix} x & \dots x \\ \vdots & \vdots \\ x & \dots x \end{bmatrix} + \begin{bmatrix} 0 & 0 \\ 0 & Y \end{bmatrix},$$

where T^- denotes the set of nodes in tree T excluding the root bus 1. It is straightforward to verify that, when Y is positive definite and x is positive, X is positive definite. This concludes the proof. $\qquad\square$

4.2.2 Local volt/var control

The goal of volt/var control on a distribution network is to provision reactive power injections $q := (q_1, \dots, q_n)$ in order to maintain the bus voltages $v := (v_1, \dots, v_n)$ to within a tight range around their nominal values v_i^{nom}, $i \in \mathcal{N}$. This can be modeled by a feedback dynamical system with state $(v(t), q(t))$ at discrete time t. A general volt/var control algorithm maps the current state $(v(t), q(t))$ to a new reactive power injections $q(t+1)$. The new $q(t+1)$ produces a new voltage magnitudes $v(t+1)$ according to (4.3). Motivated by the IEEE 1547.8 Standard [9, 10], we consider a class of local volt/var control algorithms where each bus i makes an individual decision $q_i(t+1)$ based only on its own voltage $v_i(t)$.

Definition 4.1. *A local volt/var control function $f : \mathbb{R}^n \to \Omega$ is a collection of $f_i : \mathbb{R} \to \Omega_i$ functions that map the current voltage $v_i(t)$ to a new local control $q_i(t+1)$:*

$$q_i(t+1) = f_i(v_i(t)), \quad \forall i \in \mathcal{N}, \tag{4.4}$$

where $\Omega = \prod_{i=1}^{n} \Omega_i$, with $\Omega_i = \{q_i \mid q_i^{\min} \leq q_i \leq q_i^{\max}\}$ the set of feasible reactive power injections at each bus $i \in \mathcal{N}$.

The control algorithm (4.4) is **non-incremental** as the current decision does not

depend directly on the decision at the previous time. We obtain the following dynamical system that models the non-incremental local volt/var control of a distribution network:

$$D1: \left| \begin{array}{rcl} v^{(t)} & = & Xq^{(t)} + \tilde{v}, \\ q^{(t+1)} & = & f(v^{(t)}). \end{array} \right. \tag{4.5}$$

A fixed point (v^*, q^*) of the above dynamical system represents an equilibrium operating point of the network.

Definition 4.2. (v^*, q^*) *is called an* equilibrium point, *or a* network equilibrium, *if it is a fixed point of* (4.5), *i.e.,*

$$\begin{array}{rcl} v^* & = & Xq^* + \tilde{v}, \\ q^* & = & f(v^*). \end{array} \tag{4.6}$$

4.3 Reverse Engineering Local Voltage Control in Radial Networks

In this section we will reverse engineer the local voltage control in radial networks by showing that the dynamical system $D1$ can be seen as a distributed algorithm for solving a well-defined convex optimization problem under appropriate conditions. Let us start by characterizing the equilibrium points.

4.3.1 Network equilibrium

The local volt/var control functions $f_i(\cdot)$ are usually decreasing, but are not always strictly monotone because of the deadband in control as well as the bounds on the available reactive power. We assume for each bus $i \in \mathcal{N}$ a symmetric deadband around the nominal voltage $(v_i^{\mathrm{nom}} - \delta_i/2, v_i^{\mathrm{nom}} + \delta_i/2)$, with $\delta_i \geq 0$. In the rest of this chapter we will make the following two assumptions:

A1: The local volt/var control functions f_i are nonincreasing over $\mathbb{R}$ and strictly decreasing and differentiable in $(\underline{v}_i, -\delta_i/2)$ and in $(\delta_i/2, \overline{v}_i)$.

A2: The derivative of the control function f_i is bounded, i.e., there exists a finite α_i such that $|f_i'(v_i)| \leq \alpha_i$ for all v_i in the appropriate domain, for all $i \in \mathcal{N}$. This assumption means that an infinitesimal change in voltage should not lead to a jump in reactive power.

Since f_i is nonincreasing a (generalized) inverse f_i^{-1} exists over $(q_i^{\min}, q_i^{\max})$. In particular, at the end points, we have

$$f^{-1}\left(q_i^{\min}\right) := \overline{v}_i \quad \text{and} \quad f^{-1}(q_i^{\max}) := \underline{v}_i$$

and, at the origin, we assign $f^{-1}(0) = 0$ in the deadband $[-\delta_i/2, +\delta_i/2]$. This may introduce a discontinuity at $q_i = 0$. See Figure 4.3 for an example f_i and Figure 4.4 for its inverse f_i^{-1}.

Define a cost function for each bus $i \in \mathcal{N}$:

$$C_i(q_i) \quad := \quad -\int_0^{q_i} f_i^{-1}(q)\, dq.$$

This function is convex since f_i^{-1} is decreasing. Then, given any $v_i(t)$, $q_i(t+1)$ in (4.4) is the unique solution of a simple distributed optimization:

$$q_i(t+1) \quad = \quad \operatorname*{argmin}_{q_i \in \Omega_i} C_i(q_i) + q_i v_i(t), \tag{4.7}$$

i.e., (4.4) and (4.7) are equivalent specification of $q_i(t+1)^2$.

---

[2]They are equivalent specifications even if $v_i(t) - v_i^{\mathrm{norm}}$ falls inside the deadband, i.e., if $|v_i(t) - v_i^{\mathrm{norm}}| < \delta_i/2$. Under this situation, the set of subgradients of $C_i(q_i) + q_i(v_i(t) - v_i^{\mathrm{nom}})$ at $q_i = 0$

$$\left[-\frac{\delta_i}{2} + (v_i(t) - v_i^{\mathrm{norm}}), \frac{\delta_i}{2} + (v_i(t) - v_i^{\mathrm{norm}})\right]$$

contains 0, which is exactly the optimality condition at $q_i = 0$, and hence $q_i(t+1) = 0$. In the following we ignore such subdifferentiability issue with the understanding that subgradients should be used in place of gradients where functions are not differentiable.

Now let us define the function $F : \Omega \to \mathbb{R}$:

$$F(q) \quad := \quad C(q) + \frac{1}{2} q^T X q + q^T \tilde{v}$$

where $C(q) = \sum_{i \in \mathcal{N}} C_i(q_i)$ and $\tilde{v} := \tilde{v} - v^{\mathrm{norm}}$, and the global optimization problem:

$$\min_{q \in \Omega} \quad F(q). \tag{4.8}$$

Theorem 4.1. *Suppose A1 holds. Then there exists a unique equilibrium point. Moreover a point (v^*, q^*) is an equilibrium if and only if q^* is the unique optimal solution of (4.8) and $v^* = X q^* + \tilde{v}$.*

Proof. From Lemma 2 the matrix X is positive definite. This implies that the objective function $F(q)$ is strictly convex. Hence the first order optimality condition for (4.8) is both necessary and sufficient; moreover (4.8) has a unique optimal solution. We now relate it to the equilibrium point.

The gradient of F is the (column) vector

$$\nabla F(q) \quad = \quad \nabla C(q) + X q + \tilde{v}$$

where, from the definition of $C_i(q_i)$,

$$\nabla C(q) \quad = \quad \left[-f_1^{-1}(q_1) \quad \cdots \quad -f_n^{-1}(q_n) \right]^T.$$

Hence the first order optimality condition for (4.8) is:

$$q_i^* = f_i \left(X q^* + \tilde{v} \right).$$

Hence a point (v^*, q^*) is an equilibrium if and only if q^* solves (4.8) and $v^* = X q^* + \tilde{v}$. The existence and uniqueness of the optimal solution of (4.8) then implies that of the equilibrium (v^*, q^*). $\qquad \square$

With $v = Xq + \tilde{v}$, the objective can be written as $F(q, v) = C(q) + \frac{1}{2}v^T X^{-1} v + \frac{1}{2}\tilde{v}^T X^{-1}\tilde{v}$. Note that the last term is a constant. Therefore the local volt/var control D1 tries to achieve an optimal trade-off between minimizing the cost $\frac{1}{2}(v - v^{nom})^T X^{-1}(v - v^{nom})$ of voltage deviation and minimizing the cost $C(q)$ of reactive power provisioning.

4.3.2 Dynamics

We now study the dynamic properties of local volt/var control D1.

Theorem 4.2. *Suppose A1–A2 hold. if*

$$C1: \quad A^{-1} := \mathrm{diag}\left(\frac{1}{\alpha_i}\right) \succ X, \tag{4.9}$$

i.e., if the matrix $\mathrm{diag}(\alpha_i^{-1}) - X$ is positive definite, then local volt/var control dynamic D1 converges to the unique equilibrium point (v^*, q^*).

Proof. Recall that $C(q) = \sum_{i \in \mathcal{N}} C_i(q_i)$. Its Hessian

$$\nabla^2 C(q) = \mathrm{diag}\left(-\frac{\partial f_i^{-1}(q_i)}{\partial q_i}\right).$$

By assumptions A1–A2 we have

$$\nabla^2 C(q) \succeq \mathrm{diag}\left(\frac{1}{\alpha_i}\right). \tag{4.10}$$

By the second order Taylor expansion,

$$
\begin{aligned}
&F\left(q(t+1)\right)\\
&= C(q(t+1)) + \frac{1}{2}q^T(t+1)Xq(t+1) + q^T(t+1)\tilde{v}\\
&= C(q(t)) + (\nabla C(q(t+1)))^T(q(t+1) - q(t))\\
&\quad -\frac{1}{2}(q(t+1) - q(t))^T\nabla^2 C(\tilde{q})(q(t+1) - q(t))\\
&\quad +\frac{1}{2}q^T(t)Xq(t) + (q(t+1) - q(t))^T Xq(t)\\
&\quad +\frac{1}{2}(q(t+1) - q(t))^T X(q(t+1) - q(t))\\
&\quad +q^T(t)\tilde{v} - (q(t+1) - q(t))^T\tilde{v}\\
&\leq F(q(t))\\
&\quad +(\nabla C(q(t+1)) + Xq(t) + \tilde{v})^T(q(t+1) - q(t))\\
&\quad -\frac{1}{2}(q(t+1) - q(t))^T\left(\mathrm{diag}\left(\alpha_i^{-1}\right) - X\right)(q(t+1) - q(t))\\
&\leq F(q(t))\\
&\quad -\frac{1}{2}(q(t+1) - q(t))^T\left(\mathrm{diag}\left(\alpha_i^{-1}\right) - X\right)(q(t+1) - q(t)),
\end{aligned}
$$

$$(4.11)$$

where $\tilde{q} \in \{q \in \Omega \mid q = \theta q(t) + (1-\theta)q(t+1), 0 \leq \theta \leq 1\}$, the first inequality follows from (4.10), and the last inequality follows from (4.7).

Since $\mathrm{diag}\left(\alpha_i^{-1}\right) \succ X$, the second term in (4.11) is strictly negative as long as $q(t+1) \neq q(t)$ and zero only if $q(t+1) = q(t)$. Since the fixed point to dynamic D1 is unique by Theorem 4.1, $q(t+1) = q(t)$ can only occur at the unique fixed point q^* (with $v^* = Xq^* + \tilde{v}$).

Thus we have shown the following:

- $F(q) \geq F(q^*)$ with equality if and only if $q = q^*$ by Theorem 4.1,

- $F(q(t+1)) \leq F(q(t))$ with equality if and only if $q(t+1) = q(t) = q^*$,

i.e., F is a discrete-time Lyapunov function for D1. Moreover one can extend the domain of each f_i^{-1} from $[q_i^{\min}, q_i^{\max}]$ to $\mathbb{R}$ in such a way that the above properties

hold in the entire space and F is radially unbounded. The Lyapunov stability theorem then implies that q^* is globally asymptotically stable. $\qquad\square$

Since X is not only a positive definite matrix but also a positive matrix, $\mathrm{diag}(\sum_{j \in \mathcal{N}} X_{ij}) \succeq X$. This leads to a sufficient condition for the convergence of the local volt/var control.

Corollary 3. *Suppose A1–A2 hold. If for all $i \in \mathcal{N}$*

$$\alpha_i \sum_j X_{ij} \quad < \quad 1, \tag{4.12}$$

then local volt/var control D1 converges to the unique equilibrium point (v^*, q^*). Moreover, it converges exponentially fast to the equilibrium.

Proof. By condition (4.12), $\mathrm{diag}\left(\alpha_i^{-1}\right) \succ \mathrm{diag}\left(\sum_{j \in \mathcal{N}} X_{ij}\right)$. Since X is a positive definite as well as positive matrix, $\mathrm{diag}\left(\sum_{j \in \mathcal{N}} X_{ij}\right) - X$ is diagonally dominant with non-negative diagonal entries, and is thus positive semidefinite. Thus $diag\left(\alpha_i^{-1}\right) \succ X$. By Theorem 4.2, D1 converges to the equilibrium point (v^*, q^*). Now consider the equivalent system to the dynamic D1:

$$q(t+1) \quad = \quad f(Xq(t) + \tilde{v}) \quad =: \quad g(q(t)).$$

We have

$$\frac{\partial g}{\partial q} \quad = \quad \mathrm{diag}(f_i'(v_i)) \, X$$

with $v_i := \sum_j X_{ij} q_j + \tilde{v}_i$. Condition (4.12) implies

$$\left\| \frac{\partial g}{\partial q} \right\|_\infty \quad < \quad 1,$$

where the induced matrix norm $\| \cdot \|_\infty$ is the maximum row sum. Hence

$$\| g(q) - g(\hat{q}) \|_\infty \quad \leq \quad \left\| \frac{\partial g}{\partial q} \right\|_\infty \cdot \| q - \hat{q} \|_\infty \quad < \quad \| q - \hat{q} \|_\infty,$$

i.e., g is a contraction. This implies that $(v(t), q(t))$ converges exponentially fast to the unique equilibrium point of D1. □

The following result is immediate.

Corollary 4. *if* $\max\{\alpha_i\} < \frac{1}{\lambda_{max}(X)}$ *where* λ_{max} *denotes the largest eigenvalue, then local volt/var control D1 converges to the unique equilibrium point* (v^*, q^*).

Proof. If $\max\{\alpha_i\} < \frac{1}{\lambda_{max}(X)}$, we have $\operatorname{diag}\left(\frac{1}{\alpha_i}\right) \succ \lambda_{max}(X)I \succ X$. The result follows from Theorem 4.2. □

Notice that α_i can be seen as a metric for the "aggressiveness" of the voltage control: a larger α_i value corresponds to a more aggressive response to the voltage deviation. Theorem 4.2 (and Corollary 4) implies that, in order to ensure convergence, the voltage control cannot be too aggressive. Intuitively, a too aggressive response will lead to overshoot in the control and thus oscillation.

Remark 4.1. *We have reverse-engineered the local volt/var control D1, by showing that it is a distributed algorithm for solving a convex global optimization problem. The optimization based model* (4.8) *not only provide a way to characterize the equilibrium and establish the convergence of the local volt/var control, but also suggests a principled way to engineer the control. New design goals such as fairness and economic efficiency can be revised by engineering the global objective function in* (4.8); *and new control schemes with better dynamical properties can be designed based on various optimization algorithms, e.g., the gradient algorithms.*

4.4 Case study: Inverter Control in IEEE 1547.8

A particularly interesting example control function is the piecewise linear droop control in figure 4.3 , which is proposed in the latest draft of the new IEEE 1547.8 Standard [73]. This control algorithm is incremental as at each time the reactive power is "gradually" adjusted upon the provisioning at the previous time. It is also distributed, since the reactive power provisioning decision at each node $i \in \mathcal{N}$ depends

only on the current provisioning and voltage at node i. We now apply the results of Section 4.3 to study this local inverter-based volt/var control algorithm and discuss the parameter setting for the proposed functions.

4.4.1   Reverse engineering 1547.8

The IEEE 1547 is currently being extended by the standards working group (IEEE 1547.8) to specify how to use inverters to assist in power quality control by adapting their reactive power generation. The methods being discussed in the latest draft [73] are:

1. Fixed power factor: the reactive power generation is directly proportional to the real power generation. This includes the traditional mode of operation with unity power factor where inverters are not allowed to inject or absorb reactive power under normal operating conditions.

2. Variable power factor: the reactive power generation depends not only on their active power output but also to X_{ii}/R_{ii} ratio at the point of connection.

3. Voltage-based reactive power control: an inverter monitors its terminal voltage and sets its reactive power generation based on a predefined volt-var curve.

A particularly interesting example control function is the proposed piecewise linear droop control in this document [73]:

$$f_i(v_i) := \left[-\alpha_i \left(v_i - v_i^{\text{nom}} - \frac{\delta_i}{2} \right)^+ + \alpha_i \left(-v_i + v_i^{\text{nom}} - \frac{\delta_i}{2} \right)^+ \right]_{q_i^{\text{min}}}^{q_i^{\text{max}}}, \qquad (4.13)$$

where $(x)^+ = \max\{x, 0\}$, and

$$[x]_a^b = \begin{cases} a & \text{for} \quad x \le a, \\ x & \text{for} \quad a \le x \le b, \\ b & \text{for} \quad b \le x. \end{cases}$$
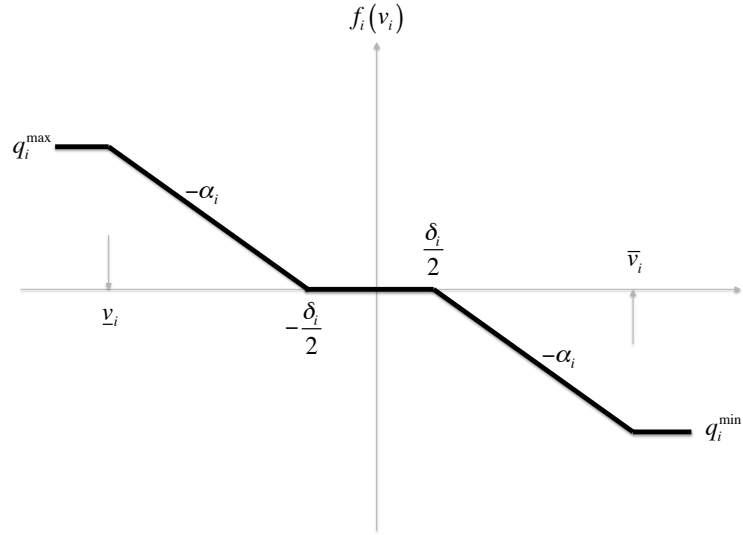
Figure 4.3: Piecewise linear volt/var control curve discussed in the latest draft of the new IEEE 1547.8 standard document.

They are specified by a deadband of width δ_i and two linear segments with a slope of $-\alpha_i$ for inverter i. In this equation, (δ_i, α_i) are the local control parameters at each bus[3].

Following the procedure described in Section 4.3.1, the inverse f_i^{-1} of the volt/var control curve over $[Q_i^{\min}, Q_i^{\max}]$ is illustrated in Figure 4.4 and given by:

$$
f_i^{-1}(q_i) \quad := \quad
\begin{cases}
-\frac{q_i}{\alpha_i} + \frac{\delta_i}{2} & \text{for } q_i \in [q_i^{\min}, 0), \\
0 & \text{for } q_i = 0, \\
-\frac{q_i}{\alpha_i} - \frac{\delta_i}{2} & \text{for } q_i \in (0, q_i^{\max}],
\end{cases}
$$

and the corresponding cost function $C_i(q_i) := \int_0^{q_i} f_i^{-1}(q) dq$ is shown in Figure 4.5 and is given by:

$$
C_i(q_i) \quad = \quad
\begin{cases}
\frac{1}{2\alpha_i} q_i^2 - \frac{\delta_i}{2} q_i & \text{if} \quad q_i \in [q_i^{\min}, 0], \\
\frac{1}{2\alpha_i} q_i^2 + \frac{\delta_i}{2} q_i & \text{if} \quad q_i \in [0, q_i^{\max}].
\end{cases}
\tag{4.14}
$$

---

[3]Here we "reload" notation, and use α_i to also denote the slope of the droop control function. It does not contradict the use of α_i in the condition A2.
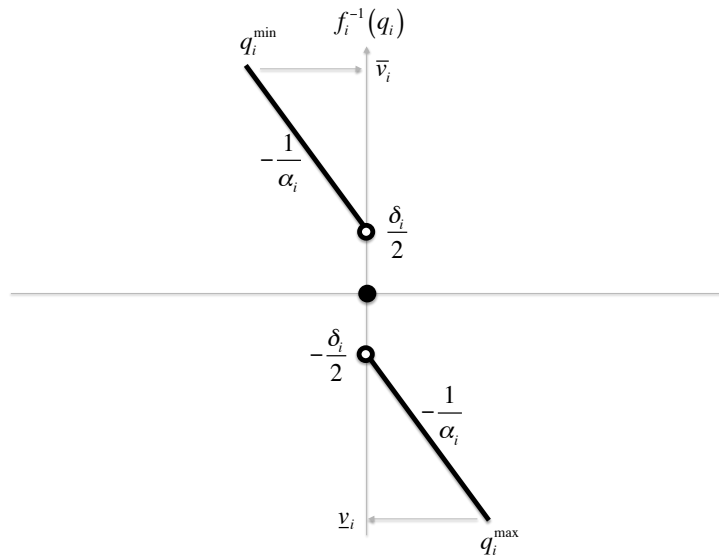
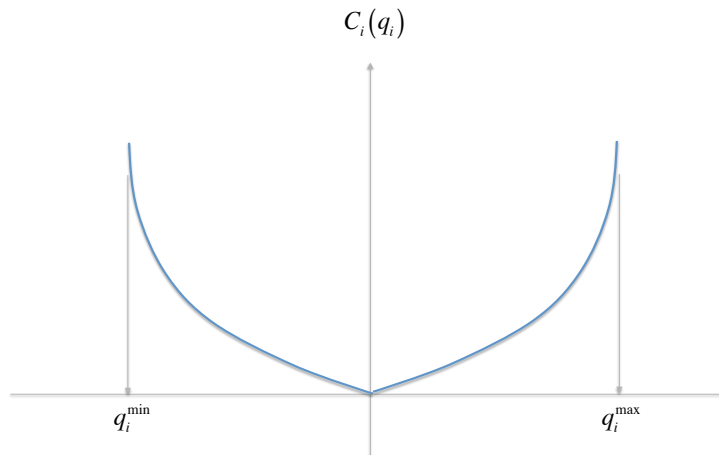Figure 4.4: The inverse f_i^{-1} of the volt/var control curve in Figure 4.3.

Figure 4.5: The cost function $C_i(q_i)$ corresponding to f_i^{-1} of Figure 4.4.

4.4.2 Parameter setting

It has been suggested to set the slope of the piecewise linear control function to $\alpha_i = 1/X_{ii}$. This is a good choice if bus i is the only bus where the inverter-based volt/var control is employed. To see this, suppose that in the beginning $v_i = \tilde{v}_i > v_i^{nom} + \delta_i/2$. Then under the control (4.13), $q_i = -(v_i - v_i^{nom} - \delta_i/2)/X_{ii}$ and $v_i = X_{ii}q_i + \tilde{v}_i = v_i^{nom} + \delta_i/2$. Therefore if the deadband δ_i is set to the range of the desired voltage, the volt/var control can bring the voltage of bus i to the desired range in just one step.

However the above choice does not take into consideration the impact of volt/var control at other buses. In particular, when the $\alpha_i = 1/X_{ii}$, condition (4.9) in Theorem 4.2 does not hold, and the local control 4.13 may not converge to the equilibrium point. Instead, by Corollary 3, a convenient choice for α_i is to set $\alpha_i = (\sum_{j \in \mathcal{N}} X_{ij} + \epsilon)^{-1}$, where $\epsilon > 0$ can be used to control the convergence speed and a larger ϵ leads to faster response. Intuitively X_{ij} characterizes the sensitivity of bus j's voltage to reactive power injected at bus i, so if a bus has a larger impact to other buses (including itself), it should control its reactive power more cautiously, i.e., use a smaller α_i.

On the other hand, as mentioned in Section 4.3.1, the local volt/var control tries to achieve an optimal tradeoff between minimizing the cost $\frac{1}{2}(v - v^{nom})^T X^{-1}(v - v^{nom})$ of voltage deviation and minimizing the cost $C(q)$ of reactive power provisioning. Seen from (4.14), a smaller α_i implies a steeper cost function of reactive power provisioning, which means that a larger voltage deviation may incur at the equilibrium. So a larger α_i and smaller ϵ is preferred for minimizing the voltage derivation. Therefore the ϵ value specifies the tradeoff between convergence speed and the voltage deviation. We will further study the optimal choice of ϵ and α_i in future work.

Seen from (4.14), a smaller deadband δ_i means a smaller marginal cost in reactive power provisioning and thus a smaller cost in reactive power provisioning. Intuitively, this implies that the smaller the deadband δ_i, the more bus i is willing/active to provision reactive power in order to achieve a narrower range of desired voltage.

The above discussion on parameter choice is based on the dynamical properties

of the local volt/var control, as well as the impact of bus i's choice on itself; e.g., if the control at a bus has a smaller impact on itself or if a bus wants to achieve a narrower voltage range, it should be more active in reactive power provisioning. We can also set parameters to balance the contribution of a bus to the network versus its gain. For example, a larger X_{ii} means bus i can help more with regulating the voltages at other buses, so it may have a tighter range of desired voltage and set a smaller deadband. A fair choice for the deadband would be $\delta_i \propto 1/X_{ii}$.

4.5 Conclusion

We have studied a general class of local volt/var control schemes where the control decision on reactive power at a bus depends only on the voltage of that bus. By interpreting the resulting feedback dynamical system as a distributed algorithm for solving a convex global optimization problem, we have shown that the network has a unique equilibrium point. Moreover, the objective function serves as a Lyapunov function, leading to a simple condition that guarantees exponential convergence. The optimization based model also suggests a principled way to engineer the control. We have applied these results to the inverter-based volt/var control in the IEEE 1547.8 standard, and discuss how to set the parameters for the proposed control functions.

Chapter 5

Incremental Local Voltage Control Algorithms

5.1 Introduction

The reverse-engineered optimization based model in (4.8) provides a way to characterize the equilibrium and establishes the convergence of the local volt/var control, as shown in Theorems 4.1 – 4.2. It also suggests a principled way to engineer the control. New design goals such as fairness and economic efficiency can be revised by engineering the objective function in (4.8); and new control schemes with better dynamical properties can be designed based on various optimization algorithms, e.g., the gradient algorithm.

In particular, the convergence condition (4.9) is hard to verify in practice for two reasons. First, it is a computationally demanding problem to verify a linear matrix inequality of potentially very large dimension. Second, matrix X depends on the reactance of every line in the network, which is practically hard to obtain. Moreover, even if you can verify the condition (4.9), it is rather restrictive in constraining "allowable" control functions, and the existing control schemes may not satisfy this condition. Indeed, it has been observed in the literature, e.g., [6], that in practical circumstances the droop-based control scheme, a commonly adopted non-incremental voltage control [73], can lead to undesirable oscillatory behaviors even in the case of a single inverter unit. This motivates us to forward-engineer the local voltage

control and apply the sub-gradient method to design an incremental voltage control algorithm that demands less restrictive condition for convergence.

Even though the sub-gradient based voltage control has less restrictive convergence condition, it has a high implementation complexity because of the need to choose the proper sub-gradient direction and to compute the inverse of the control function. Therefore, we follow up by proposing a pseudo-gradient based voltage control algorithm that not only admits a less restrictive convergence condition but also has a low implementation complexity. We show that the dynamical system with the new voltage control algorithm solves the same optimization problem and gives the condition on the stepsize under which the system converges. We further compare all the three voltage control algorithms analytically, as well as numerically based on a real world distribution feeder in Southern California with multiple large PV generation units through simulations.

5.2   An incremental control algorithm

As mentioned in the above, for a given optimization problem, there may exist different optimization algorithms. In this subsection, we will apply the (sub)gradient method to the problem (4.8) to design a new voltage control algorithm:

$$
q_i(t + 1) \quad = \quad \left[q_i(t) - \gamma \frac{\partial F(q)}{\partial q_i} \right]_{q_i^{min}}^{q_i^{max}}, \tag{5.1}
$$

where $\gamma > 0$ is the stepsize, '$[\ ]_b^a$' denotes the projection onto $[a, b]$, and

$$
\frac{\partial F(q)}{\partial q_i} = \begin{cases} C_i'(q_i(t)) + v_i(t) & \text{if } q_i(t) \neq 0 \\ 0 & \text{if } q_i(t) = 0 , \ -\frac{\delta}{2} \leq v_i(t) \leq \frac{\delta}{2} \\ -\frac{\delta}{2} + v_i(t) & \text{if } q_i(t) = 0 , \ v_i(t) > \frac{\delta}{2} \\ \frac{\delta}{2} + v_i(t) & \text{if } q_i(t) = 0 , \ v_i(t) < -\frac{\delta}{2} \end{cases} . \tag{5.2}
$$

The above control algorithm is **incremental** as at each time the reactive power is "gradually" adjusted upon the provisioning at the previous time. It is also distributed,

since the reactive power provisioning decision at each node $i \in \mathcal{N}$ depends only on the current provisioning and voltage at node i.

We thus obtain the following dynamical system:

$$D2: \left| \begin{array}{rcl} v^{(t)} & = & Xq^{(t)} + \tilde{v}, \\ q_i^{(t+1)} & = & \left[q_i(t) - \gamma \frac{\partial F(q)}{\partial q_i} \right]_{q_i^{min}}^{q_i^{max}}. \end{array} \right. \tag{5.3}$$

The following result is immediate.

Theorem 5.1. *Suppose A1 holds. Then there exists a unique equilibrium point for the dynamical system D2. Moreover, a point (v^*, q^*) is an equilibrium if and only if q^* is the unique optimal solution of problem (4.8) and $v^* = Xq^* + \tilde{v}$.*

5.2.1 Convergence

We now analyze the convergence of the dynamical system $D2$.

Theorem 5.2. *Suppose A1 holds. If the stepsize γ_g satisfies*

$$C2: \quad \gamma_g < \frac{2}{\lambda_{max}(\nabla^2 C(q) + X)}, \tag{5.4}$$

where λ_{max} denotes the maximum eigenvalue, then the dynamical system D2 converges to the unique equilibrium.

Proof. Consider first the case when $q_i(t) \neq 0$, $\forall i \in \mathcal{N}$. By the second order Taylor expansion,

$$\begin{aligned} & F(q(t+1)) \\ = & F(q(t)) + (\nabla F(q(t)))^T (q(t+1) - q(t)) \\ & + \frac{1}{2}(q(t+1) - q(t))^T (\nabla^2 C(\tilde{q}) + X)(q(t+1) - q(t)), \end{aligned} \tag{5.5}$$

where $\tilde{q} = \theta q(t) + (1 - \theta)q(t+1)$ for certain $\theta \in [0, 1]$. By Projection Theorem[74],

we have $(\nabla F)^T(q(t+1) - q(t)) \le -\frac{1}{\gamma_g}||q(t+1) - q(t)||^2$, which leads to

$$
\begin{aligned}
&F(q(t+1)) \\
&\le F(q(t)) - \frac{1}{\gamma_g}||q(t+1) - q(t)||^2 \\
&\quad + \frac{1}{2}(q(t+1) - q(t))^T(\nabla^2 C(\tilde{q}) + X)(q(t+1) - q(t)) \\
&= F(q(t)) \\
&\quad + (q(t+1) - q(t))^T(-\frac{2}{\gamma_g}I + \nabla^2 C(\tilde{q}) + X)(q(t+1) - q(t)). \quad (5.6)
\end{aligned}
$$

When the condition (5.7) holds, $-\frac{2}{\gamma_g}I + \nabla^2 C(\tilde{q}) + X$ is negative definite, and thus the second term in (5.6) is strictly negative as long as $q(t+1) \ne q(t)$ and zero only if $q(t+1) = q(t)$. So, $F(q(t+1)) \le F(q(t))$ with the equality if and only if $q(t+1) = q(t)$. Since the equilibrium of the dynamical system $D2$ is unique by Theorem 5.1, $q(t+1) = q(t)$ can only occur at the unique equilibrium q^* (with $v^* = Xq^* + \tilde{v}$). Thus, $F(q(t+1)) \le F(q(t))$ with the equality if and only if $q(t+1) = q(t) = q^*$. Also, notice that $F(q) \ge F(q^*)$ with equality if and only if $q = q^*$. So, F is a discrete-time Lyapunov function for $D2$, and the Lyapunov stability theorem then implies that q^* is globally asymptotically stable [75].

Consider now the case when $q_i(t) = 0$ and thus $C_i(q_i(t))$ in the function $F(q(t))$ is not differentiable for some $i \in \mathcal{N}$. The complication here is to use well-defined derivatives in the Taylor expansion. We have three sub-cases; see equation (5.2):

1. $v_i(t) > \delta/2$: The subgradient in $D2$ is chosen as $\frac{\partial F}{\partial q_i} = -\frac{\delta}{2} + v_i(t) > 0$, so $q_i(t+1) = -\gamma_g\frac{\partial F}{\partial q_i} < 0$. We can use the left derivative $C_i'(0^-)$, which is well-defined, in the Taylor expansion.

2. $v_i(t) < -\delta/2$: The subgradient in $D2$ is chosen as $\frac{\partial F}{\partial q_i} = \frac{\delta}{2} + v_i(t) < 0$, so $q_i(t+1) = -\gamma_g(\frac{\delta}{2} + v_i(t)) > 0$. We can use the right derivative $C_i'(0^+)$, which is well-defined, in the Taylor expansion.

3. $-\delta/2 \le v_i(t) \le \delta/2$: The subgradient in $D2$ is chosen as $\frac{\partial F}{\partial q_i} = 0$. So, $q_i(t+1) = q_i(t) = 0$. In this case, the Taylor expansion on C_i is not needed, and

$F(q(t+1)) \leq F(q(t))$ still holds.

With the above choice of the derivatives in the Taylor expansion, we can similarly show that F is a discrete-time Lyapunov function for $D2$ and q^* is globally asymptotically stable. □

Notice that for any control functions f_i (that satisfies A1), the convergence condition (5.7) can be always satisfied by a properly chosen stepsize γ_g. Even though the range of γ_g depends on the control functions, the condition (5.7) does not constrain the allowable control functions. In contrast, the convergence condition (4.9) for the non-incremental voltage control (4.4) does constrain the allowable control functions f_i.

For the piecewise linear droop control functions (4.13), we have the following result on convergence.

Corollary 5. *Suppose A1 holds. If the stepsize γ_g satisfies*

$$\gamma_g < \frac{2}{\lambda_{max}(\mathrm{diag}(\frac{1}{\alpha_i}) + X)}, \tag{5.7}$$

then the dynamical system $D2$ with the piecewise linear droop control functions (4.13) converges to the unique equilibrium.

Proof. For the piecewise linear control functions (4.13), $\nabla^2 C(q) = \mathrm{diag}(\frac{1}{\alpha_i})$. The result follows from Theorem 5.2. □

Recall that α_i can be seen as a metric for the "aggressiveness" of the voltage control. Theorem 5.2 (and Corollary 5) implies that a more aggressive voltage control allows a larger range of the stepsize for the convergence. This is different from the convergence of the non-incremental voltage control (4.4) where the control cannot be too aggressive. On the other hand, a bound (5.7) on the "allowable" stepsize also means that the control cannot be too aggressive.
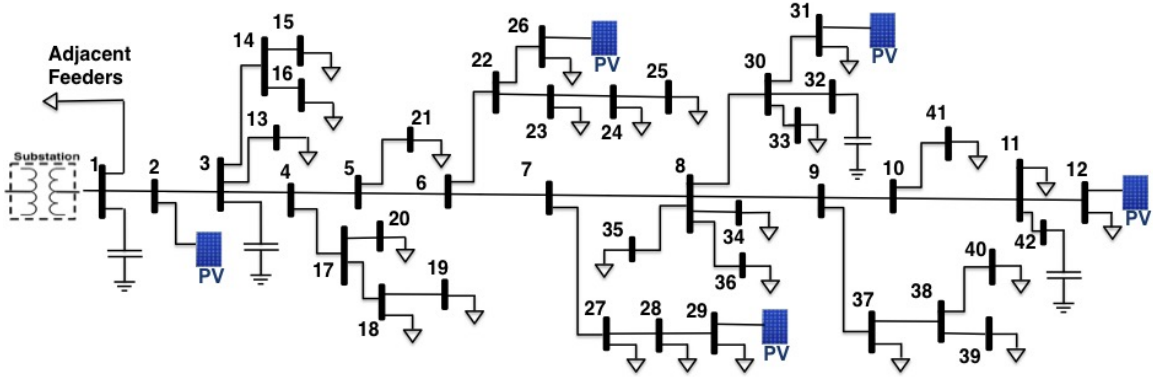
Figure 5.1: Circuit diagram for SCE distribution system.

Table 5.1: Network of Fig. 5.1: Line impedances, peak spot load KVA, capacitors, and PV generation's nameplate ratings.

Network Data																
Line Data				Line Data				Line Data				Load Data		Load Data		PV Generators
From Bus.	To Bus.	R (Ω)	X (Ω)	From Bus.	To Bus.	R (Ω)	X (Ω)	From Bus.	To Bus.	R (Ω)	X (Ω)	Bus No.	Peak MVA	Bus No.	Peak MVA	Bus No.	Capacity MW
1	2	0.259	0.808	8	34	0.244	0.046	18	19	0.198	0.046	11	0.67	28	0.27		
2	3	0.031	0.092	8	36	0.107	0.031	22	26	0.046	0.015	12	0.45	29	0.2	2	1
3	4	0.046	0.092	8	30	0.076	0.015	22	23	0.107	0.031	13	0.89	31	0.27	26	2
3	13	0.092	0.031	8	9	0.031	0.031	23	24	0.107	0.031	15	0.07	33	0.45	29	1.8
3	14	0.214	0.046	9	10	0.015	0.015	24	25	0.061	0.015	16	0.67	34	1.34	31	2.5
4	17	0.336	0.061	9	37	0.153	0.046	27	28	0.046	0.015	18	0.45	35	0.13	12	3
4	5	0.107	0.183	10	11	0.107	0.076	28	29	0.031	0	19	1.23	36	0.67		
5	21	0.061	0.015	10	41	0.229	0.122	30	31	0.076	0.015	20	0.45	37	0.13		
5	6	0.015	0.031	11	42	0.031	0.015	30	32	0.076	0.046	21	0.2	39	0.45		
6	22	0.168	0.061	11	12	0.076	0.046	38	39	0.107	0.015	23	0.13	40	0.2		
6	7	0.031	0.046	14	16	0.046	0.015	38	40	0.061	0.015	24	0.13	41	0.45		
7	27	0.076	0.015	14	15	0.107	0.015	43	44	0.061	0.015	25	0.2	$V_{base} = 12.35$ KV			
7	8	0.015	0.015	17	18	0.122	0.092	43	45	0.061	0.015	26	0.07	$S_{base} = 1000$ KVA			
8	35	0.046	0.015	17	20	0.214	0.046					27	0.13	$Z_{base} = 152.52\ \Omega$			

5.3   Numerical Examples

Focusing on the piecewise linear droop control functions (4.13), we evaluate the proposed incremental var/volt control algorithm (5.1) and compare it against the existing non-incremental algorithm (4.4) on a distribution feeder of South California Edison with a high penetration of photovoltaic (PV) generation.[1]

Fig. 5.1 shows a 42-bus model of this feeder, where bus 1 is the substation and five photovoltaic generators are integrated at buses 2, 12, 26, 29, and 31. As we aim

---

[1]This feeder is a modified version of the original feeder published in [2], where zero impedance lines have been removed, and also the location and capacity of the PV generators have changed for demonstration purpose.

to study the volt/var control through PV inverters, all shunt capacitors are assumed to be off. Table 5.1 contains the network data including the line impedance, the peak MVA demand of loads, and the capacity of the PV generators. It is important to note that all studies are run with a full AC power flow model (not the linearized model). Droop parameters at voltage controlling nodes are such that the deadband is from $0.98^{p.u.}$ to $1.02^{p.u.}$, and the hard voltage thresholds are $\bar{v}_i = 0.97^{p.u.}, \underline{v_i} = 0.97^{p.u.}$ on all inverters.
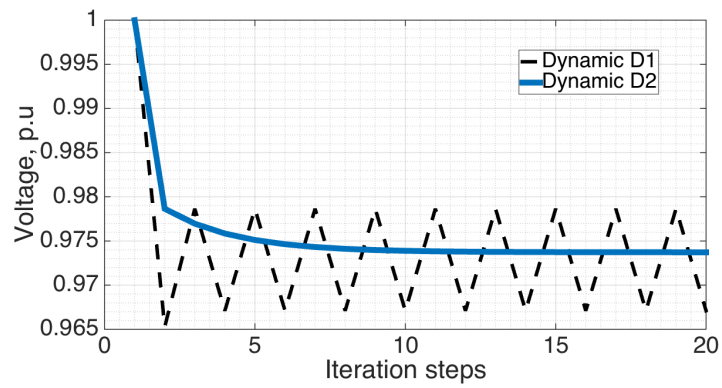
5.3.1 Case of a single inverter

We first provide a simple example to illustrate the potential instability of the non-incremental voltage control scheme (4.4). In the feeder in Fig. 5.1, assume that all loads are at 80% of their peak value with a constant 0.9 Power Factor (PF), i.e., a total demand of 8.24^{MW} and 3.99^{MVar}. We further assume that all five PV generators are running at 60% of their nameplate capacity with PF=1, except for the generator at bus 12, which is enabled to inject/absorb reactive power within a range of PF $\in [0.8, 1]$, corresponding to $q_{12}^{max} = 1.35^{MVar}$. In this setup, it is observed that the reactive power output of the inverter at bus 12 oscillates between 0.18 and 1.35^{Mvar} (dash line in Fig. 5.2a), corresponding to a voltage oscillation between 0.967 and $0.979^{p.u.}$ (dash line in Fig. 5.2b). In contrast, when the proposed incremental control algorithm (5.1) with $\gamma = 20$ is applied, there is no oscillation and the system converges very quickly to the equilibrium point of 0.85^{MVar}, $0.974^{p.u.}$ at bus 12 (solid lines in Fig. 5.2a, 5.2b).

5.3.2 Multiple inverter interactions

As demonstrated above, the non-incremental voltage control (4.4) can potentially be unstable even with just a single inverter. With multiple inverters operating simultaneously in a distribution feeder, instability is even more of a serious concern. To see this, suppose that all five PV units of the feeder in Fig. 5.1 are active in controlling their inverters. Now let all spot loads be at their peak value with a constant 0.9 PF,
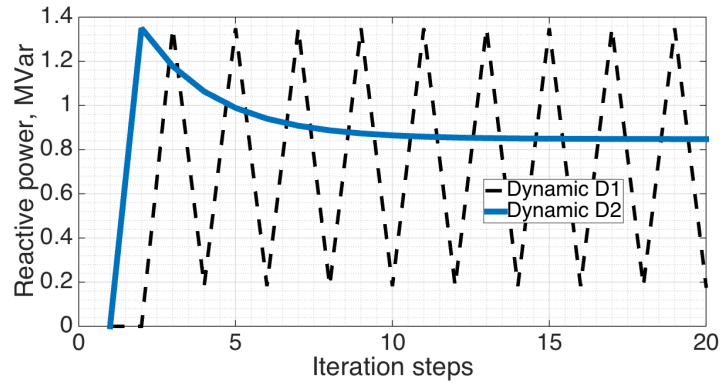
(a)

(b)

Figure 5.2: Dynamics in reactive power injection and voltage magnitude for the case of a single inverter.
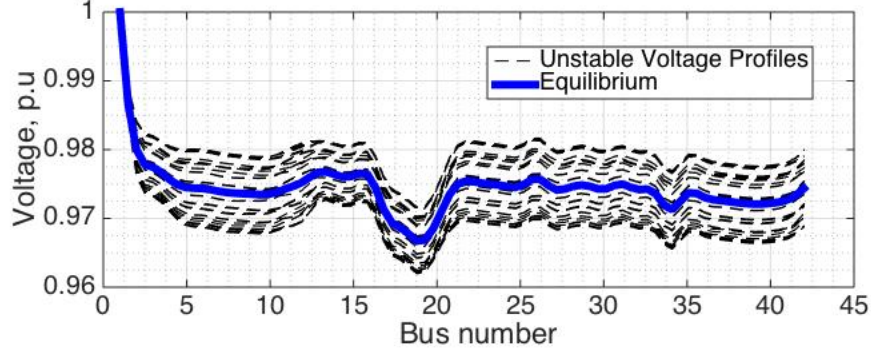
Figure 5.3: Oscillation in voltage profile when all inverters operate.

and let the PV units be running at 70% of their capacity, all enabled to control their reactive power output within a range of PF $\in [0.8, 1]$. Again, as shown in Fig. 5.3, it is observed that in this case the non-incremental control scheme fails to converge, causing the voltage profile of the feeder to oscillate around the equilibrium (dashed blue line). Also, notice that, when the control at an inverter oscillates, it causes oscillation at all buses except for the substation bus.

In contrast, with the incremental voltage control algorithm (5.1) there is no oscillation and the system converges with appropriate stepsizes, as shown in Fig. 5.8. We see that with "small" enough stepsize γ, the proposed incremental voltage control scheme converges to the equilibrium; and the larger the stepsize, the faster the convergence, which is a typical characteristics of the gradient algorithm. Also notice that, as shown in Fig. 5.8(d), if the stepsize is too large, the system will oscillate. In practice, we can start with an analytical estimate of the bound on the stepsize (5.7), and then run some numerical experiments around the bound to choose a stepsize that achieves a good tradeoff between convergence speed and robustness.

5.4 pseudo-gradient based local voltage control

Despite the condition $C2$ being less restrictive, the above incremental voltage control based on the (sub)gradient algorithm incurs lots of implementation complexity. The (sub)gradient (5.2) requires tracking the value of v_i with respect to $\pm \delta_i / 2$, and takes

(a) $\gamma = 10$: fast convergence

(b) $\gamma = 1$

(c) $\gamma = 0.1$: slow convergence
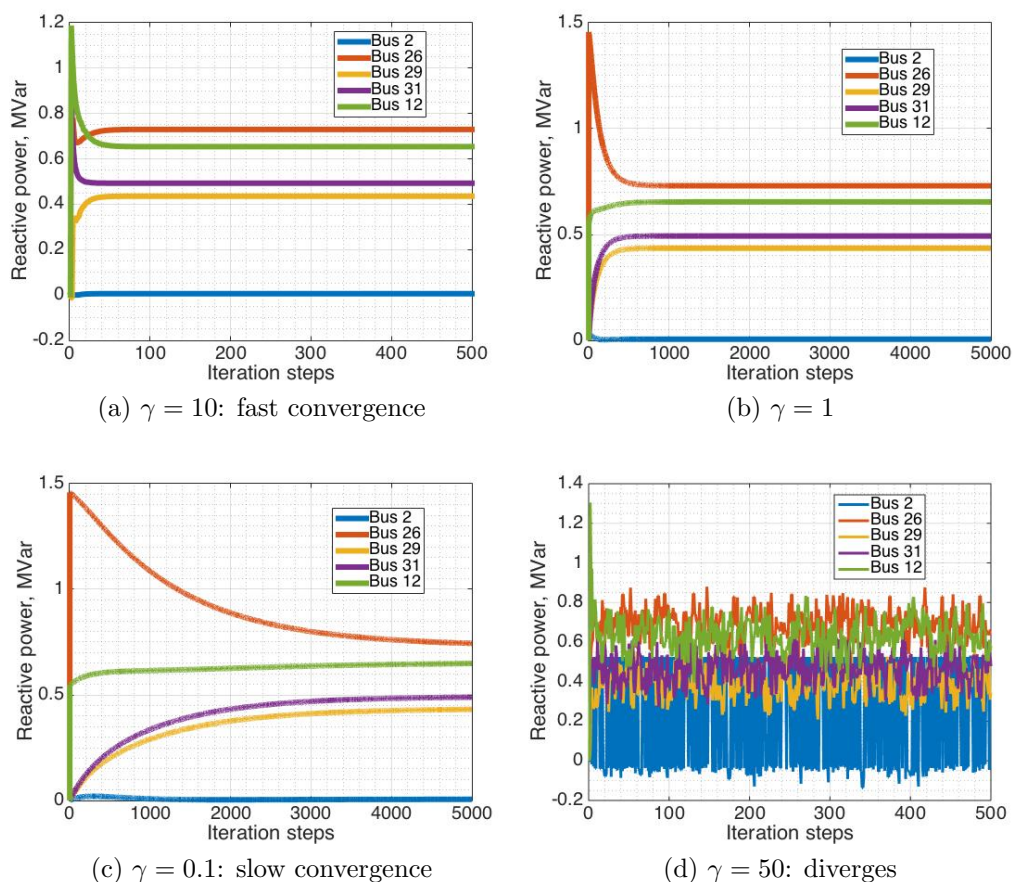
(d) $\gamma = 50$: diverges

Figure 5.4: Convergence of the proposed incremental voltage control with different stepsizes.

different forms accordingly. Furthermore, it requires the computation of the inverse of the control function f_i, which is computationally expensive for a general control function. This high implementation complexity of the gradient algorithm motivates us to seek an incremental voltage control algorithm with less restrictive conditions on the control function as well as low implementation complexity. In the next section, we will present such a control algorithm based on the pseudo-gradient algorithm for the optimization problem ((4.8)) and study its equilibrium and dynamical properties.

Consider the following incremental local voltage control based on the pseudo-

gradient algorithm for solving the optimization problem (4.8):

$$
\begin{aligned}
q_i(t+1) &= \left[(1-\gamma_p)q_i(t) + \gamma_p f_i(v_i(t))\right]_{q_i^{min}}^{q_i^{max}} \\
&= \left[q_i(t) - \gamma_p\left(q_i(t) - f_i(v_i(t))\right)\right]_{q_i^{min}}^{q_i^{max}},
\end{aligned}
\tag{5.8}
$$

where $\gamma_p > 0$ is the stepsize or the weight. With the given control functions f_i, the implementation of the algorithm (5.8) is straightforward and does not have any implementation issues that the (sub)gradient based control algorithm D2 has. It is also interesting to notice that, when the weight $\gamma_p = 1$, we recover the non-incremental voltage control in (4.5).

With the control (5.8), we obtain the following dynamical system:

$$
D3 : \left| \begin{aligned}
v(t) &= Xq(t) + \tilde{v}, \\
q_i(t+1) &= \left[q_i(t) - \gamma_p\left(q_i(t) - f_i(v_i(t))\right)\right]_{q_i^{min}}^{q_i^{max}}.
\end{aligned} \right.
\tag{5.9}
$$

The dynamical system $D3$ has the same equilibrium condition as the dynamical system $D1$. The following result is immediate.

Theorem 5.3. *Suppose A1 holds. There exists a unique equilibrium point for the dynamical system D3. Moreover, a point (v^*, q^*) is an equilibrium if and only if q^* is the unique optimal solution of problem (4.8) and $v^* = Xq^* + \tilde{v}$.*

We now analyze the convergence of the dynamical system $D3$.

Lemma 3. *Suppose $A1 - A2$ hold. With any $q_a, q_b \in [q_i^{min}, q_i^{max}]$, we have*

$$
\left((-f_i^{-1}(q_a)) - (-f_i^{-1}(q_b))\right)(q_a - q_b) \geq \frac{1}{\alpha_i}(q_a - q_b)^2.
\tag{5.10}
$$

Proof. By the condition $A2$, we have the bound on the derivative of the control function $|f_i'(v_i)| \leq \alpha_i$, and thus the bound for its inverse $|(-f_i^{-1}(q_i))'| = |\frac{1}{f'(f^{-1}(q_i))}| \geq \frac{1}{\alpha_i}$.

If q_a and q_b are both positive (or both negative), then the corresponding $v_a = f_i^{-1}(q_a)$ and $v_b = f_i^{-1}(q_b)$ are both smaller than $v_i^{nom} - \delta_i/2$ (or larger than $v_i^{nom} + \delta_i/2$).

We thus have $|(-f_i^{-1}(q_a)) - (-f_i^{-1}(q_b))| \geq \frac{1}{\alpha_i}|q_a - q_b|$. Equality is achieved if the linear control function (4.13) is used. On the other hand, if one of q_a and q_b is positive and the other is negative, then as long as $\delta \neq 0$ we have $|(-f_i^{-1}(q_a)) - (-f_i^{-1}(q_b))| > \frac{1}{\alpha_i}|q_a - q_b|$. Combined with the monotonicity of f^{-1}, the inequality (5.10) follows. $\square$

Theorem 5.4. *Suppose A1-A2 hold. If the stepsize γ_p satisfies the following condition C3:*

$$C3: \quad \gamma_p < \frac{2}{\max\{\alpha_i\}\lambda_{max}(\nabla^2 C(q) + X)}, \tag{5.11}$$

then the dynamical system D3 converges to its unique equilibrium.

Proof. We first consider the case when $q_i(t) \neq 0$, $\forall i$, i.e., when objective function F is differentiable. By the second-order Taylor expansion, we have

$$
\begin{aligned}
&F(q(t+1)) \\
= \ &F(q(t)) - \gamma_p \sum_i (-f_i^{-1}(q_i(t)) + v_i(t))(q_i(t) - f_i(v_i(t))) \\
&+ \frac{\gamma_p^2}{2}(q(t) - f(v(t)))^T (\nabla^2 C(\tilde{q}) + X)(q(t) - f(v(t))),
\end{aligned}
\tag{5.12}
$$

where $f(v(t)) := \Big(f_1(v_1(T)), \ldots, f_n(v_n(t)) \Big)^T$, and $\tilde{q} = \theta q(t) + (1-\theta)q(t+1)$ for some $\theta \in [0,1]$. By Lemma 3, we have $(-f_i^{-1}(q_i(t)) + v_i(t))(q_i(t) - f_i(v_i(t))) \geq \frac{1}{\alpha_i}(q_i(t) - f_i(v_i(t)))^2$. Thus the Taylor expansion follows as

$$
\begin{aligned}
&F(q(t+1)) \\
\leq \ &F(q(t)) + \frac{1}{2}(q(t) - f(v(t)))^T \\
&(\gamma_p^2(\nabla^2 C(\tilde{q}) + X) - 2\gamma_p A^{-1})(q(t) - f(v(t))).
\end{aligned}
\tag{5.13}
$$

When the condition $C3$ holds, $\gamma^2(\nabla^2 C(\tilde{q}) + X) - 2\gamma A^{-1}$ is always negative definite. As a result, the second term in (5.13) is always non-positive. In fact, this part is

equal to zero if and only if $q(t) = f(v(t))$, or equivalently, $q(t) = q(t+1)$. Therefore $F(q(t+1)) \leq F(q(t))$, where the equality is obtained if and only if $q(t+1) = q(t)$. Additionally, because of the uniqueness of the equilibrium point as shown in Theorem 5.3, $F(q(t+1)) = F(q(t))$ if and only if $q(t+1) = q(t) = q^*$. So, F can be seen as a discrete-time Lyapunov function for the dynamical system $D3$, and by the Lyapunov stability theorem, the equilibrium q^* is globally asymptotically stable.

Next we consider the case when $q_i(t) = 0$ for some i. For bus i with $q_i(t) = 0$, the dynamics, irrelevant of derivative, is still well-defined, giving $q_i(t+1) = \gamma f_i(v_i(t)) = 0$. However, its Taylor expansion involves the derivative of $C_i(q(t))$, which doesn't exist at $q_i = 0$. We thus assign the subgradient value for bus i as $\frac{\partial F(q)}{\partial q_i}\big|_{q_i=0} = 0$, and then the proof follows similarly with this well-defined Taylor expansion, and the conclusion holds as well. $\qquad\square$

Theorem 5.4 shows that the pseudo-gradient based local voltage control has the same advantage as the gradient based control, as opposed to the nonincremental voltage control; and in particular, its convergence condition does not restrict the allowable control functions f_i. We will provide more detailed comparison between the three algorithms in the next section.

Remarks: Notice that in the pseudo-gradient algorithm it is usually assumed that $\gamma_p \leq 1$. This gives a nice interpretation of the new decision $q_i(t+1)$ being a convex combination of the previous decision $q_i(t)$ and the local control $o_i(t) = f_i(v(t))$ in reactive power. However, here we do not require $\gamma_p \leq 1$, as long as the condition $C3$ is met.

5.5   Comparative Study of Convergence Conditions and Rates

We have presented three different local voltage control algorithms in the previous two sections. In this section, we compare these three control schemes regarding the corresponding convergence conditions and convergence rates. As we will see,

the gradient and pseudo-gradient based algorithms have very close performance in terms of convergence. So, as discussed in the previous sections, the advantage of the pseudo-gradient based algorithm over the gradient based algorithm is its much lower implementation complexity. However, this low implementation complexity provides strong enough motivation for adopting the pseudo-gradient based local voltage control in the distribution network.

5.5.1   Analytical characterization

5.5.1.1   Comparison of D3 and D1

As indicated earlier, $D1$ can be viewed as a special case of $D3$. The following result is immediate.

Proposition 1. *The non-incremental voltage control in the dynamical system $D1$ is a special case of the control in $D3$ with the stepsize $\gamma_p = 1$.*

As a result of Proposition 1, when the condition $C1$ holds, the largest stepsize that $D3$ can take is no smaller than 1. On the other hand, if the condition $C3$ gives a upper bound for γ_p that is smaller than 1, $D1$ will not converge.

5.5.1.2   Comparison of D3 and D2

We investigate the relationship between the dynamical systems $D2$ and $D3$, in terms of their available ranges of the step sizes γ_g and γ_p for convergence and the convergence speed, by looking at the descent rates of their objective value. We'll show that $D2$ and $D3$ are very closely related, and under some circumstances equivalent.

Proposition 2. *The dynamical systems $D2$ and $D3$ have the same (one-to-one corresponding) ranges of stepsizes γ_g and γ_p to converge, i.e., for any $\gamma_p \in (0, B_p]$, there exists a corresponding $\gamma_g = \max\{a_i\}\gamma_p \in (0, B_g]$, where B_g and B_p are upper bounds of the convergence range for $D2$ and $D3$, respectively.*

Proof. The result follows from the proofs of the sufficiency of the conditions $C2$ and $C3$ for convergence. □

Moreover, we expect similar convergence speeds, or descent rates from dynamical systems $D2$ and $D3$.

Proposition 3. $D2$ *and $D3$ have convergence speeds of the same order, when corresponding stepsizes are chosen.*

Proof. We pick a feasible stepsize γ_p for $D3$, and a corresponding feasible $\gamma_g = \max\{a_i\}\gamma_p$ for $D2$. By second-order Taylor expansions, we have the descent from $q(t+1)$ to $q(t)$, i.e., $F(q(t+1)) - F(q(t))$, of the pseudo-gradient algorithm as

$$\frac{1}{2}\Big(q(t) - f(v(t))\Big)^T \Big(\gamma_p^2(\nabla C(\tilde{q}) + X) - 2\gamma_p A^{-1}\Big)\Big(q(t) - f(v(t))\Big), \qquad (5.14)$$

while that of the gradient algorithm is

$$\frac{1}{2}\Big(v(t) - f^{-1}(q(t))\Big)^T \Big(\gamma_g^2(\nabla C(\tilde{q}) + X) - 2\gamma_g I\Big)\Big(v(t) - f^{-1}(q(t))\Big). \qquad (5.15)$$

Notice that from the proof of Lemma 3, there exists a factor of $\max\{\alpha_i\}$ between $(q(t) - f(v(t)))$ and $(v(t) - f^{-1}(q(t)))$, which compensates for the factor $1/\max\{a_i\}$ between γ_p and γ_g. As a result, the above two decent terms are in the same order, with the only difference coming from the gap between A and $\max\{\alpha_i\}I$. $\qquad\square$

Corollary 6. $D2$ *and $D3$ have identical convergence speeds if homogeneous control functions are applied.*

5.5.2 Numerical examples

We now provide some numerical examples to illustrate the difference between the convergence conditions and rates of the three algorithms based on piecewise linear droop control functions (4.13). The network topology (Fig. 5.1) and parameters (TABLE 5.1) are based on a distribution feeder of South California Edison. As shown in Fig. 5.1, Bus 1 is the actual "0" bus, and five PVs are installed on Bus 2, 12, 26, 29, and 31 respectively.[2] AC power flow model is applied in our simulation,

---

[2]Unlike what is implied in the system model and its analysis, in practice we may not have control at all buses. As a result, the convergence conditions $C1$, $C2$, and $C3$ need to be modified accordingly,

and calculated with MatLab package MatPower[76], instead of the linear model we use in the analytical characterization.

The deadband for control function is chosen to be $[0.98^{p.u.}, 1.02^{p.u.}]$ for all buses, and the hard voltage threshold $\overline{v}_i$ and $\underline{v}_i$ in control function is designed to be a variable, adjusted for the purpose of comparison of convergence conditions by $\alpha_i = q_i^{max}/(\overline{v}_i - \delta/2)$.

5.5.2.1 Convergence condition

We start with observing the difference among the convergence conditions of the three algorithms.

- We first present in Fig.5.5 that, once we design control functions and stepsize such that convergence conditions for $C2$ and $C3$ are met, the dynamical systems $D2$ and $D3$ converge monotonically to the same equilibrium. However, the dynamical system $D1$ converges but may not monotonically.

- We then change the slope of the control function such that we have a larger A^{-1} (i.e., smaller α_i). This will give $D2$ a more strict condition, and $D3$ a less strict one. Resultantly, as we see in Fig.5.6(a), $D2$ no longer converge. However, by simply decreasing stepsize γ_g, $D2$ can be brought back to convergence, as shown in Fig. 5.6(b).

- Lastly, we change the slope of control function to get a smaller A^{-1} (i.e., larger α_i). This affects the convergence conditions for $D1$ and $D3$, while leaving that for $D2$ inviolated. Similarly, $D3$ can be back to convergence by having a smaller stepsize. This is shown in Fig. 5.6(c-d).

5.5.2.2 Range of the stepsize for convergence

Proposition 2 shows that the upper bounds for the stepsizes in $D2$ and $D3$ are related with a factor $\max\{\alpha_i\}$. Since $\max\{\alpha_i\}$ is just a bound, it is interesting to see how

---

based on an "effective" reactance matrix that takes into consideration non-control buses.
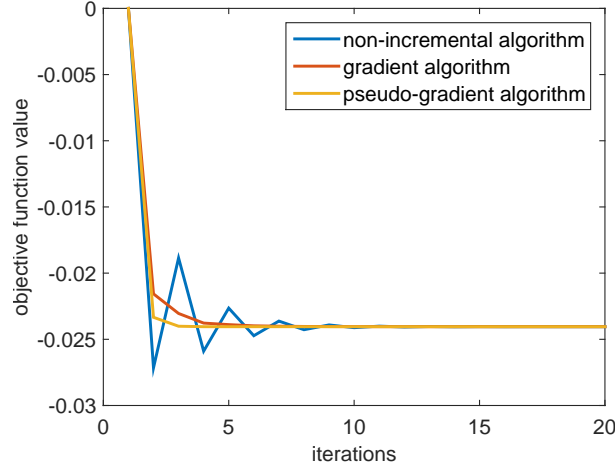
Figure 5.5: $D2$ and $D3$ both converge

tight it is. For the linear control function, $\max\{\alpha_i\} = \max(q_i^{max}/(\overline{v} - \delta/2))$, assuming we have universal and symmetric hard voltage threshold $\overline{v} - v^{nom} = v^{nom} - \underline{v}$. We tune $\overline{v}$ such that the value of $\overline{v} - v^{nom}$ ranges from $0.03^{p.u.}$ to $0.18^{p.u.}$ with granularity of $0.01^{p.u.}$, and value of $\max(\alpha_i)$ ranges from 158 to 9.84 accordingly. We examine the largest possible stepsize $\max(\gamma_g)$ and $\max(\gamma_p)$, and compare their ratio with the theoretical convergence boundary factor $\max(\alpha_i)$. The granularity for γ_g and γ_p is 1 and 0.05, respectively. The results in Fig.5.7 illustrates that the simulated relationship of convergence ranges for gradient algorithm and pseudo-gradient algorithm is close to the theoretical one, which serves well as a conservative upper bound. It supports our analysis in Proposition 2 that these two algorithms have a one-to-one corresponding convergence ranges for γ_g and γ_p.

5.5.2.3 Convergence rate

We observe the convergence rates under certain fixed control functions, with stepsizes γ_g and γ_s tuned within convergence conditions.[3] Since $D1$ is a special case for $D3$ with $\gamma_p = 1$ and fixed convergence rate, assuming it still fits the convergence condition, we won't specifically involve it.

---

[3]Since simulations run under non-linear model, the boundary for stepsizes will usually be different from that obtained under linear model. We carefully choose the values of step size so that convergence results are still obtained.
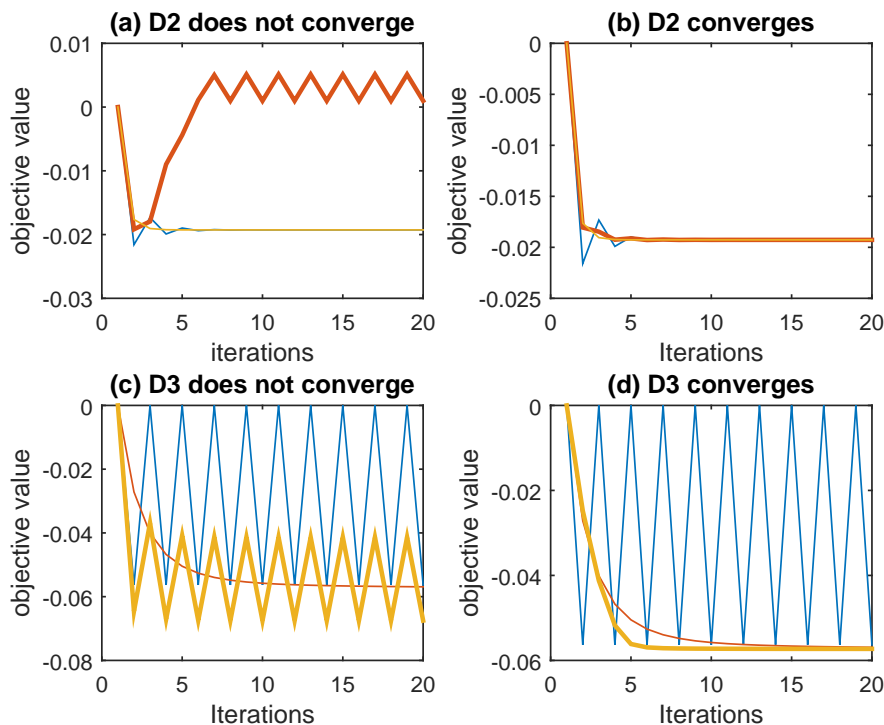
Figure 5.6: D2 and D3 can be brought back to convergence by changing stepsizes γ_g and γ_p to small enough values.

We fixed the hard voltage threshold as $\overline{v}_i = 0.92^{p.u.}$, and $\underline{v}_i = 1.08^{p.u.}$, change the stepsize until it reaches the convergence condition boundary. The results are shown in Fig. 5.8a and 5.8b. We can see that the convergence rates for both gradient algorithm and pseudo-gradient algorithm increase monotonically with the stepsizes before they reach upper bounds, where oscillation of objective function value takes place, i.e., when $\gamma_g = 11$, and $\gamma_p = 0.6$, and starts bringing down the convergence rates. Also, both algorithms perform similarly in terms of convergence rates, with a minimal number of steps less than 10.

5.6 Conclusion

Motivated by the oscillatory behavior of the existing non-incremental local var/volt control schemes, we applied our reverse-engineering results of the previous chapter to
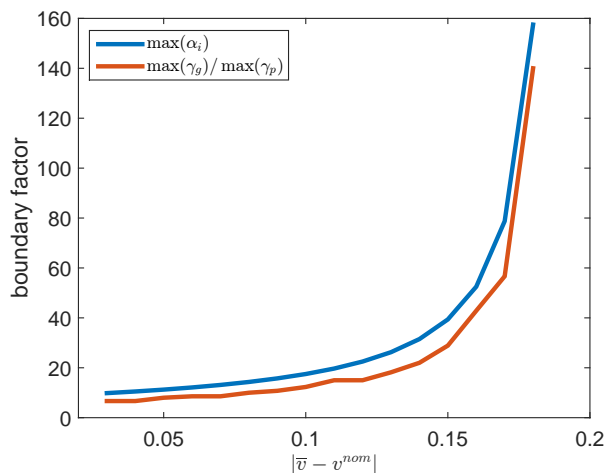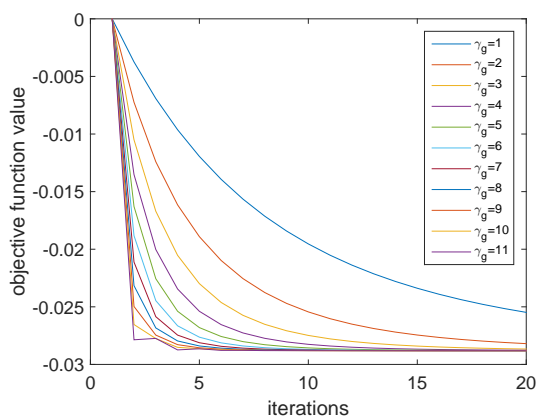
Figure 5.7: The upper bounds for γ_g and γ_p is related by a factor close to theoretical value $\max(\alpha_i)$.

(a) larger γ_g leads to faster convergence rates.
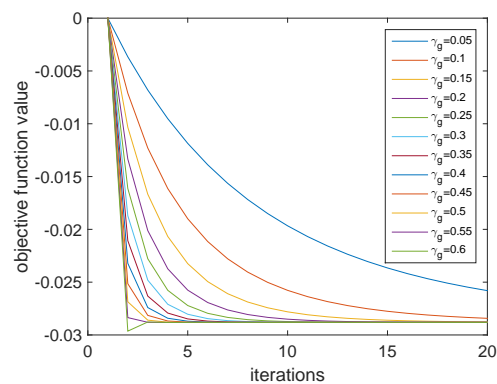
(b) larger γ_p leads to faster convergence rates

Figure 5.8: Convergence of the gradient (left), and pseudo-gradient (right) algorithms with different step-sizes.

design two incremental voltage control algorithms that demand less restrictive condition for convergence: a sub-gradient based method, and a pseudo-gradient method that admits lower implementation complexity. We characterize the convergence of these two methods and compare them in terms of the convergence condition and the convergence rate as well.

Bibliography

[1] Saad Sayeef and Commonwealth Scientific. *Solar Intermittency: Australia's Clean Energy Challenge: Characterising the Effect of High Penetration Solar Intermittency on Australian Electricity Networks.* CSIRO Sydney, Australia, 2012.

[2] Konstantin Turitsyn, Petr Sulc, Scott Backhaus, and Michael Chertkov. Options for control of reactive power by distributed photovoltaic generators. *Proceedings of the IEEE*, 99(6):1063–1073, 2011.

[3] JW Smith, W Sunderman, R Dugan, and Brian Seal. Smart inverter volt/var control functions for high penetration of pv on distribution systems. In *Power Systems Conference and Exposition (PSCE), 2011 IEEE/PES*, pages 1–6. IEEE, 2011.

[4] Masoud Farivar, Christopher R. Clarke, Steven H. Low, and K. Mani Chandy. Inverter var control for distribution systems with renewables. In *IEEE SmartGridComm*, pages 457–462, 2011.

[5] Brett A Robbins, Christoforos N Hadjicostis, and Alejandro D Domínguez-García. A two-stage distributed architecture for voltage control in power distribution systems. *Power Systems, IEEE Transactions on*, 28(2):1470–1482, 2013.

[6] Aliprantis D.C. Jahangiri, P. Distributed volt/var control by pv inverters. *Power Systems, IEEE Transactions on*, 28(3):3429–3439, July 2013.

[7] Jason C Neely, Sigifredo Gonzalez, Michael Ropp, and Dustin Schutz. Accelerating development of advanced inverters: Evaluation of anti-islanding schemes with grid support functions and preliminary laboratory demonstration. Technical report, Northern Plains Power Technologies, Brookings, SD; Sandia National Laboratories (SNL-NM), Albuquerque, NM (United States), 2013.

[8] Tim Basso. Ieee standard for interrconnecting distributed resources with the electric power system. In *IEEE PES Meeting*, page 1, 2004.

[9] Standards Coordinating Committee 21 of Institute of Electrical and Inc. Electronics Engineers. *Recommended Practice for Establishing Methods and Procedures that Provide Supplemental Support for Implementation Strategies for Expanded Use of IEEE Standard 1547.* IEEE ballot document, 2014.

[10] Institute of Electrical and Inc. Electronics Engineers. *IEEE Standard for Interconnecting Distributed Resources with Electric Power Systems Amendment 1.* IEEE ballot document, 2014.

[11] R.A. Jabr. Radial distribution load flow using conic programming. *IEEE Transactions on Power Systems*, 21(3):1458–1459, 2006.

[12] J. Lavaei and S. H. Low. Zero duality gap in optimal power flow problem. *IEEE Transactions on Power Systems*, 27(1):92–107, 2012.

[13] Petr Sulc, Scott Backhaus, and Michael Chertkov. Optimal distributed control of reactive power via the alternating direction method of multipliers. *Energy Conversion, IEEE Transactions on*, 29(4):968–977, 2014.

[14] Na Li, Guannan Qu, and Munther Dahleh. Real-time decentralized voltage control in distribution networks. In *Communication, Control, and Computing (Allerton), 2014 52nd Annual Allerton Conference on*, pages 582–588. IEEE, 2014.

[15] Jeries Shihadeh, Seungil You, and Lijun Chen. Signal-anticipating in local voltage control in distribution systems. In *Smart Grid Communications (Smart-*

GridComm), 2014 IEEE International Conference on, pages 212–217. IEEE, 2014.

[16] Masoud Farivar and Steven H. Low. Branch flow model: relaxations and convexification (part i). *IEEE Transactions on Power Systems*, 28(3):2554–2564, 2013.

[17] Masoud Farivar and Steven H. Low. Branch flow model: relaxations and convexification (part ii). *IEEE Transactions on Power Systems*, 28(3):2565–2572, 2013.

[18] M. Farivar and S.H. Low. Branch flow model: Relaxations and convexification. In *Decision and Control (CDC), 2012 IEEE 51st Annual Conference on*, pages 3672–3679, 2012.

[19] Masoud Farivar, Lijun Chen, and Steven Low. Equilibrium and dynamics of local voltage control in distribution systems. In *Decision and Control (CDC), 2013 IEEE 52nd Annual Conference on*, pages 4329–4334. IEEE, 2013.

[20] Masoud Farivar, Xinyang Zhouy, and Lijun Chen. Local voltage control in distribution systems: An incremental control algorithm. In *Smart Grid Communications (SmartGridComm), 2015 IEEE International Conference on*. IEEE, 2015.

[21] M. Farivar, R. Neal, C. Clarke, and S. Low. Optimal inverter var control in distribution systems with high pv penetration. In *Power and Energy Society General Meeting, 2012 IEEE*, pages 1–7, July 2012.

[22] J. Carpentier. Contribution to the economic dispatch problem. *Bulletin de la Societe Francoise des Electriciens*, 3(8):431–447, 1962.

[23] J. A. Momoh. *Electric Power System Applications of Optimization*. Power Engineering. Markel Dekker Inc.: New York, USA, 2001.

[24] M. Huneault and F. D. Galiana. A survey of the optimal power flow literature. *IEEE Transactions on Power Systems*, 6(2):762–770, 1991.

[25] J. A. Momoh, M. E. El-Hawary, and R. Adapa. A review of selected optimal power flow literature to 1993. Part I: Nonlinear and quadratic programming approaches. *IEEE Transactions on Power Systems*, 14(1):96–104, 1999.

[26] J. A. Momoh, M. E. El-Hawary, and R. Adapa. A review of selected optimal power flow literature to 1993. Part II: Nonlinear and quadratic programming approaches. *IEEE Transactions on Power Systems*, 14(1):105–111, 1999.

[27] K. S. Pandya and S. K. Joshi. A survey of optimal power flow methods. *Journal of Theoretical and Applied Information Technology*, 4(5):450–458, 2008.

[28] B. Stott and O. Alsac. Fast decoupled load flow. *IEEE Transactions on Power Apparatus and Systems*, PAS-93(3):859–869, 1974.

[29] O. Alsac, J. Bright, M. Prais, and B. Stott. Further developments in lp-based optimal power flow. *IEEE Transactions on Power Systems*, 5(3):697–711, 1990.

[30] K. Purchala, L. Meeus, D. Van Dommelen, and R. Belmans. Usefulness of DC power flow for active power flow analysis. In *Proc. of IEEE PES General Meeting*, pages 2457–2462. IEEE, 2005.

[31] B. Stott, J. Jardim, and O. Alsac. Dc power flow revisited. *IEEE Transactions on Power Systems*, 24(3):1290–1300, 2009.

[32] X. Bai, H. Wei, K. Fujisawa, and Y. Wang. Semidefinite programming for optimal power flow problems. *International Journal of Electrical Power and Energy Systems*, 30(6-7):383–392, 2008.

[33] X. Bai and H. Wei. Semi-definite programming-based method for security-constrained unit commitment with operational and optimal power flow constraints. *IET Generation, Transmission and Distribution*, 3(2):182–197, 2009.

[34] J. Lavaei. Zero duality gap for classical OPF problem convexifies fundamental nonlinear power problems. In *Proc.of the American Control Conf.*, 2011.

[35] Somayeh Sojoudi and Javad Lavaei. Physics of power networks makes hard optimization problems easy to solve. In *IEEE Power and Energy Society General Meeting*, pages 1–8, 2012.

[36] Subhonmesh Bose, Dennice F Gayme, Steven Low, and K Mani Chandy. Optimal power flow over tree networks. In *Allerton*, pages 1342–1348, 2011.

[37] B. Zhang and D. Tse. Geometry of feasible injection region of power networks. In *Allerton Conf. on Communication, Control, and Computing*, pages 1508–1515, 2011.

[38] S. Bose, D.F. Gayme, K.M. Chandy, and S.H. Low. Quadratically constrained quadratic programs on acyclic graphs with application to power flow. *Control of Network Systems, IEEE Transactions on*, 2(3):278–287, Sept 2015.

[39] B. Lesieutre, D. Molzahn, A. Borden, and C. L. DeMarco. Examining the limits of the application of semidefinite programming to power flow problems. In *Allerton*, pages 1492–1499, 2011.

[40] I. A. Hiskens and R. Davy. Exploring the power flow solution space boundary. *IEEE Trans. Power Systems*, 16(3):389–395, 2001.

[41] Yuri V. Makarov, Zhao Yang Dong, and David J. Hill. On convexity of power flow feasibility boundary. *IEEE Trans. Power Systems*, 23(2):811–813, May 2008.

[42] Dzung T. Phan. Lagrangian duality and branch-and-bound algorithms for optimal power flow. *Operations Research*, 60(2):275–285, March/April 2012.

[43] Mesut E Baran and Felix F Wu. Network reconfiguration in distribution systems for loss reduction and load balancing. *IEEE Transactions on Power Delivery*, 4(2):1401–1407, 1989.

[44] M. E. Baran and F. F. Wu. Optimal sizing of capacitors placed on a radial distribution systems. *IEEE Transactions on Power Delivery*, 4(1):735–743, 1989.

[45] J. A. Taylor. *Conic optimization of electric power systems*. PhD thesis, MIT, 2011.

[46] J. A. Taylor and F. S. Hover. Convex models of distribution system reconfiguration. *IEEE Transactions on Power Systems*, 27(3):1407–1413, 2012.

[47] R. Cespedes. New method for the analysis of distribution networks. *IEEE Trans. Power Del.*, 5(1):391–396, January 1990.

[48] A. G. Exposito and E. R. Ramos. Reliable load flow technique for radial distribution networks. *IEEE Transactions on Power Systems*, 14(3):1063–1069, 1999.

[49] R. A. Jabr. A Conic Quadratic Format for the Load Flow Equations of Meshed Networks. *IEEE Trans. on Power Systems*, 22(4):2285–2286, Nov 2007.

[50] Lingwen Gan, Na Li, Ufuk Topcu, and Steven Low. Branch flow model for radial networks: convex relaxation. In *Proceedings of the 51st IEEE Conference on Decision and Control*, 2012.

[51] H-D Chiang and Mesut E Baran. On the existence and uniqueness of load flow solution for radial distribution power networks. *IEEE Transactions on Circuits and Systems*, 37(3):410–416, 1990.

[52] Hsiao-Dong Chiang. A decoupled load flow method for distribution power networks: algorithms, analysis and convergence study. *International Journal Electrical Power Energy Systems*, 13(3):130–138, June 1991.

[53] L. R. Foulds. *Graph Theory Applications*. Springer-Verlag, 1992.

[54] Norman Biggs. *Algebraic graph theory*. Cambridge University Press, 1993. Cambridge Mathematical Library.

[55] Narain G Hingorani, Laszlo Gyugyi, and Mohamed El-Hawary. *Understanding FACTS: concepts and technology of flexible AC transmission systems*, volume 1. IEEE press New York, 2000.

[56] Zhang Xiao-Ping, C Rehtanz, and B Pal. Flexible ac transmission systems: Modelling and control, 2006.

[57] Ray D Zimmerman, Carlos E Murillo-Sánchez, and Robert J Thomas. Matpower's extensible optimal power flow architecture. In *Power & Energy Society General Meeting, 2009. PES'09. IEEE*, pages 1–7. IEEE, 2009.

[58] Jos F Sturm. Using sedumi 1.02, a matlab toolbox for optimization over symmetric cones. *Optimization Methods and Software*, 11(1-4):625–653, 1999.

[59] S. Bose, S.H. Low, and K.M. Chandy. Equivalence of branch flow and bus injection models. In *Allerton*, pages 1893–1899, 2012.

[60] Dimitri P. Bertsekas. *Nonlinear programming.* Athena Scientific, 1995.

[61] JJ Grainger and S Civanlar. Volt/var control on distribution systems with lateral branches using shunt capacitors and voltage regulators part i: The overall problem. *Power Apparatus and Systems, IEEE Transactions on*, (11):3278–3283, 1985.

[62] T Niknam, AM Ranjbar, and AR Shirani. Impact of distributed generation on volt/var control in distribution networks. In *Power Tech Conference Proceedings, 2003 IEEE Bologna*, volume 3, pages 7–pp. IEEE, 2003.

[63] Konstantin Turitsyn, Petr Sulc, Scott Backhaus, and Michael Chertkov. Distributed control of reactive power flow in a radial distribution circuit with high photovoltaic penetration. In *Power and Energy Society General Meeting, 2010 IEEE*, pages 1–6. IEEE, 2010.

[64] K. Turitsyn, P. Sulc, S. Backhaus, and M. Chertkov. Local control of reactive power by distributed photovoltaic generators. In *IEEE SmartGridComm*, pages 79–84, 2010.

[65] Kevin P Schneider, J Fuller, F Tuffner, and Ruchi Singh. Evaluation of conservation voltage reduction (cvr) on a national level. *Pacific Northwest National Laboratory report*, 2010.

[66] Ted Soubdhan, Richard Emilion, and Rudy Calif. Classification of daily solar radiation distributions using a mixture of dirichlet distributions. *Solar energy*, 83(7):1056–1063, 2009.

[67] Y Liu, Jovan Bebic, B Kroposki, J De Bedout, and W Ren. Distribution system voltage performance analysis for high-penetration pv. In *Energy 2030 Conference, 2008. ENERGY 2008. IEEE*, pages 1–8. IEEE, 2008.

[68] M Braun. Reactive power supplied by pv inverters–cost-benefit-analysis. In *22nd European Photovoltaic Solar Energy Conference and Exhibition*, pages 3–7, 2007.

[69] Michael Grant, Stephen Boyd, and Yinyu Ye. Cvx: Matlab software for disciplined convex programming. online at `http://cvxr.com/cvx/`, 2008.

[70] M. E. Baran and F. F Wu. Optimal Capacitor Placement on radial distribution systems. *IEEE Transactions on Power Delivery*, 4(1):725–734, 1989.

[71] Anthony Kam and James Simonelli. Stability of distributed, asynchronous var-based closed-loop voltage control systems. In *PES General Meeting— Conference & Exposition, 2014 IEEE*, pages 1–5. IEEE, 2014.

[72] Filip Andrén, Benoit Bletterie, Serdar Kadam, Panos Kotsampopoulos, and Christof Bucher. On the stability of local voltage control in distribution networks with a high penetration of inverter-based generation. 2014.

[73] IEEE P1547. *Recommended Practice for Establishing Methods and Procedures that Provide Supplemental Support for Implementation Strategies for Expanded Use of IEEE Standard 1547.* IEEE ballot document, 2012.

[74] Dimitri P Bertsekas and John N Tsitsiklis. *Parallel and distributed computation: numerical methods.* Prentice-Hall, Inc., 1989.

[75] Hassan K Khalil and JW Grizzle. *Nonlinear systems*, volume 3. Prentice hall New Jersey, 1996.

[76] Ray D Zimmerman, Carlos E Murillo-Sánchez, and Deqiang Gan. Matpower: Steady-state operations, planning, and analysis tools for power systems research and education. *IEEE Transactions on Power Systems*, 26(1):12–19, 2010.

[77] Steven H Low. Convex relaxation of optimal power flow – part i: Formulations and equivalence. *IEEE Transactions on Control of Network Systems*, 1(1):15–27, 2014.

[78] SH Low. Convex relaxation of optimal power flow – part ii: Exactness. *Control of Network Systems, IEEE Transactions on*, 1(2):177–189, 2014.

[79] Subhonmesh Bose, Steven H Low, Thanchanok Teeraratkul, and Babak Hassibi. Equivalent relaxations of optimal power flow. *Automatic Control, IEEE Transactions on*, 60(3):729–742, 2015.

[80] Qiuyu Peng and Steven H Low. Distributed algorithm for optimal power flow on a radial network. In *Decision and Control (CDC), 2014 IEEE 53rd Annual Conference on*, pages 167–172. IEEE, 2014.

[81] Steven H Low. Convex relaxation of optimal power flow: a tutorial. In *2013 IREP Symposium Bulk Power System Dynamics and Control-IX Optimization, Security and Control of the Emerging Power Grid*, 2013.

[82] Zhaoyu Wang and Jianhui Wang. Review on implementation and assessment of conservation voltage reduction. *Power Systems, IEEE Transactions on*, 29(3):1306–1315, 2014.

[83] Hieu D Nguyen and Konstantin S Turitsyn. Appearance of multiple stable load flow solutions under power flow reversal conditions. In *PES General Meeting— Conference & Exposition, 2014 IEEE*, pages 1–5. IEEE, 2014.

[84] Carleton Coffrin, Hassan L Hijazi, and Pascal Van Hentenryck. Strengthening convex relaxations with bound tightening for power network optimization. In *Principles and Practice of Constraint Programming*, pages 39–57. Springer, 2015.

[85] Lingwen Gan. *Distributed Load Control in Multiphase Radial Networks*. PhD thesis, California Institute of Technology, 2015.

[86] Mohammadhafez Bazrafshan and Nikolaos Gatsis. Decentralized stochastic programming for real and reactive power management in distribution systems. In *Smart Grid Communications (SmartGridComm), IEEE International Conference on*, pages 218–223, 2014.

[87] Xinyang Zhou, Masoud Farivar, and Lijun Chen. Pseudo-gradient based local voltage control in distribution networks. In *Communication, Control, and Computing (Allerton), 53nd Annual Allerton Conference on*, 2015.

[88] Hamed Firouzi, Masoud Farivar, Massoud Babaie-Zadeh, and Christian Jutten. Approximate sparse decomposition based on smoothed l0-norm. *arXiv preprint arXiv:0811.2868*, 2008.

[89] Emiliano Dall'Anese, Sairaj V Dhople, and Georgios Giannakis. Optimal dispatch of photovoltaic inverters in residential distribution systems. *Sustainable Energy, IEEE Transactions on*, 5(2):487–497, 2014.

[90] Bernard C Lesieutre, Daniel K Molzahn, Alex R Borden, and Christopher L DeMarco. Examining the limits of the application of semidefinite programming to

power flow problems. In *Communication, Control, and Computing (Allerton), 49th Annual Allerton Conference on*, pages 1492–1499, 2011.

[91] Daniel K Molzahn, Bernard C Lesieutre, and Christopher L DeMarco. Investigation of non-zero duality gap solutions to a semidefinite relaxation of the optimal power flow problem. In *System Sciences (HICSS), 47th Hawaii International Conference on*, pages 2325–2334, 2014.

[92] Mohamadreza Baradar. *On the Efficiency and Accuracy of Simulation Methods for Optimal Power System Operation: Convex Optimization Models for Power System Analysis, Optimal Utilization of VSC-type DC Wind Farm Grids and FACTS Devices*. PhD thesis, KTH Royal Institute of Technology, 2015.

[93] Joshua Adam Taylor. *Convex Optimization of Power Systems*. Cambridge University Press, 2015.

[94] Xiangjing Su, Mohammad Masoum, Peter J Wolfs, et al. Optimal pv inverter reactive power control and real power curtailment to improve performance of unbalanced four-wire lv distribution networks. *Sustainable Energy, IEEE Transactions on*, 5(3):967–977, 2014.

[95] Baosen Zhang, Alejandro D Dominguez-Garcia, and David Tse. A local control approach to voltage regulation in distribution networks. In *North American Power Symposium (NAPS), 2013*, pages 1–6, 2013.

[96] Ahmad Reza Malekpour, Anil Pahwa, and Sanjoy Das. Inverter-based var control in low voltage distribution systems with rooftop solar pv. In *North American Power Symposium (NAPS), 2013*, pages 1–5. IEEE, 2013.

[97] Pedram Jahangiri. *Voltage and reactive power regulation by photovoltaics in distribution systems*. PhD thesis, Iowa State University, 2014.

[98] Devendra Shelar and Saurabh Amin. Analyzing vulnerability of electricity distribution networks to der disruptions. In *American Control Conference (ACC)*, pages 2461–2468, 2015.

[99] Seungil You and Qiuyu Peng. A non-convex alternating direction method of multipliers heuristic for optimal power flow. In *Smart Grid Communications (SmartGridComm), IEEE International Conference on*, pages 788–793, 2014.

[100] Jeries Shihadeh, Seungil You, and Lijun Chen. Signal-anticipating in local voltage control in distribution systems. In *Smart Grid Communications (SmartGridComm), IEEE International Conference on*, pages 212–217, 2014.

[101] Shahab Bahrami, Vincent WS Wong, and Juri Jatskevich. Optimal power flow for ac-dc networks. In *Smart Grid Communications (SmartGridComm), IEEE International Conference on*, pages 49–54, 2014.